C1 Chemistry for the Production of Clean Liquid Transportation Fuels and Hydrogen

Annual report
Research conducted May 1, 2001-September 30, 2002
DOE Cooperative Agreement No. DE-FC26-99FT40540
Prepared by the Consortium for Fossil Fuel Science

Gerald P. Huffman, Director
CFFLS / University of Kentucky
533 S. Limestone Street, Suite 107
Lexington, KY 40506
Phone: (859) 257-4027
FAX: (859) 257-7215
E-mail: huffman@engr.uky.edu

Consortium for Fossil Fuel Science
University of Kentucky
West Virginia University
University of Pittsburgh
University of Utah
Auburn University

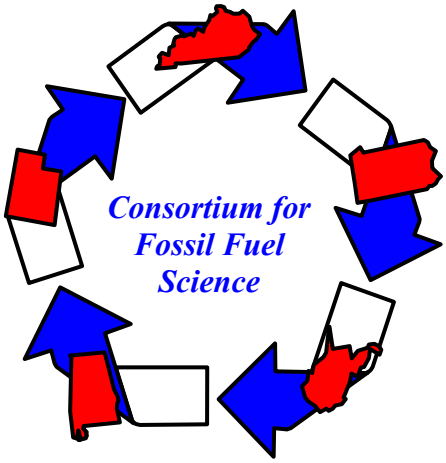

Table of Contents

Abstract

Faculty and students from five universities – the University of Kentucky, University of Pittsburgh, University of Utah, West Virginia University, and Auburn University - are collaborating in a research program to develop C1 chemistry processes to produce ultra-clean liquid transportation fuels and hydrogen, the zero-emissions transportation fuel of the future. The feedstocks contain one carbon atom per molecular unit. They include synthesis gas (syngas), a mixture of carbon monoxide and hydrogen produced by coal gasification or reforming of natural gas, methane, methanol, carbon dioxide, and carbon monoxide. An important objective is to develop C1 technology for the production of transportation fuel from domestically plentiful resources such as coal, coalbed methane, and natural gas. An Industrial Advisory Board with representatives from Chevron-Texaco, Eastman Chemical, Conoco-Phillips, Energy International, the Department of Defense, and Tier Associates provides guidance on the practicality of the research. The current report presents results obtained in this program in its third year, as briefly summarized below.

1. Nanoscale iron-based catalysts containing molybdenum, palladium, or nickel and supported on alumina have been developed that are very effective for the dehydrogenation of methane and ethane to produce pure hydrogen and carbon nanotubes, a potentially valuable by-product. Some of the nanotube structures are being investigated as a safe storage medium for hydrogen. Dehydrogenation of higher hydrocarbons, including several liquids that are compatible with vehicular transportation under fuel cell power, is currently under investigation.
2. Operation of Fischer-Tropsch (FT) synthesis under supercritical fluid (SCF) solvent conditions increases liquid fuel yields and improves the selectivity of the process to produce desired products.
3. Small additions (~1%) of organic probe molecules with carbon-carbon triple bonds to the FT reaction markedly shift the molecular weight distribution and increase the oxygenate content of the products. The goal is to develop better technology for producing cleaner burning diesel fuel and other fuels.
4. Several different types of catalyst are under investigation to develop better control of FT fuel product distributions.
5. C1 processes have been developed for producing ethylene and propylene, two high-value products, from methanol. Novel silicoaluminophosphate (SAPO) catalysts containing nickel and other metals are used.
6. Binary tungsten-cobalt carbide catalysts have been found to have excellent activities and lifetimes for reforming of methane into synthesis gas using carbon dioxide. This type of catalyst is being further investigated for synthesis gas reactions relevant to the goal of producing hydrogen from coal.

Executive Summary

Introduction

The Consortium for Fossil Fuel Science (CFFS) is a research consortium with participants from five universities – the University of Kentucky, University of Pittsburgh, University of Utah, West Virginia University, and Auburn University. The CFFS universities are collaborating in a research program to develop C1 chemistry processes to produce clean transportation fuel from resources such as coal and natural gas, which are more plentiful domestically than petroleum. The processes under development will convert feedstocks containing one carbon atom per molecular unit into ultra clean liquid transportation fuels (gasoline, diesel, and jet fuel) and hydrogen, which many believe will be the transportation fuel of the future. The feedstocks include syngas, a mixture of carbon monoxide and hydrogen produced by coal gasification or reforming of natural gas, methane, methanol, carbon dioxide, and carbon monoxide. An Industrial Advisory Board with representatives from Chevron, Eastman Chemical, Energy International, the Department of Defense, Conoco, and Tier Associates provides guidance on the practicality of the research.

The major objectives of the program are to develop C1 technology for the production of:

1. Ultra-clean, high efficiency, liquid transportation fuels; and
2. Hydrogen, the zero-emissions transportation fuel of the future.

The current report contains results obtained during the third year of the CFFS C1 chemistry program. Some of the more interesting results are briefly summarized below.

1. Nanoscale iron-based catalysts containing molybdenum, palladium, or nickel and supported on alumina have been developed that are very effective for the dehydrogenation of methane and ethane to produce pure hydrogen and carbon nanotubes. Pure hydrogen is the fuel required by vehicles powered by fuel cells, while carbon nanotubes are a potentially valuable by-product. Very open traffic cone structures in nanotubes derived from ethane show promise as a safe storage medium for hydrogen. Currently, this research project is focused on dehydrogenation of higher hydrocarbons, including several liquids that are compatible with vehicular transportation under fuel cell power.
2. Operation of Fischer-Tropsch (FT) synthesis under supercritical fluid (SCF) solvent conditions increases liquid fuel yields and increases the selectivity of the process to produce desired products. Under SCF conditions, gaseous diffusion and liquid thermal conduction conditions prevail. This makes tuning the molecular products by temperature and pressure variation feasible.
3. Small additions (~1%) of organic probe molecules with carbon-carbon triple bonds to the FT reaction markedly shift the molecular weight distribution and increase the oxygenate content of the products. This research is being further pursued with the goal of developing better technology for producing cleaner burning diesel fuel and other fuels.
4. Several different types of catalyst are under investigation to develop for better control of FT fuel products. These include platinum supported on tungstated-zirconia catalysts, which are very effective at cracking FT wax into diesel fuel and lube oil, and sol-gel catalysts containing iron and cobalt that result in more selective FT synthesis.

5. C1 processes have been developed for producing ethylene and propylene, two high-value products, from methanol. Novel silicoaluminophosphate (SAPO) catalysts containing nickel are used.
6. Binary transition tungsten-cobalt carbide catalysts have been found to have excellent activities and lifetimes for reforming of methane into synthesis gas using carbon dioxide. This type of catalyst is being further investigated for synthesis gas reactions relevant to the goal of producing hydrogen from coal.

These topics are discussed in more detail in the remainder of this Executive Summary.

Novel Approaches to Fischer-Tropsch Synthesis

Fischer-Tropsch (FT) synthesis is the best-known C1 chemistry process for producing transportation fuel from syngas. CFFS research has produced a number of innovations on the FT process. In research conducted at the University of Pittsburgh, it has been discovered that small (~1%) additions of probe molecules with carbon-carbon triple bonds dramatically enhance the presence of oxygenated products. This significantly decreases emissions of particulate matter (PM), which is a critical issue for diesel and jet fuels. Using 1-hexyne as the probe molecule additive, much higher yields of FT products in the C_6 to C_{20} range were obtained. GC/MS analysis detected such oxygenated species as 1-heptanal, 2-heptanal, 1 heptanol, 1-octanol, 1-undecanol, and 1-tetradecanol.

Addition of acetylenic hydrocarbons as probe molecules to the FT synthesis has revealed that a homogeneous hydroformylation reaction can take place with both cobalt and iron catalysts. Although both acetylenes and CO contain triple bonds, the acetylenic molecule is adsorbed more rapidly on the catalyst surface and initiates the FT synthesis. Addition of sulfur to the FT synthesis, in the presence of 1-hexyne, poisons the reaction, especially with the cobalt catalyst but does not affect the hydroformylation reaction. Addition of pyridine to a cobalt-catalyzed FT synthesis, again in the presence of 1-hexyne, poisons the hydrformylation reaction without affecting the FT synthesis. The latter two reactions, addition of sulfur and pyridine, have little effect on an iron-catalyzed FT synthesis. Cobalt-catalyzed FT synthesis evidently proceeds by addition of CH_x units to a growing chain. It is likely that iron-catalyzed FT synthesis involves a different mechanistic path, one proceeding via oxygenated surface intermediates.

Other work at the University of Pittsburgh has focused on catalytic hydrocracking of FT wax, which is typically 65-75% of the FT product. $Pt/W/ZrO_2$ catalysts have been developed that are very effective at converting FT wax into a product that is approximately 70% diesel fuel, 25% gasoline, and 5% lube oil.[1,2]

FT synthesis in supercritical fluid (SCF) solvents is under investigation at Auburn University. The SCF media has the advantage of gas-like diffusivities and liquid-like solubilities and heat transfer properties. In experiments using SCF hexane and a commercial cobalt FT catalyst, total syngas conversion was increased over the gas-phase reaction from approximately 50% to 80% and selectivity to heavier products and olefins was increased.[3,4] The yield of C_1-C_3 gases was decreased by approximately 40% in the SCF reaction, while the C_7-C_{24} 1-olefin yield was markedly increased. Under steady-state operation, the temperature distribution along the reactor is significantly flatter in the supercritical phase comparing to gas phase suggesting that the SCF

medium does a much better job in distributing the generated heat. The maximum temperature deviation along the reactor in the supercritical phase is around 5°C compared to 15°C in the gas-phase. It should be noted that the CO conversion in the SCF phase was 70% where the conversion in the gas phase was only 50%. Pressure tuning is found to significantly affect SCF FT synthesis. For example, increasing the pressure moderately leads to the production of more long chain compounds. Future research will focus on other SCF solvents (propane, pentane, carbon dioxide, and mixtures), novel catalyst designs, and pressure tuning to alter product selectivity and yield.

The porosity of xerogel and aerogel supports for cobalt nanoparticle FT catalysts can be adjusted by a judicious combination of ambient drying conditions and supercritical CO_2 drying of the sol-gels. A nanoporous (pores under 4 nm in diameter) xerogel containing 7 nm diameter cobalt particles yields a product which contains diesel fuel range hydrocarbons from the Fischer-Tropsch reaction of syngas at 225°C and 30 psi. Future work will investigate catalyst lifetimes and hydrocarbon product distribution from a fully automated continuous flow reactor loaded with a cobalt-xerogel catalyst. Promoter metals and iron and binary sol-gel catalysts will also be investigated.

Hydrogen

Traditionally, hydrogen has been produced by partial oxidation of methane or gasification of coal to produce synthesis gas, followed by the water-gas shift reaction to convert CO to CO_2 and produce more hydrogen. To achieve the purity required by polymer-electrolyte proton exchange membrane (PEM) fuel cells (<10 ppm CO), further purification (reverse methanation or catalytic oxidation of CO) and separation procedures are required. Research at the University of Kentucky is focused on producing pure hydrogen in a single step by catalytic dehydrogenation of hydrocarbons. Nanoscale, binary Fe-based catalysts containing Mo, Pd or Ni and supported on high surface area alumina have been developed that are very effective for the non-oxidative catalytic decomposition of methane into pure hydrogen and carbon nanotubes.[1] The key factor influencing catalyst activity is the efficient removal of carbon from the catalyst surface in the form of multi-walled nanotubes (MWNT), a valuable by-product with potential applications in electronics, high strength materials, and hydrogen storage. More recent experiments on the catalytic dehydrogenation of ethane have also produced promising results.[2] Yields of 80-90% of pure hydrogen have been obtained from both methane and ethane at relatively low temperatures of 700-800 °C. The nanotube structure produced by ethane exhibits an interesting stacked traffic cone structure at low decomposition temperatures. Such open nanotube structures appear promising for hydrogen storage. This is being investigated in collaboration with Dr. Brad Bockrath, a scientist at the U.S. DOE National Energy Technology Laboratory.

The structures of the binary Fe-M/Al_2O_3 (4.5%Fe-0.5%M, M=Mo, Ni, or Pd) catalysts have been thoroughly characterized[7]. STEM established that the Fe-M catalyst particles are binary in nature and typically ~10-30 nm in mean diameter. The molecular structures of the Fe and secondary metals were determined using XAFS and Mössbauer spectroscopy in their as-prepared, pre-reduced, and after reaction (TOS) states. The results indicate suggest that the key factors that account for the high activity and comparatively long lifetimes of these catalysts are:

★ Binding of the catalyst particles to the alumina support by the formation of hercynite, preventing deactivation by demetallization.

★ Dehydrogenation of methane with simultaneous formation of carbon nanotubes. The nanotubes grow away from the surfaces of the bound Fe-M-C alloy catalyst nanoparticles, which are non-magnetic and austenitic, preventing deactivation by coking.

Future research will be focused on catalytic dehydrogenation of liquid hydrocarbons, a critical problem for fuel cell-powered vehicles, and on development of a continuous process for catalytic production of pure hydrogen and carbon nanotubes from light alkanes.

Synthesis gas

The first and often most expensive step in FT synthesis and many other C1 processes is the production of synthesis gas (syngas). One of the perennial problems in this area has been the deactivation of catalysts by coking. Binary transition metal carbide catalysts developed at West Virginia University have been shown to have excellent activities and lifetimes for reforming of methane to syngas using carbon dioxide. A cobalt tungsten carbide (Co_6W_6C) catalyst exhibited stable activity for CO_2 reforming of CH_4 for more than 150 hours at elevated pressures and high temperatures. The catalyst showed stabilization with increasing activity when heated for over 20 hours at 850 ^oC in the presence of the feed mixture at 850^oC and 5 atm. total pressure. The stabilized catalyst gave CH_4 and CO_2 conversions of 82 and 78 % respectively, with CO yields of 76 % and H_2/CO ratio close to unity at 850^oC and 5 atm total pressure. XRD patterns of the transformed catalyst suggest a phase transformation, at 850 ^oC, from Co_6W_6C to a mixture of WC + Co + C. Hence coke is not a factor in the performance of these catalysts, unlike that of conventional catalysts.

High-value C1 products

An important component of the eventual development of Vision 21 plants that produce electricity and transportation fuels will be the production of other high-value C1 products. C1 processes for producing ethylene and propylene from methanol are being developed at Auburn University. These processes use novel silicoaluminophosphate (SAPO) catalysts. Several SAPO catalysts were successfully synthesized by hydrothermal crystallization and tested in syngas and MeOH conversion reactions. Ethylene selectivities of up to 63 mol% and overall C2-C4 olefin yields of 94% were achieved in MeOH conversion reactions. Inclusion of water in the MeOH feed increased selectivities of C2-C4 olefins to 99.6%. A 100 hr run was made with a Co modified SAPO-34:SAPO-5 composite catalyst. Results suggest that it may be possible to tailor the olefins product composition (e.g., C2/C3 ratio) by adjustment of the SAPO-34:SAPO-5 phase ratio in a composite catalyst.

Extensive characterization of these catalysts by XRD has been performed at West Virginia University to determine whether the desired products are being formed under controlled conditions. This has greatly assisted the Auburn group in optimizing conditions for the controlled synthesis of SAPO catalysts. SAPO's modified by the addition of transition metals (Mn, Co, Ni) showed interesting changes in selectivities and activities. Characterization of the metals using electron spin resonance (ESR) and SQUID magnetometry at West Virginia University, and XAFS spectroscopy at the University of Kentucky is in progress.

Synthesis of Hydrocarbons and Alcohols from Syngas

The production of mixed alcohols and hydrocarbons from synthesis gas was studied over Mo-Ni-K/C catalysts. The effect of reaction temperature, H_2/CO ratio, and contact time were investigated. Increasing the reaction temperature increases the space-time yield of both total alcohols and hydrocarbons. Decreasing the GHSV decreases the space-time yield of total alcohols and increases the space-time yield of hydrocarbons, indicating that short contact times favor production of alcohols, while long contact times favor formation of hydrocarbons. The H_2/CO ratio is a key- parameter to control the productivity of higher alcohols. Increasing the H_2/CO ratio increases production of methanol and decreases production of higher alcohols. Increasing the H_2/CO ratio also increases the space-time yield of hydrocarbons. Conversely, the increase in carbon monoxide concentration on the feed stream decreases the space-time yield of hydrocarbons and increases the productivity of total alcohols.

References:

1. N. Shah, D. Panjala, and G.P. Huffman, *Energy & Fuels,* **15** (2001) 1528-1534.
2. A. Makkuni, D. Panjala, N. Shah, and G.P. Huffman, *ACS, Fuel Chem. Div. Preprints,* **47(2)** (2002), to be published.
3. S. Zhang, Y. Zhang, J.W. Tierney and I. Wender, *Fuel Process. Technol.,* **69**, (2001) 59-71.
4. S. Zhang, Y. Zhang, J.W. Tierney and I. Wender, *Applied Catalysis A: General,* **193** (2000) 155-171.
5. X. Huang, C.W. Curtis, C.B. Roberts, *ACS, Fuel Chem. Div. Preprints,* 47(1), 150-153, (2002).
6. X. Huang, C.B. Roberts, "Supercritical Fluid Hexane Based Fischer-Tropsch Synthesis on a Cobalt Catalyst" submitted to *Ind. Eng. Chem. Res.* (2002).
7. N. Shah, F. E. Huggins, Sidharta Pattanaik, D. Panjala, and G. P. Huffman "XAFS and Mössbauer spectroscopy characterization of supported binary catalysts for non-oxidative dehydrogenation of methane", *Fuel Processing Technology*, special issue on C1 chemistry, in press, edited by Christopher Roberts.

Inside Fischer-Tropsch

L. Hou, Y. Zhang, G.D. Holder, J.W. Tierney and I. Wender
University of Pittsburgh

Although the mechanism of the Fischer-Tropsch synthesis (FTS) reaction has been extensively investigated for decades, it is still controversial due to its complexity. The principal objective of the present research is to investigate the FTS synthesis mechanism by addition of small probe molecules. Our initial experiments tested the effect of adding small molecules including vinyl ethers, epoxides and compounds containing a carbon-carbon triple bond to cobalt and iron-catalyzed FTS reactions. The most interesting results were obtained using acetylenic hydrocarbons; these are incorporated into FTS products yielding oxygenated products, mostly aldehydes and alcohols.. This finding led to the possibility of modifying the FTS synthesis to increase the amounts and types of oxygenated products, while helping to elucidate the mechanism of the synthesis. A major aim was to increase the amount of jet and diesel fuel while decreasing the emission of particle matter (PM).

We decided to pursue this research pathway since diesel engines are much more efficient than gasoline (spark-ignited) engines, but they emit large amounts of PM. It is known that the addition of oxygenates to diesel fuel from petroleum can significantly lower PM emissions. A study has been made[1] of the addition of various types of oxygen-containing compounds, including ethers, alcohols, carbonates, acetals and esters, to diesel fuel to determine their effects on exhaust emissions. The oxygenates were blended with diesel fuel in amounts needed to obtain an oxygen content of 7 wt%. However, just adding oxygenated compounds to diesel fuel has problems involving availability, toxicity, solubility, lubricity and biodegradability, among other properties.

The addition of acetylenic hydrocarbons to the FTS appears to be a way of modifying the synthesis so as to increase the amount of oxygenated products without addition of oxygenated compounds. This effect is of great interest. Acetylenes contain carbon-carbon triple bonds; carbon monoxide has a carbon-oxygen triple bond. Our research has led us to believe that the carbon-carbon triple bond in acetylenic molecules initiates the FTS reaction; the FTS synthesis then proceeds with addition of carbon monoxide and hydrogen (synthesis gas). It is possible that the formation of oxygenated FTS products upon addition of an acetylenic hydrocarbon proceeds via a homogeneously catalyzed reaction similar to the well-known hydroformylation (oxo)

$$\mathrm{R-CH_2=CH_2+CO+H_2\rightarrow R-CH_2-CH_2-CH_2OH} \quad + \quad \mathrm{R-CH_2-CH_2-CH_2OH} \quad (1)$$

$$\mathrm{CH_3}$$

synthesis[2] (Equation 1). Our approach to this research path was to investigate the addition of 1-

and 2-hexynes to both cobalt and iron catalyzed FTS reactions. Later reactions were carried out with additions of 1-heptyne and 1-decyne to the FTS.

Catalyst Preparation

Supported cobalt catalysts were prepared by incipient-wetness impregnation of cobalt nitrate on calcined (500ºC) γ-alumina. The catalyst with a composition of Co (10 wt%) and Al_2O_3 (90 wt%) was dried in air at 120ºC for 10 hours, followed by calcination at 300ºC for 5 hours. Before reaction, catalysts were activated in flowing hydrogen at 350ºC for 10 hours.

Our iron catalyst was obtained from Dr. B. Davis of the University of Kentucky. It was prepared by a precipitation method and had a composition of 100Fe/51Si/2.0Cu/50K_2O.

Experimental Reaction System

Experiments were carried out with the automatic reaction system shown below. Briefly, the apparatus consists of a gas supply, a fixed bed reactor, condensers and analysis by on-line G-C and off-line GCMS.

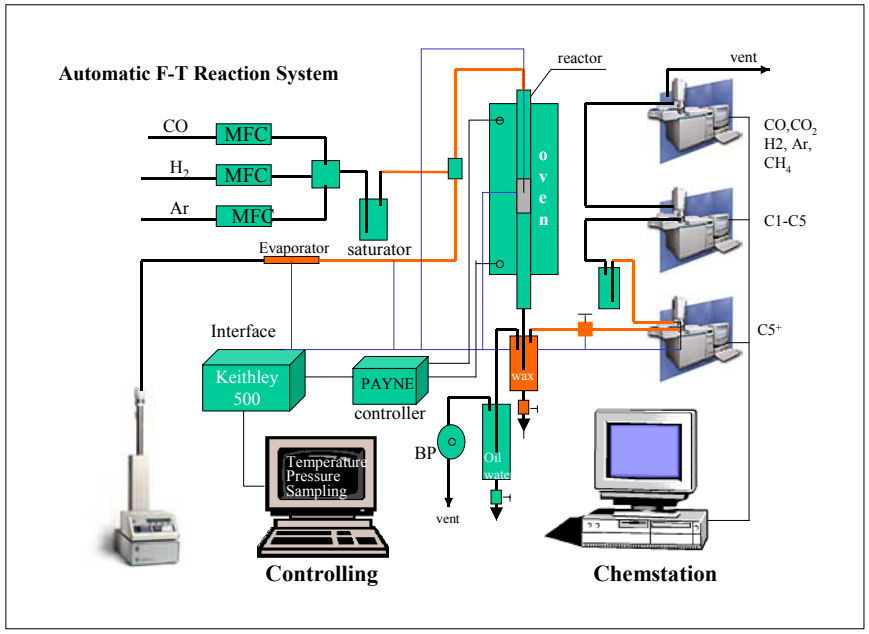

Schematic Diagram of Experimental Apparatus

Typically, 0.2 to 1 grams of catalyst were mixed with 1 gram of quartz. CO and H_2 were introduced into the reactor with a fixed ratio of 0.5 for cobalt and 1.5 for iron. Acetylenic compounds were added either by a saturator kept at 0ºC in an ice-water bath or by a syringe pump; the additives were dissolved in pentane. Thiophene was injected into the system with a micro syringe. Pyridine was added as a blend with 1-hexyne and pentane.

The first cooling trap was maintained at about 150˚C in order to collect higher boiling hydrocarbons which would be deposited in solid form in the cold trap. The second trap was held at 0˚C to separate liquid hydrocarbons. Liquid products were analyzed by GCMS. A small gas

flow withdrawn from the main stream behind the hot trap was analyzed by two on-line GCs to get the full spectra of carbon distribution and CO and H_2 concentrations.

Metals that are good FTS catalysts (Co, Fe, Ru) are able to dissociate the carbon monoxide molecule; metals that cannot dissociate CO (Cu, Pt, Pd) are methanol synthesis catalysts. Both CO and acetylenic compounds contains triple bonds. Our research has led us to conclude that the molecules with a carbon-carbon triple bond can initiate the FTS. We have found that FTS catalysts incorporate the C≡C entity as such, but it is possible that, like the CO molecule, dissociation of the carbon-carbon triple bond in acetylenes can occur to some extent. The bond dissociation energy of acetylene (230 kcal/mole) is slightly lower than that of carbon monoxide (257 kcal/mole).

We will first discuss the reaction of acetylenic compounds with a cobalt FTS catalyst. It is of interest that the FTS was discovered in early 1920s by Franz Fischer working with alkalized iron catalysts. However, the FTS was first operated commercially in Germany using cobalt catalysts during the 1935-1945 period. The standard catalyst was Co-ThO_2-Keiselguhr. However, cobalt was found to be too expensive so that these plants were then operated with cheaper iron catalysts. In 1955, in South Africa, SASOL started operation of a coal-based FTS plant using iron catalysts. Recently, there has been a large switch back to the use of cobalt catalysts in the FTS. This is due chiefly to the change in feedstock from coal, which yields synthesis gas with high CO/H_2 ratios on gasification, to natural gas (methane) which, on gasification, yields high H_2/CO ratios. Iron is a good water-gas shift catalyst; cobalt is not. ThO_2 was probably added to the old German cobalt catalyst to make the catalyst more tolerant to the presence of sulfur in the synthesis gas. Cobalt is more active than iron, and gives high yields of straight-chain alkanes and wax. Iron tends to yield more olefins and oxygenates than cobalt.

Experiments were carried out with a cobalt catalyst, with and without the addition of 1-hexyne. A GC analysis showed that the hexyne initiated the carbon chain; the C_7 peak, which includes hydrocarbons and oxygenates, is high, probably derived from 1-hexyne (Figure 1). The large C_{12} peak is due to dimerization of 1-hexyne. The presence of heptanol (Figure 2) is due to a type of hydroformylation reaction of hexyne adsorbed on the catalyst. Later results showed that addition of acetylenic compounds to both cobalt and iron catalyzed FTS gave C_7 aldehydes and C_7 alcohols, typical of the hydroformylation reaction of a C_6 olefin.

Carbon-carbon type bonds are readily adsorbed on the FTS catalyst when acetylenic hydrocarbons with chains longer than 1-hexyne are added to the FTS. The oxygen contents of the products decrease while the FTS products increase over the usual cobalt catalyzed FTS (Table 1).

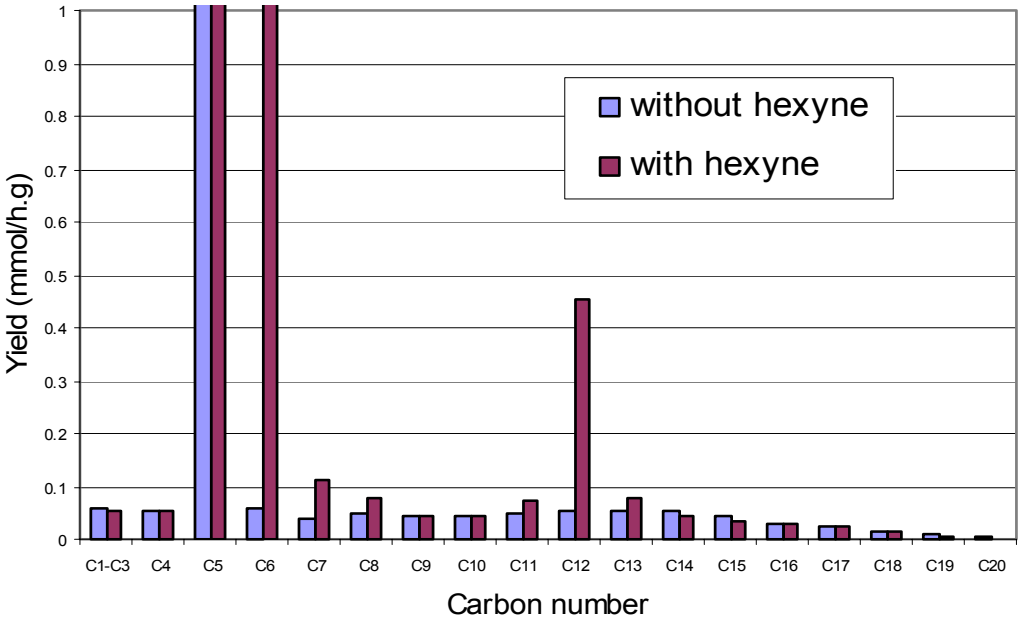

Figure 1. Product distribution with/without 1-hexyne on a cobalt catalyst at 220˚C. Co10Al90, H2/CO=2, P=100 psi, 1-hexyne in pentane (10% by volume) was added by a syringe pump with a flow rate of 2 ml/hr.

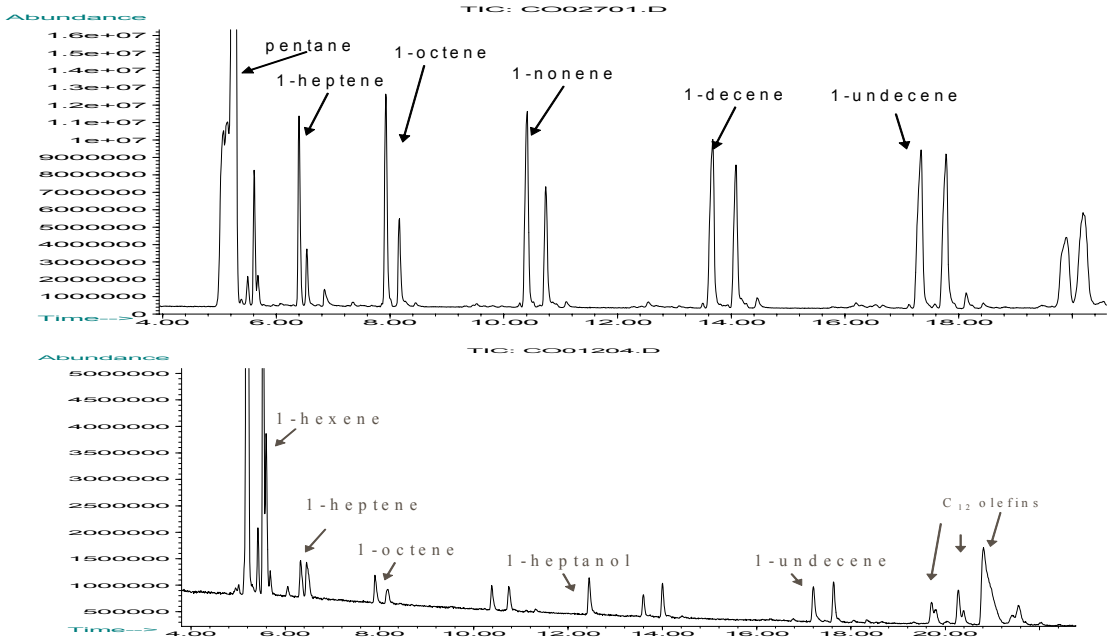

Figure 2 F-T product distribution without/with 1-hexyne addition on a cobalt catalyst Co10Al90, T=220C, P=100psi, H2/CO=2. Pentane or 1-hexyne in pentane (10% in volume) was added by a syringe pump with a flow rate of 2ml/h.

Table 1. Incorporation of Acetylenes with Different Chain Lengths		
Probe Molecule	Increase of Product Over Normal FTS	Oxygenate content
1-Hexyne	C7 197%	23%
1-Heptyne	C8 123%	18%
1-Decyne	C11 34%	2.5%

Co10Al90, T=220˚C, P=100 psi, $H_2/CO=2$.
Acetylenic compounds in pentane (10% by volume) were added with syringe pump 2 ml/hr.

The hydroformylmation reaction consists of the reaction of an olefin with synthesis gas to form aldehydes and alcohols. The reaction was discovered by Roelen[3] while he was studying the effect of added olefins to the FTS using a heterogeneous cobalt catalyst. Indeed, the hydroformylation reaction was first conducted in Germany as if it were a heterogeneous reaction but it was found necessary to add cobalt salts continuously to the reactor. It was found that the reactor was sometimes plugged by an orange-yellow substance that was identified as cobalt carbonyl ($Co_2(CO)_8$. Roelen recognized that the reaction was catalyzed by soluble cobalt carbonyls. It was later found[4] that the soluble $Co_2(CO_8)$ and cobalt hydrocarbonyl (HCo(CO)4) were the catalytic species or precursors for the hydroformylation reaction.

The hydroformylation of an olefin is shown below:

$$RCH=CH_2+CO+H_2 \rightarrow RCH_2CH_2CHO + RCH_2CHCHO$$
$$\qquad\qquad\qquad\qquad\qquad\qquad\qquad\qquad\qquad\qquad\qquad\quad |$$
$$\qquad\qquad\qquad\qquad\qquad\qquad\qquad\qquad\qquad\qquad\qquad\quad CH_3$$

+ the corresponding alcohols (2)

With cobalt, therefore, there is the possibility that a homogeneous reaction could take place concurrently with the FTS. Indeed, Pichler[5] stated that "the optimum condition of pressure and temperature for hydrocarbon synthesis on nickel, cobalt, iron and ruthenium are close to the condition at which formation of carbonyls and carbonyl hydrogen compounds can be detected. Pressure "requirements" for the catalytic synthesis and for carbonyl formation appear to be closely parallel in the case of metallic catalysts."

The following experiments were carried out on a cobalt catalyzed FTS to provide evidence that a hydroformylation reaction had indeed occurred. Since the FTS is easily poisoned by the presence of sulfur, thiophene was added to the reaction, in the presence of 1-hexyne, to poison the FTS. On the other hand, the hydroformylation reaction takes place in the presence of sulfur compounds with essentially no deactivation. The results of experiments of cobalt catalyzed FTS in the presence and in the absence of thiophene are shown in Figure 3. Thiophene poisons the FTS but the C_7 oxygenate peak is not affected; heptanal appears rather than heptanol because cobalt is a better hydrogenation catalyst than is iron.

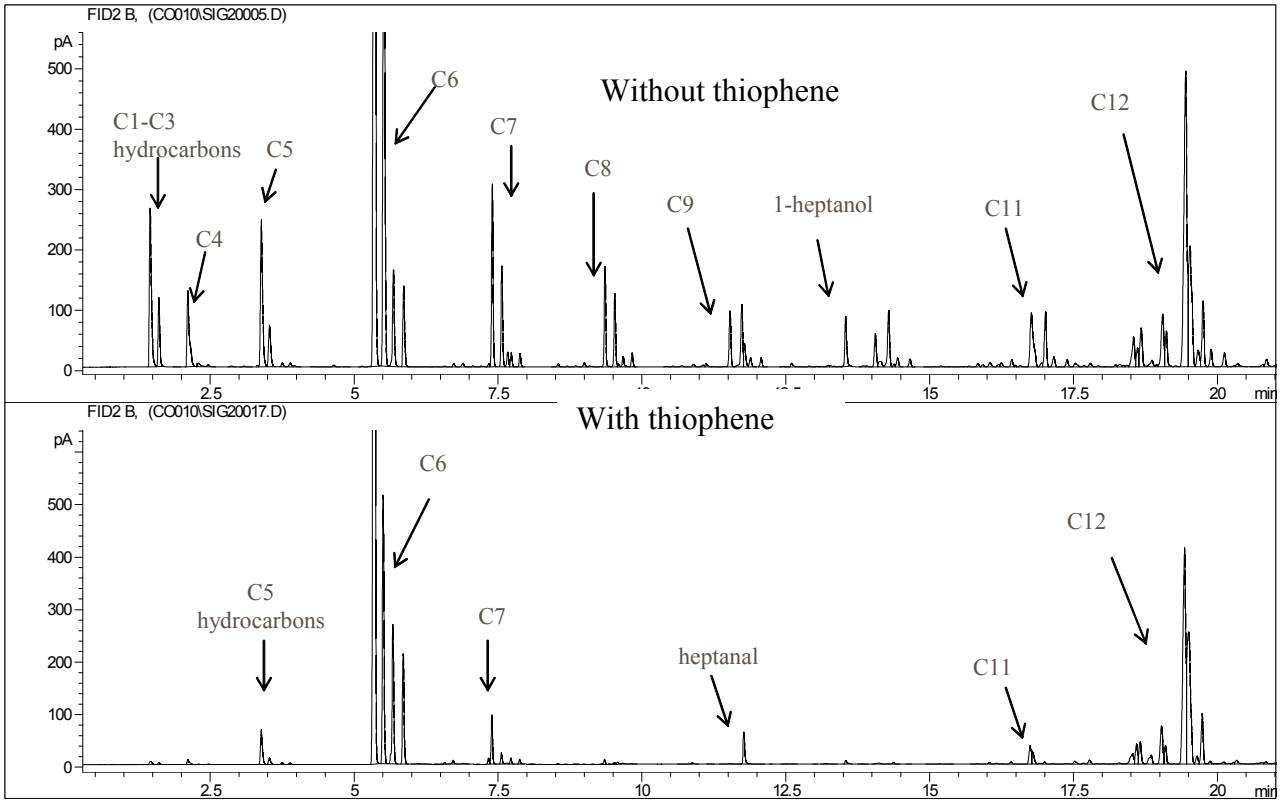

Figure 3 Effect of thiophene addition on a cobalt catalyst. Co10Al90, T=220C, P=100psi, H2/CO=2. 1-Hexyne was added by a saturator at 0˚C; 4.0 micro liters of thiophene were added in 28 hours

It is also possible, by addition of pyridine to the FTS, in the presence of 1-hexyne, to poison the hydroformylation reaction without significantly affecting the FTS. Without pyridine addition (Figure 4), the FTS reaction proceeds and the heptanol peak is present as before. Added pyridine reacts with the essential hydroformylation catalyst [6], $HCo(CO)_4$, which is a strong acid.

$$Py + HCo(CO)_4 \rightarrow PyHCo(CO)_4$$

Pyridine also reacts with cobalt carbonyls, so that the hydroformylation reaction does not occur.

Information about the mechanism of the FTS can be obtained by adding small amounts of a probe molecule, 1-hexyne in this instance, as shown in Figure 5. The acetylene molecule is adsorbed on a cobalt catalyst in the same way that an olefin would be adsorbed; the acetylenic molecules initiate the FTS, but a double bond remains on the adsorbed 1-hexyne. The hydroformylation reaction then takes place since cobalt carbonyls are present during the FTS.

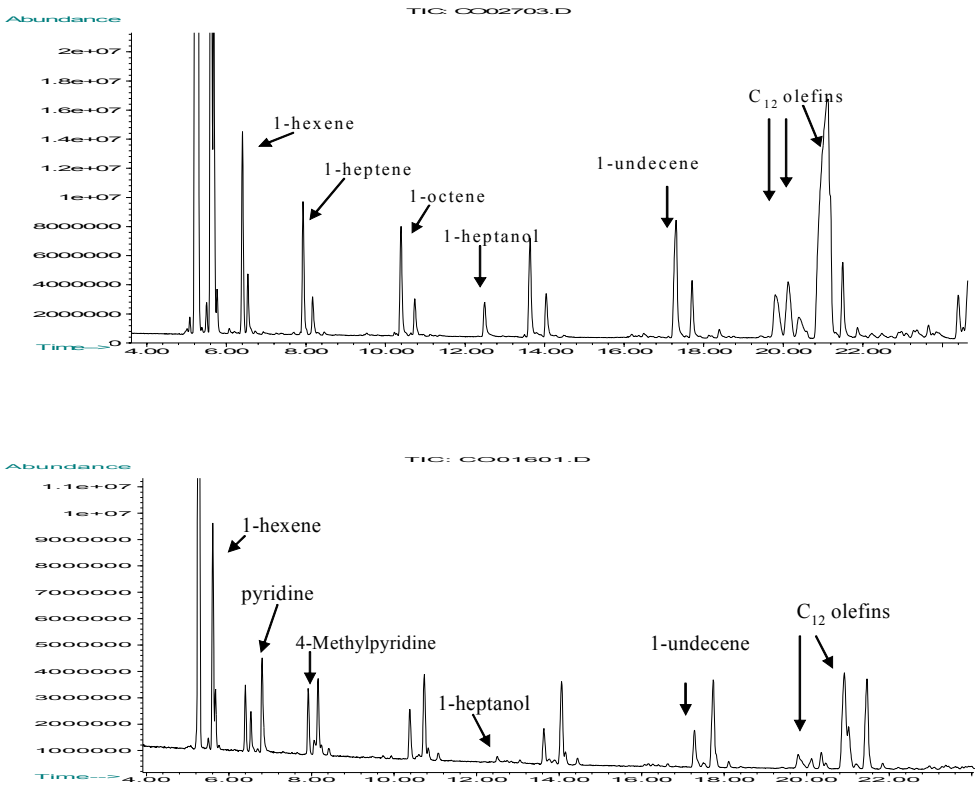

Figure 4 Effect of pyridine addition on a cobalt catalyst Co10Al90, T=220C, P=100psi, H2/CO=2, 1-hexyne: pyridine=1:1

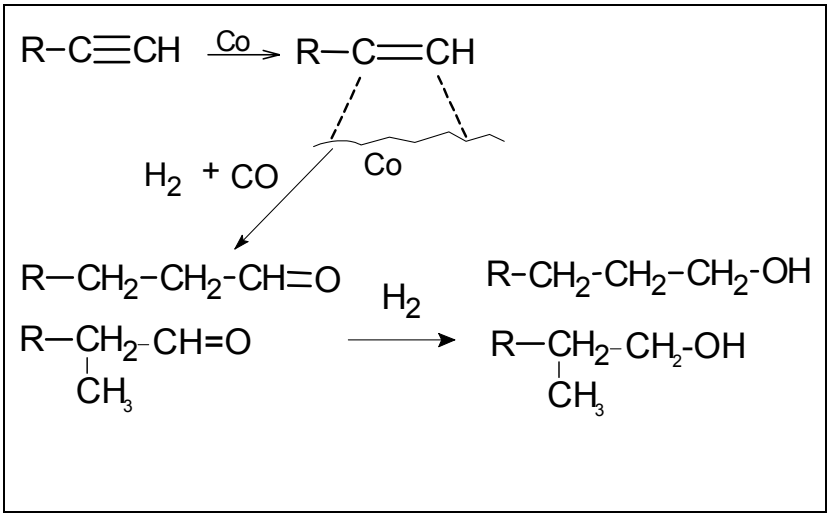

Figure 5 Possible mechanism of oxygenate formation with 1-hexyne addition on a cobalt catalyst

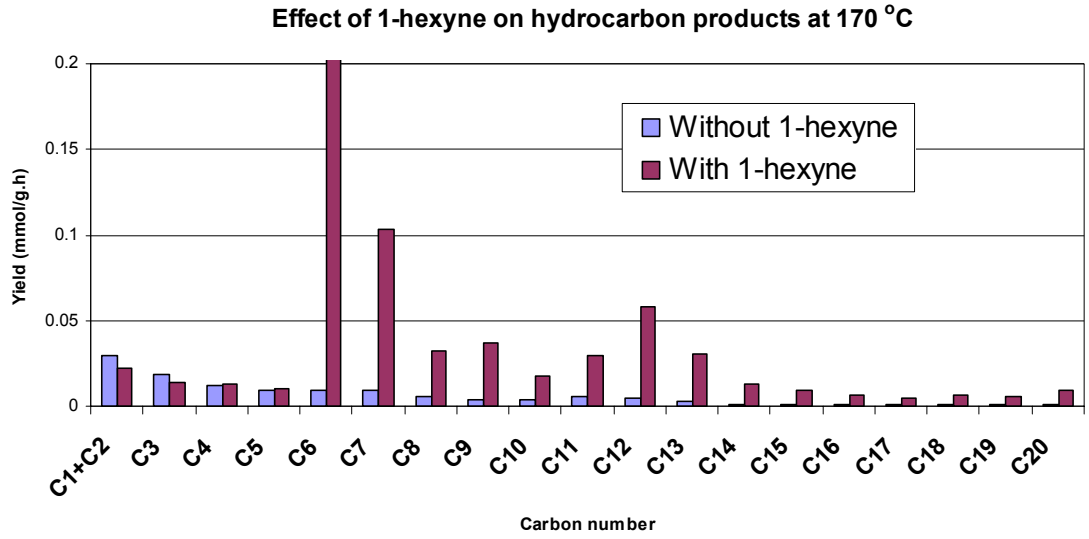

Figure 6 Product distribution of FTS synthesis without/with 1-hexyne on an iron catalyst 100Fe-5.1Si-2.0Cu-5.0K2O, T=170˚C, P=100psi, H2/CO=2/3, 1-hexyne was added by a saturator at 0˚C

The same type of reaction with acetylenic probe molecules is obtained with iron catalysts in the FTS. Adding 1-hexyne to the FTS on iron catalysts at 170°C greatly increases C_7 oxygenates and hydrocarbons (Figure 7). It clearly indicates that 1-hexyne initiates the FTS and produces C_7+ carbon chains. Typical liquid products of the FTS with addition of 1-hexyne are shown in Figure 8. Besides heptanol and heptanal, some C_7+ oxygenates are also produced.

Similar thiophene poisoning experiments were carried out with iron catalysts. It appears that iron catalysts at 170°C are much more tolerant to sulfur than are cobalt catalysts. With cobalt catalysts, 4 µl of thiophene deactivate the FTS; with iron catalysts, 250 µl of thiophene are needed to deactivate the catalyst. With iron catalysts, both the FTS and oxygenates are decreased (Figure 9).

The response to pyridine addition on iron catalysts is also different from that with cobalt catalysts. Pyridine does not decrease oxygenate formation on the iron catalyst (Figure 10). Similar results are obtained without or with pyridine addition. Unlike cobalt catalysts, methylpyridine could not be detected with the iron catalyst, indicating that there are not many CH_x intermediates to be scavenged by pyridine.

We have also incorporated 2-hexyne into the FTS on an iron catalyst. Branched hydrocarbons and branched oxygenates are produced in addition to normal hydrocarbons and oxygenates. This shows that the initial position of the triple bond in the acetylenic compounds is very important. When the carbon-carbon triple bond lays down on the surface of the catalyst, it may isomerize to produce terminal intermediates and produce normal products, or start the reaction at the internal triple bond and produce branched products.

It is well known that the FTS on iron catalysts produces more oxygenates than are obtained with cobalt catalysts. There is little doubt that formation of oxygenates on cobalt catalysts may result

from a hydroformylation reaction via a homogeneous mechanism. Formation of oxygenates on iron catalyst are likely heterogeneously catalyzed. Oxygenates appear to be intermediates on iron catalysts. The cobalt mechanism probably involves propagation via CH_x intermediates.

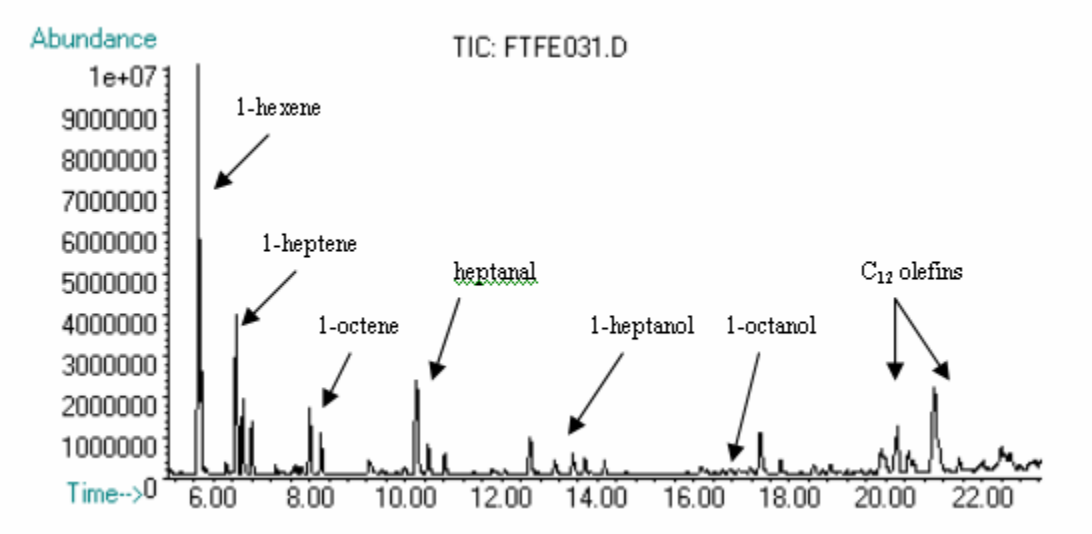

Figure 7. GC-MS of FTS products with 1-hexyne addition on an iron catalyst 100Fe-5.1Si-2.0Cu-5.0K2O, T=170˚C, P=100psi, H2/CO=2/3, 1-hexyne was added by a saturator at 0˚C

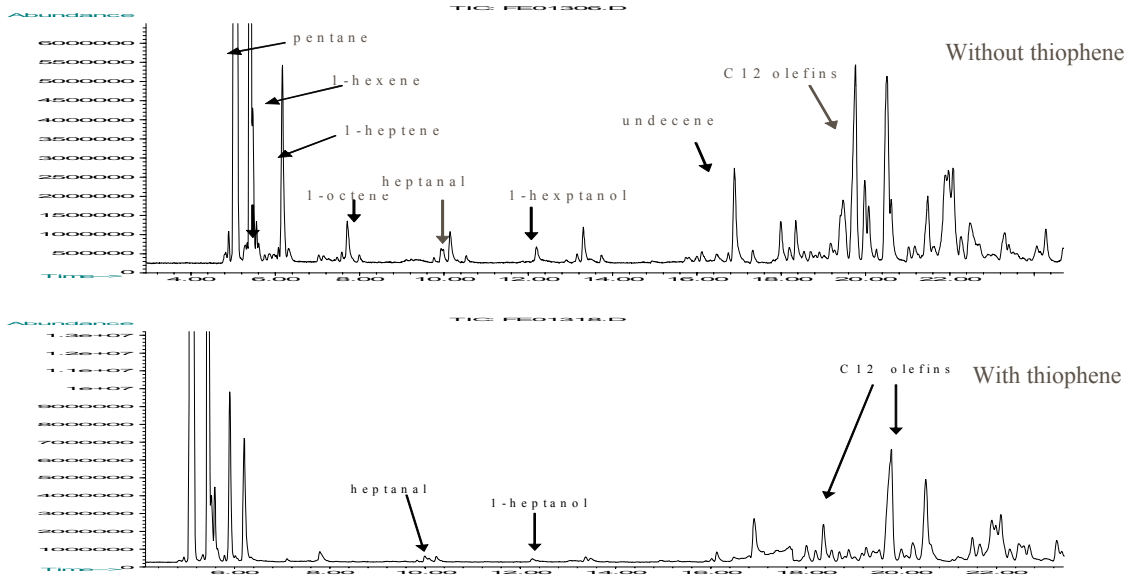

Figure 8. Effect of thiophene addition on an iron catalyst. 100Fe-5.1Si-2.0Cu-5.0K_2O, T=170˚C, P=100 psi, H_2/CO=2/3, 250 micro liters of thiophene were added in 54 hours.

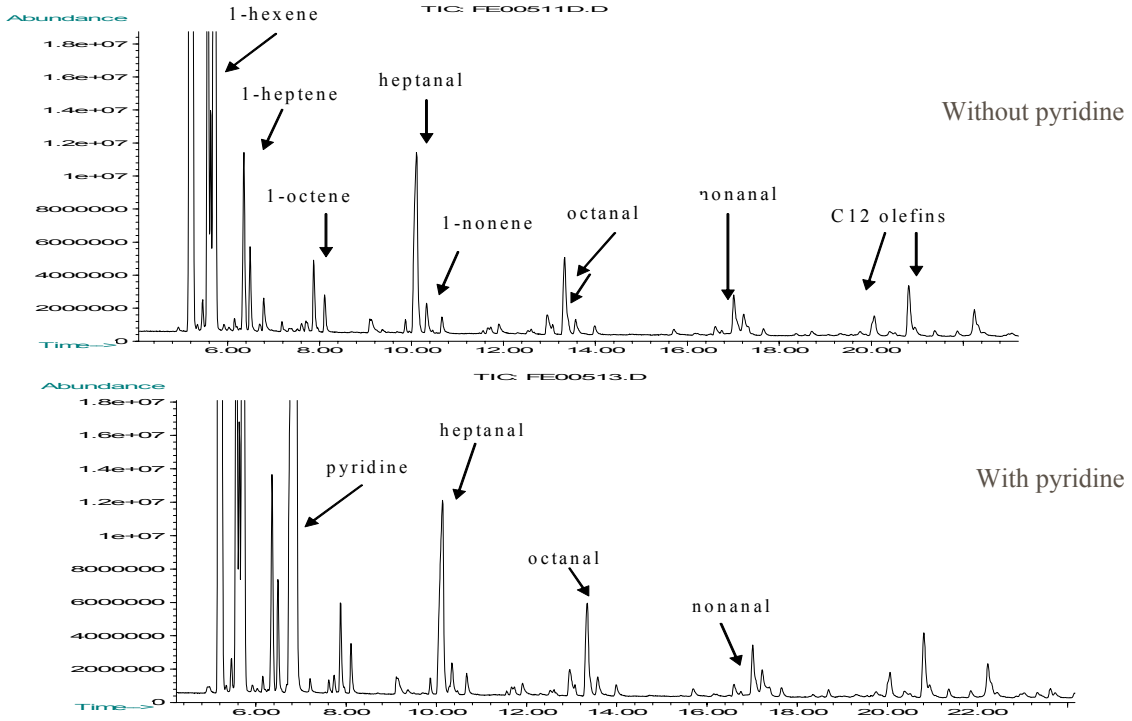

Figure 9. Effect of pyridine addition on an iron catalys. 100Fe-5.1Si-2.0Cu-5.0K_2O, T=170˚C, P=100 psi, H2/CO=2/3, 1-hexyne: pyridine=1:1

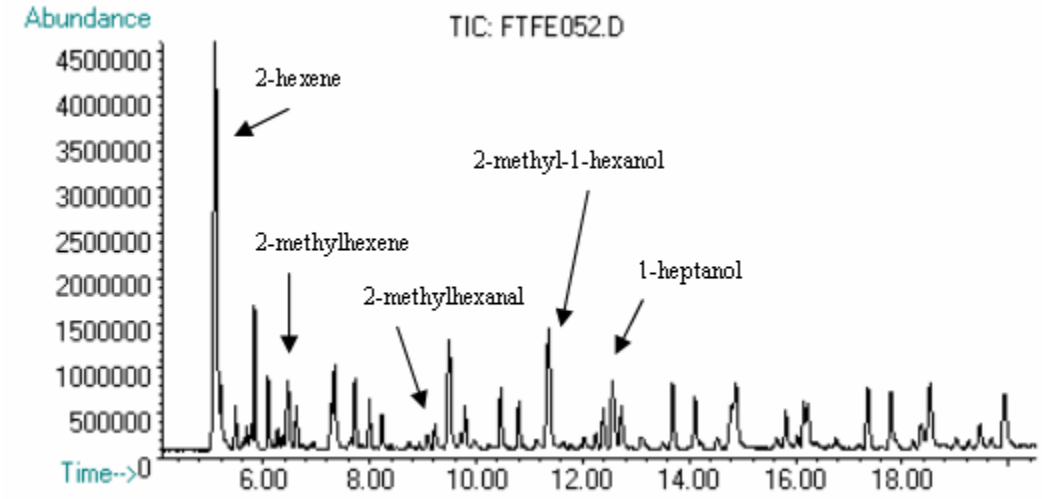

Figure 10. GC-MS analysis of FTS products with 2-hexyne on an iron catalyst. 100Fe-5.1Si-2.0Cu-5.0K_2O, T=170˚C, P=100 psi, H_2/CO=2/3, 2-hexyne was added by a saturator at 0˚C.

Conclusions

Addition of acetylenic hydrocarbons as probe molecules to the FTS has revealed that a homogeneous hydroformylation reaction can take place with both cobalt and iron catalysts. Although both acetylenes and CO contain triple bonds, the acetylenic molecule is adsorbed more rapidly on the catalyst surface and initiates the FTS. Addition of sulfur to the FTS, in the presence of 1-hexyne, poisons the reaction, especially with the cobalt catalyst but does not affect the hydroformylation reaction. Addition of pyridine to a cobalt-catalyzed FTS, again in the presence of 1-hexyne, poisons the hydrformylation reaction without affecting the FTS. The latter two reactions, addition of sulfur and pyridine, have little effect on an iron-catalyzed FTS. Cobalt-catalyzed FTS evidently proceeds by addition of CH_x units to a growing chain. It is likely that iron-catalyzed FTS involves a different mechanistic path, one proceeding via oxygenated surface intermediates.

Knowledge gained by addition of probe molecules to the FTS will lead to a better understanding of the FTS mechanism and provide a basis for the design of FTS catalysts tailor made to produce specific transportation fuels.

References

[1] D.W. Naegeli, S. Moulton, B.C. Owens and E.A. Frame, "Oxygenates for Advanced Petroleum-Based Diesel Fuels," Interim Report, Southwest Research Institute, February, 2001.
[2] P. Pino, F. Piacenti and M. Bianichi, "The Hydroformylation (OXO) Reaction" in *Organic Syntheses via Metal Carbonyls*," edited by I. Wender and P. Pino, John Wiley & Sons, p. 233-296, 1975.
[3] O. Roelen, German patent 849,548 (1938); Chem Zentr, 1953, 1953, p 297; U.S. Patent 2,317,066,(1943).
[4] I. Wender, H.W. Sternberg and M. Orchin, *J. Am. Chem. Soc.*, **75**, 3043 (1953).
[5] H. Pichler, *Advances in Catalysis 4*, 336 (1952).
[6] L. Hou, Y. Zhang, J.W. Tierney and I. Wender, "Acetylenic Molecules as Probes in Fischer-Tropsch Reactions," Pittsburgh-Cleveland Catalysis Society Spring Meeting, May 10 (2002).

Application of Supercritical Fluids as Reaction Medium for Fischer-Tropsch Synthesis

Xiwen Huang, Nimir O. Elbashir, Christopher B. Roberts
Auburn University

Introduction

Fischer-Tropsch synthesis (FTS) holds great potential for the alternative production of ultra-clean transportation fuels, chemicals, and other hydrocarbon products through the conversion of readily available syngas (CO/H_2) resources. The syngas can be produced from a variety of carbon-bearing feedstocks including natural gas, coal, and biomass through gasification and reforming technologies. FTS results in high quality petroleum products that can be further processed to specific boiling-point fractions. Of special interest is the FTS derived diesel fuel fraction for its desirable characteristics including very low sulfur and aromatic content, high cetane index, and the fact that it is exceptionally clean burning in a compression-ignition engine.

Supercritical fluids (SCFs) offer several advantages over traditional solvents as reaction media for catalytic reactions including the ability to manipulate the reaction environment through simple changes in pressure to enhance solubility of reactants and products, to eliminate interphase transport limitations, and to integrate reaction and separation unit operations. Supercritical fluid solvents offer attractive physical properties including; low viscosity and high diffusivity resulting in superior mass transfer characteristics; low surface tension enabling easy penetration into the pores of a solid matrix (catalyst) for extraction of nonvolatile materials from within the pores; high compressibility near the critical point inducing large changes in density with very small changes in pressure and/or temperature enabling separation of the dissolved material easily and completely. The unique properties of SCFs can be exploited in various ways for the design of heterogeneous catalytic reaction systems. As a result, several classic industrial processes are conducted under SCF conditions such as ethylene polymerization, ammonia synthesis and methanol synthesis.

The advantages of utilizing a supercritical hexane (ScH) phase over traditional gas-phase and liquid-phase reactions in the FTS were initiated by Fujimoto and coworkers[1]. They concluded that the supercritical phase FTS reaction offers rapid transportation of reactants and products within the catalyst bed and pellets, efficient heat transfer and in situ wax extraction. Burkur, et al.[2,3] studied the effect of process conditions on olefin selectivity in conventional and supercritical propane FTS. They observed that the total olefin and 2-olefin selectivity were essentially independent of reaction temperature but changed significantly from the conventional operation to supercritical operation. Subramaniam et al.[4,5] exploited the pressure-tunable density and transport properties of the near-critical hexane reaction medium. They observed that isothermal pressure tuning from 1.2-2.4P_c in the supercritical region could enhance the catalyst effectiveness factor through alleviation of pore-diffusion limitations at higher pressure, which results in significant improvement in syngas conversion and product selectivity. Davis, et al.[6] studied the SCF-FT reaction using an unpromoted Co/SiO_2 catalyst, and a pentane-hexane mixture as the supercritical solvent. They found the supercritical phase F-T reaction can significantly inhibit the deactivation of the catalyst due to the extraction of heavy hydrocarbon products from the catalyst pores possibly improving the heat transfer inside the reactor.

Roberts, et al.[7-10] reported the FTS reaction activity and the product distribution of 15% Co-0.5% Pt/ Al_2O_3 at 250 °C. Supercritical hexane (ScH) was used as reaction medium and the pressure of the reaction in the ScH phase was varied from 35 bar up to 80 bar. We also showed a comparison between the ScH-FTS reaction and that in gas-phase at the same temperature and at syngas partial pressure of 20 bar. Steady state operation was quickly achieved under ScH-phase conditions and the overall product distributions obtained were quite constant over extended periods of operation (over 40 hr). Our results showed that the reaction in the ScH gave slightly higher syngas conversion with lower (40% less) selectivity towards light hydrocarbons (e.g. methane). As a result of enhanced solubility in the ScH media the selectivity towards the 1-oelfins (C_7-C_{20}) is always higher than in gas phase reaction. Over the experimental range of pressure studied in the ScH we reported an interesting result that there is the existence of an optimum pressure (65 bar) whereby maximum conversion and olefin selectivity were obtained. This has been attributed to the fine balance between the bulk diffusion of reactants and products and the pore diffusion at catalyst active site.

Research Objective

The objective of our project is to establish optimum operating conditions for FTS within the supercritical region itself and to investigate the product selectivity alteration when the FTS is operated in a SCF medium vs. a liquid or gas medium. We are also evaluating the feasibility of maintaining catalyst activity by continuous in situ extraction of products with the SCF medium. We plan to establish an optimum method to increase the selectivity to desired products such as diesel and high-octane gasoline to improve the economics of the FTS. One of our objectives is also to develop a kinetic model and mechanism for the FTS in supercritical fluid medium that will assist the optimization of the reaction conditions towards the desired products.

Recent work

FTS under the ScH conditions was examined in our continuous high-pressure reactor by employing traditional promoted Co catalysts (15%Co-0.5%Pt/Al_2O_3). The reaction was also studied in gas phase under the same conditions. The catalyst activity (CO conversion), product (olefins, and paraffins) distributions, and the temperature profile in the catalyst bed were measured for both the ScH phase and gas-phase reactions. The effect of tuning the pressure of the ScH phase on CO conversion, olefin selectivity, and product distribution was also evaluated. We are currently studying the effect of reaction temperature on the activity and selectivity for the reaction in the ScH. The effect of residence time was also examined by varying both the syngas flow rate and the total operating pressure of the system. A kinetic model describing the mechanism of the reaction in the supercritical fluid is currently under development by our group. This model will be used to determine the reaction constants and parameters and will be compared to those measured experimentally.

Experimental

Reactor Design

The reactor (1.27 cm×2.5.4 cm; effective volume: 32 cm^3; High Pressure Company) used in this study is a conventional down flow fixed bed reactor. A 15mm (diameter), 2-3mm(thickness) and 4-15micron (porosity) fused quartz disc (Quartz Plus, Inc.) is fixed in the middle of the reactor to establish the cobalt catalyst 15%Co-0.5%Pt/Al_2O_3 (United Catalyst Inc.) in its position. In order to position the disc in the middle of the reactor, the inner diameter of the reactor above the disc

was machined exactly to match the disc diameter, which is a little larger than the diameter of the section underneath the disc. The quartz disc was employed to avoid the use of any Fe-containing metal near the reaction zone. An 1/8" (0.318 cm) diameter hole was machined in center of the quartz disc to allow insertion of the profile thermocouple with 6 equally-spaced (3.63 cm) probes (OMEGA) along the reactor length (see Fig 1). This profile thermocouple allows axial tracking of the temperature distribution in the reactor.

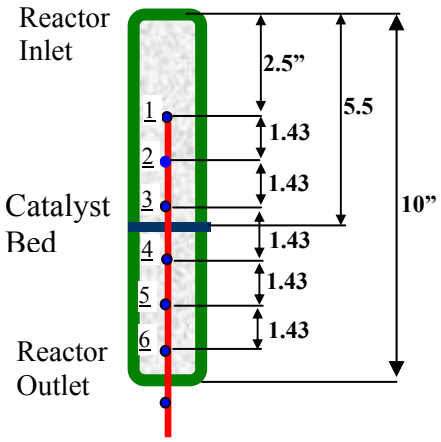

Fig. 1: Profile thermocouple location along the reactor

Reactant Delivery, Reaction and Analysis System

The flowrate of the syngas and nitrogen (internal standard) gas mixtures (Air Product) is controlled by the mass-flow controller (Brooks 5850E) and the solvent hexane is delivered through the HPLC pump. The hexane and syngas are combined in a static mixer (OMEGA) before entering the reactor, where the high temperature results in a supercritical hexane phase. The reactor is situated in a furnace with a programmed temperature controller system. The reaction pressure is controlled by a back pressure regulator (Tescom Inc.) located between the reactor and a hot trap. After leaving the reactor, the products pass through a hot trap (200 °C) to condense some heavy components prior to sampling into the on-line GC analysis. All lines between the reactor outlet and the GC are heated to 200 °C preventing product condensation. Two GCs are used in the analysis system. A Varian 3300 GC with a capillary column (DB-5) and an FID was used for the analysis of C2-C30 hydrocarbons and oxygenates. The overall experimental apparatus is shown in Fig. 2.

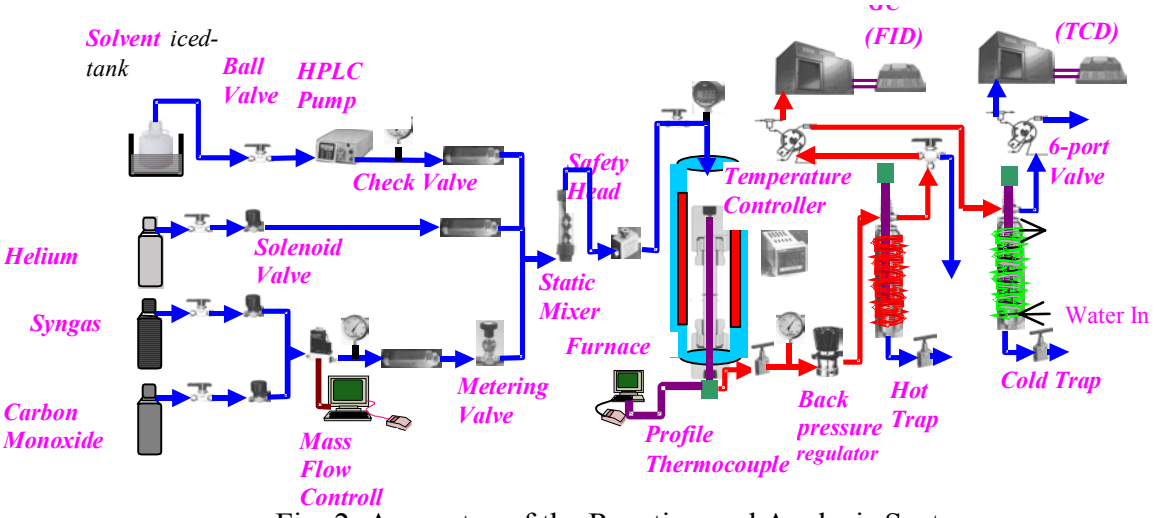

Fig. 2: Apparatus of the Reaction and Analysis System

The reaction conditions employed in our experiments are shown Table 1.

Table 1. The reaction conditions for the FTS reaction in the ScH and in the gas-phase.

Reactor	Fixed bed: 1.27cm(0.5in)*25.4cm(10in) with an effect volume:32 cm^3
Catalyst	15%Co-0.5%Pt-Al_2O_3
Solvent	Hexane (Pc=29.7bar, Tc=233.7°C); Flowrate:1.0 ml/min
Syngas	Space velocity: 50 sccm/g cat, and 40 sccm/g cat ; Ratio: H_2/CO: 2.0
Pretreatment	Reducing gas type: CO; Flowrate: 50sccm Time: 20 hr; Temperature, Pressure: 280°C, 1atm.
Reaction Condition	Temperature: 250°C; Pressure: varied between 35 bar to 80 bar, while for the gas-phase the pressure is 20 bar. Time: until steady state is achieved and kept at steady state for at least 24h

Results and Discussion

CO conversion and catalyst activity

Since the reactants (syngas) mass transport and the product bulk diffusion rates are higher in the gas phase than in the supercritical phase, it might be expected that a higher syngas conversion would be obtained under gas phase FTS. However, the experimental results presented in Fig. 3 show a considerably higher CO conversion under supercritical phase operation (up to 80%) relative to the gas phase reaction (up to 60%). The SCH phase experiment presented in Fig. 3 was performed at a total pressure of 80 bar while the gas phase reaction was performed at 20 bar in the absence of any hexane solvent. The 20 bar pressure in the gas phase was used to achieve the same partial pressure of syngas compared to the supercritical phase experiment at 80 bar. Steady state operation was achieved more rapidly under SCF-FTS than in gas phase FTS.

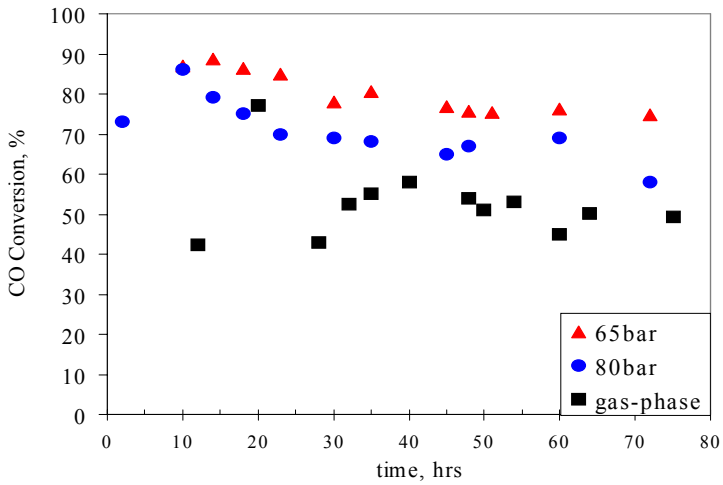

Fig. 3: CO conversion in gas phase and supercritical phase FTS (Temperature: 250°C; Pressure (SCF Phase): 65 bar, 80 bar; Syngas Partial Pressure (Gas Phase): 20 bar; Hexane flowrate: 1ml/min; syngas flowrate: 50sccm/g cat; syngas ratio (H_2/CO): 2/1)

Under the ScH phase FTS, the formation rate of heavy products and coke precursors is balanced by their removal rate as a result of the liquid-like solubility and in-situ extractability of the supercritical medium[9]. The rapid desorption of the extracted and dissolved heavy hydrocarbons effectively creates more vacant reactive sites available to the reactants.

Product Distribution

The products from FTS often involve a wide distribution of C1-C40 hydrocarbons and oxygenates depending on the reaction conditions and catalysts. If the hydrocarbon chain is formed stepwise by insertion or addition of C1 intermediates with a constant chain growth probability, then the chain length distribution is described by the Anderson-Schulz-Flory (ASF) law. The ASF distribution implies that the chain propagation and termination probabilities are independent of carbon number[11]. However, FTS on both iron and cobalt catalysts often shows a marked deviation from the ASF law, as observed in many publications[12-17]. In Fig. 4a, we showed the comparison of the product distribution in gas/SCF phase FTS. The experimental data exhibits the so-call double value phenomenon (non-ASF distribution). We can observe the appearance of an obvious shoulder around C7 indicating two chain growth probability α values under both gas phase and SCF FTS. For the light products ($n<7$), no significant difference of the α value (α =0.71) was observed in either gas phase or SCF phase. However, for those heavy products ($n>10$), the α value (α =0.87) is larger in SCF phase than in the gas phase process (α =0.75). This result demonstrates that the SCF-FTS process more favors the heavy compound production than the gas phase process. There are various theoretical explanations for this deviation[12, 18-20]. One of the well-recognized explanations for this deviation is the diffusion-enhanced readsorption of 1-alkene model provided by Iglesia and Madon[21-23]. This model describes that diffusion limitations within the liquid-filled pores slows down the removal of 1-alkenes which causes an increase of their residence time within the catalyst pores. From Fig. 4b, we can clearly see that the product distribution shifts to higher carbon number in SCF-FTS, although they have similarly shaped distributions including a decline in hydrocarbon content at

the higher carbon numbers. Furthermore, the undesirable production of methane can be significantly reduced under SCF operation.

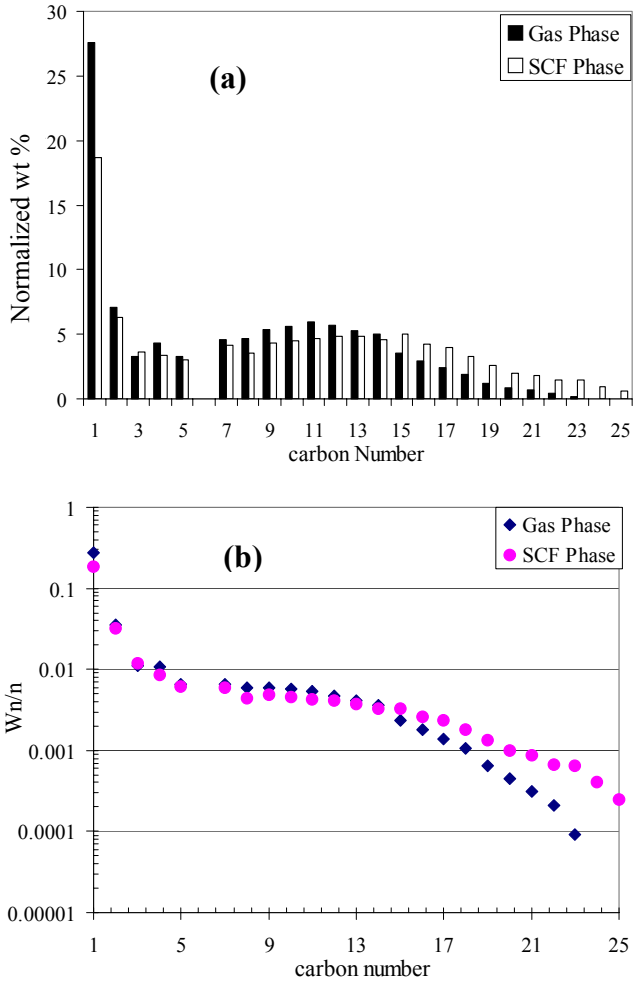

Fig. 4a,b: Product Distribution in gas-phase and ScH phase (Temperature: 250°C; Pressure (SCF Phase): 80bar; Syngas Partial Pressure(Gas Phase): 20 bar; Hexane flowrate: 1ml/min; syngas flowrate: 50sccm/g cat; syngas ratio (H_2/CO): 2/1)

α-Olefins content

α-Olefins are very important chemical intermediates for a number of industrial and consumer products. Significant economic benefits can be achieved by increasing the α-olefins selectivity of the raw FTS products and thus reducing the cost of product separation. Based on thermodynamics arguments, Anderson and coworkers concluded that α-olefins and oxygenates were the primary products of the FTS reaction[24].

We examined differences between the olefin selectivities in the gas phase and supercritical phase processes (Fig. 5), from which we can observe significantly higher olefin selectivity in ScH-FTS than in the gas-phase process for products with carbon numbers greater than 7. For light compounds, there is no significant difference in the olefin selectivity between the SCF and gas phase processes. Olefin content decreases with an increase in carbon number at a much slower rate in the supercritical phase than in the gas phase FTS resulting in significantly higher olefin

production. For example, within the carbon number range of 10 to 15, the olefin selectivity decreases only slightly, with olefins representing at least 65% of the hydrocarbon products at each of these carbon numbers. In these experiments, we observed little 2-olefin formation in either gas phase or supercritical phase.

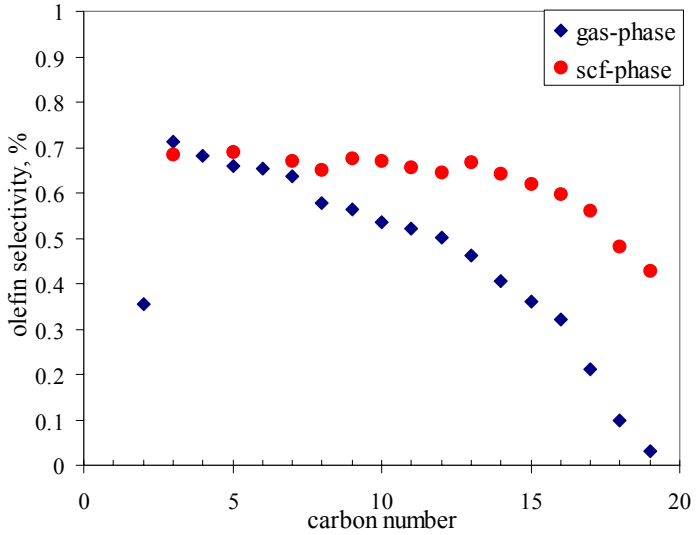

Fig. 5: Olefins Selectivity in ScH phase and gas-phase reaction (Temperature: 250^{o}C; Pressure(SCF Phase): 80bar; Syngas Partial Pressure(Gas Phase): 20 bar; Hexane flowrate: 1ml/min; syngas flowrate: 50sccm/g cat; syngas ratio (H2/CO):2/1)

Temperature Profile

Supercritical fluid posses significantly higher thermal conductivity than corresponding gases and consequently heat transfer is enhanced in this medium. The FTS process is highly exothermic resulting in local overheating on the catalyst surface. If the heat transfer process is low on the catalyst surface, then more undesired light compounds (such as methane) will be formed coupled with possible catalyst deactivation.

We investigated the temperature profile along the length of the reactor during ScH-FTS and gas-phase FTS (Fig. 6). Under steady-state operation, the temperature distribution along the reactor is significantly flatter in the supercritical phase comparing to gas phase suggesting that the SCF medium does a much better job in distributing the generated heat. The maximum temperature deviation along the reactor in the supercritical phase is around 5^{o}C compared to 15^{o}C in the gas-phase. It should be noted that the CO conversion in the SCF phase was 70% where the conversion in the gas phase was only 50%. Therefore, the results would be even more dramatic had the conversions been matched. These data suggest that heat transfer in the SCF-phase is more effective than in the gas-phase and is close to that in the liquid-phase.

Pressure Effect on Conversion

Fig. 7 presents the influence of pressure on the syngas conversion in the SCF-FTS process. From these results, we observe that the syngas conversion increases with increases in pressure from 35 to 41 to 65 bar. As the pressure is increased within this range, the hexane medium possesses increasingly liquid-like density which enables enhanced extraction of heavy

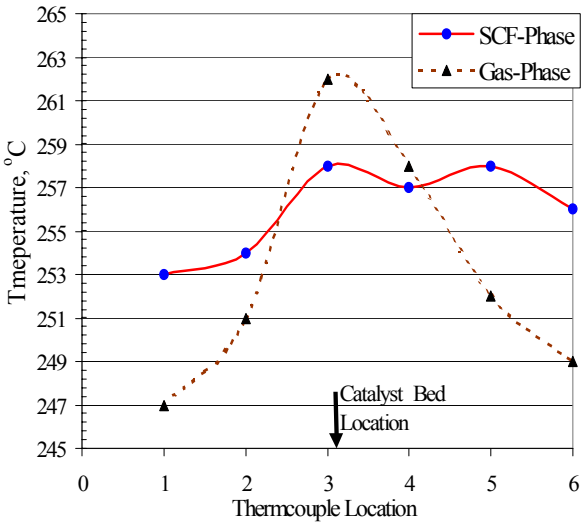

Fig. 6: Temperature distribution in gas/ ScH Phases along the length of the reactor (see Fig. 1).

hydrocarbons. This enhanced extraction maintains wider catalyst pore channels, reduces pore diffusion limitations, and increases the availability of reactive sites. This favors greater CO and H_2 absorption onto reactive sites thereby increasing CO conversion. This result in the range of 35 to 65 bar suggests that the SCF-FTS process is not externally diffusion controlled. If this process were externally diffusion controlled the CO conversion would decrease with increases in pressure since the bulk diffusivity decreases with increasing pressure. However, when the pressure increases beyond a certain point (in our case 65 bar), the syngas conversion begins to decrease with further increases in pressure. This is due to significant decreases in bulk diffusivity at very high pressures. Beyond an optimal pressure, the negative influence of the

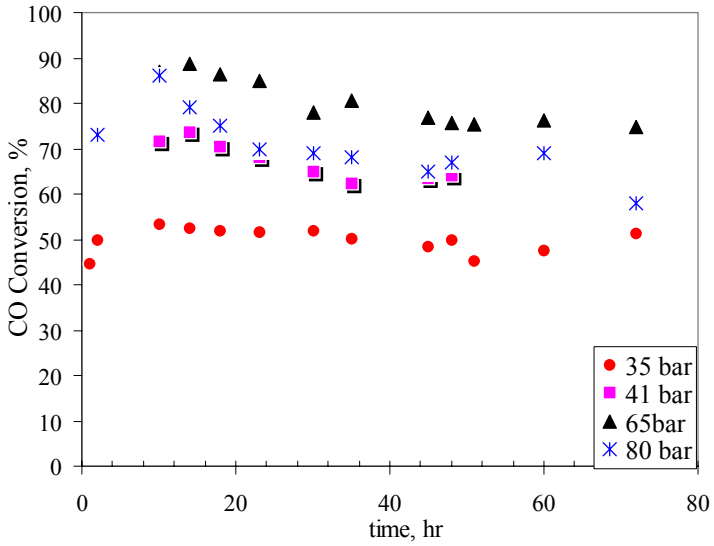

Fig. 7: Pressure effects on syngas conversion in ScH phase (Temp.: 250°C; Pressure: 35 bar, 41bar, 65bar, 80bar; Hexane flowrate: 1ml/min; syngas flowrate: 50sccm/g cat; syngas ratio (H_2/CO): 2/1).

decreasing bulk diffusivity may outweigh the positive enhancement in heavy product extractability and enhanced pore diffusion at high pressures.

Pressure effect on the 1-olefin selectivity

The effect of pressure on the olefin selectivity is presented in Fig. 8. With an increase in pressure from 35 to 65 psi the olefin content increases particularly in the carbon number range of C3 to C15. Again, as the pressure is further increased from 65 to 80 bar the 1-olefin content decreased within this C3 to C15 range. Therefore, olefin selectivity exhibits a maximum with respect to operating pressure similar to the observed maximum in CO conversion at intermediate pressures.

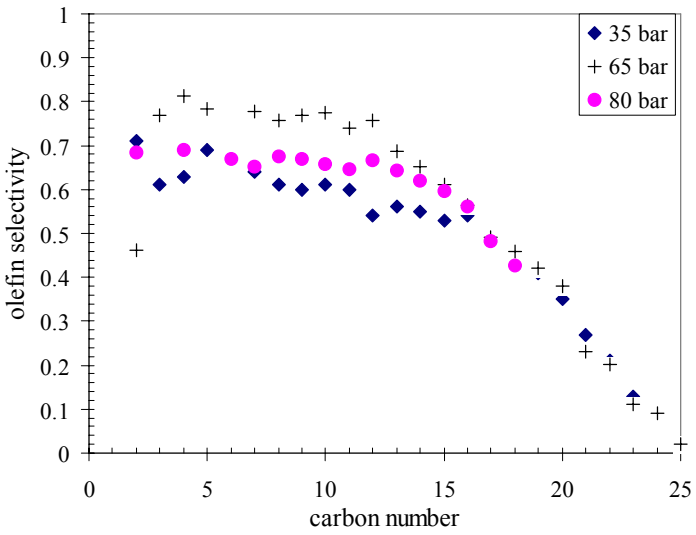

Fig. 8: Pressure effects on olefin selectivity (Temperature: 250°C; Pressure: 35 bar, 65bar, 80bar; Hexane flowrate: 1ml/min; syngas flowrate: 50sccm/g cat; syngas ratio (H_2/CO): 2/1)

Production Distribution

Fig. 9 exhibits the pressure tuning effects on the product distribution. For the light compounds (n<=8), we can observe there is no obvious effect of the pressure on the chain growth probability with an □value ca. 0.71 (greater than C10) at 35bar, 65 bar, and 80 bar. However, for heavy compounds, the pressure tuning effects gradually become more significant based on the difference in the α values: 0.83 (35bar), 0.90 (65bar) and 0.87 (80 bar). This result demonstrates that increasing pressure moderately helps the production of more long chain compounds.

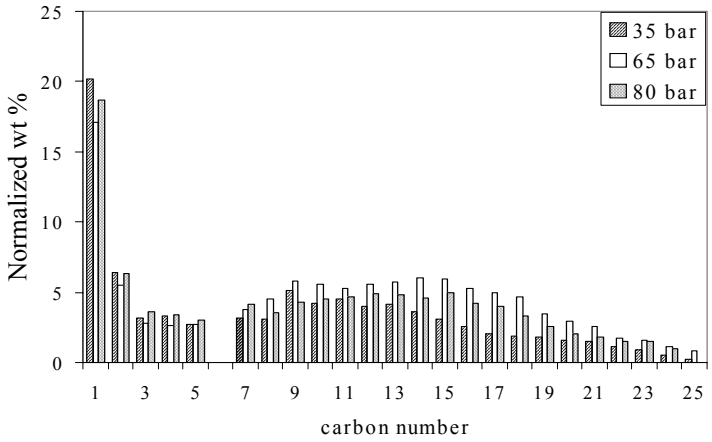

Fig. 9 Pressure-tuning Effects on the hydrocarbon product distribution

Future Plan

- ★ Perform detailed SCF-FT reaction studies on traditional Fe and Co catalysts in the SCF solvents: propane, n-pentane, hexane, and mixtures of these solvents at temperatures up to 300oC and pressures up to 200 bar. Analyze reaction products to determine the effect of the reaction parameters and catalysts. A variety of solvent/syngas flowrates and feed compositions will be explored.
- ★ A kinetic model describing the mechanism of the reaction in the supercritical fluid is currently under development by our group. This model will be used to determine the reaction constants and parameters that will be compared to those measured experimentally.
- ★ We are currently working on the design of slurry bubble reactor (SBR) using one liter Parr reactor to study and to compare the FTS reaction in liquid phase to the measured reaction performance in gas phase and SCF.
- ★ A variety of catalyst materials will be examined including traditional iron and cobalt based catalysts.
- ★ Perform comparative studies of FT reactions (with the catalysts of interest here) under liquid and gas phase conditions in order to make comparisons of the syngas conversion, product selectivity, reaction rates and catalyst activity in SCF, liquid, and gas phase media.
- ★ In addition to varying the syngas flow rate, the effect of residence time will also be discussed under different contact time experiments through variation of the mass of catalyst combined with inert quartz at constant catalyst bed volume.

References

1. Yokota K., Y. Hanakata, and K. Fujimoto, *Chem. Eng. Sci.* **45(8)** (1990) 2743.
2. Bukur D. B., X. Lang, A. Akgerman, and Z. Feng *Ind. Eng. Chem. Res.* **36** (1997) 2580.
3. Lang X., A. Akgerman , D. B. Bukur, *Ind. Eng. Chem. Res.* **34** (1995) 72.
4. David J. B. and Subramaniam B. *AIChE J.,* **44(8)** (1998) 1889.
5. Subramaniam B., *Appl. Catal. A: Gen.* **212** (2001) 199.
6. Davis B*., Energeia* (1997), 8(3),1-5.
7. Huang X., C. W. Curtis, C. B. Roberts, *AIChE 2001 Annual Meeting*.
8. Huang X., C. W. Curtis, C. B. Roberts, *ACS 2002 National meeting*, *Fuel Chemistry Division Preprints* **47(1)** (2002) 150.
9. Huang X., C. W. Curtis, C. B. Roberts, submitted to *Fuel and Processing Technology* (2002).

10. Huang, X., Curtis, C.W., and Roberts, C.B. 10th International Symposium on Supercritical Fluid Chromatography, Extraction and Processing, Myrtle Beach, SC, August 19-22, 2001.
11. Anderson R.B., R. A. Friedel, and H. H. Storch, *J. Chem. Phys.* **19** (1951) 313.
12. Huff G. A. and C. N. Satterfield. *J. Catal.* **85** (1984) 370.
13. Iglesia E., S.C. Reyes and R. J. Madon. *J. Catal.* **129** (1991) 238.
14. Schliebs B. and J. G. B. Bunsenges. *Phys. Chem.* **89** (1985) 68.
15. Donnelly T. J., I. C. Yates and C. N. Satterfield. *Energy & Fuels* **2** (1988) 734.
16. Donnelly T. J. and C. N. Satterfield. *Appl. Catal.* **52** (1989) 93.
17. Dictor R. A. and A. T. Bell. *J. Catal.* **97** (1986) 124.
18. Stenger H. G. , *J. Catal.* **92** (1985) 426.
19. Kuipers E.W., C. Scheper, J.H. Wilson, I.H. Vinkenburg and H. Oosterbeek *J. Catal.* **158** (1996) 288.
20. Kuipers V., I. H. Vinkenburg and H. Osterbeek. *J. Catal.* **152** (1995) 137.
21. Madon R.J., S.C. Reyes and E. Iglesia. *J. Phys. Chem.* **95** (1991) 7795.
22. Madon R.J. , and E. Iglesia. *J. Catal.* **139** (1993) 576
23. Iglesia E., S.C. Reyes, R.J. Madon and S.L. Soled. *Adv. Catal.* **39** (1993) 221.
24. Friedel R. A., R. B. Anderson, *J. Am. Chem. Soc.* **72** (1950) 1212.

Publications and presentations resulting from this project during the last year

1. Huang, X.; Curtis, C.W.; Roberts, C.B.; "Supercritical Fluid Solvent Effects on Fischer-Tropsch Synthesis", 10th International Symposium on Supercritical Fluid Chromatography, Extraction and Processing, Myrtle Beach, SC, August 19-22, 2001.
2. Huang, X.; Park, Y.; Curtis, C.W.; Roberts, C.B.; "Supercritical Fluid s as an Alternative Reaction Medium for Fischer-Tropsch Synthesis", AIChE Annual Meeting, Reno, NV, November 4-9, 2001.
3. Roberts, C.B.; "Alternative Processing with Supercritical Fluid Solvents", Ciba Specialty Chemicals, Macintosh, AL, December 5, 2001 (Invited Seminar)
4. Roberts, C.B.; "Supercritical Fluids in Chemical Synthesis and Materials Processing", Eastman Chemical, Kingsport, TN, March 21, 2002 (Invited Seminar).
5. Huang X., C. W. Curtis, C. B. Roberts, *ACS 2002 National meeting*, *Fuel Chemistry Division Preprints* 47(1) (2002) 150.
6. Huang X., C. W. Curtis, C. B. Roberts, submitted to *Fuel and Processing Technology* (2002).
7. Huang X., N. O. Elbashir, Roberts, C. B. will be presented in AIChE 2002 Annual Meeting (2002).

Sol-Gel Supported Cobalt Catalysts for Fischer-Tropsch Synthesis of Diesel Range Fuel

E. M. Eyring, H. L. C. Meuzelaar and R. J. Pugmire
University of Utah

Two largely independent synthetic chemistry research efforts are reported below that both involve the use of carbon monoxide. In the one project, completed in January, 2002, some of the experimental details of the synthesis of diethyl carbonate (DEC) from ethanol, carbon monoxide and molecular oxygen were clarified with a continuous flow reactor monitored by GC/MS. The motivation for this study is the known suitability of DEC to be an oxygenated fuel additive to diesel fuel for the purpose of diminishing smoke output from a diesel engine.

The other project, that is still underway, is the synthesis and characterization of cobalt catalysts on sol-gel supports to facilitate the Fischer-Tropsch (F-T) conversion of syngas to diesel fuel. This second project is motivated by the interest in finding heterogeneous catalyst supports that favor the formation of diesel range automotive fuels from syngas.

What we already knew on May 1, 2001 about the diethyl carbonate synthesis, largely from previous batch reactor studies, was the following: 1) A hydroxide promoter enhances the yield of DEC from the oxidative carbonylation of gaseous ethanol over a heterogeneous $CuCl_2/PdCl_2$/activated carbon catalyst; 2) short residence times (of the order of 10 seconds) favor DEC formation to the exclusion of byproducts; 3) higher pressures enhance the DEC yield; 4) reactions forming DEC and the byproducts occur in parallel making it likely that a better DEC synthesis catalyst may be found.

On May 1, 2001, the Utah research group had had no experience with Fischer-Tropsch reactions carried out over cobalt catalysts.

Results

Dr. Nam-Sun Roh, a Korean scientist in the Eyring lab from Feb. 2001 to January 2002, used a laboratory-scale continuous flow reactor (Figure 1) to establish the following additional insights concerning the DEC synthesis: 1) Undesirable byproduct diethoxymethane forms in significantly higher yields when ethanol is introduced in excess; 2) catalyst pretreatment with KOH is better for DEC yield and selectivity than with any of five other metal hydroxides tested (see Figure 2); 3) a higher OH:Cu mole ratio than 2.0 in the composition of the $CuCl_2/PdCl_2$/AC-KOH catalyst drops the conversion rate to DEC below that found when no KOH has been added to the catalyst (see Figure 3). These results were presented in a symposium at the Orlando American Chemical Society meeting in April 2002. A scientific paper reporting these results has also been prepared for publication.

Turning now to results of the Fischer-Tropsch (F-T) project, we note first that there are several published reports[1-5] of F-T syntheses being carried out over cobalt metal catalysts supported by sol-gels. The hydrolysis and condensation of a tetramethyl orthosilicate (TMOS) or tetraethyl orthosilicate (TEOS) after several days of drying of the "sol" (to remove water and alcohol) produces a porous "gel" that superficially resembles ordinary silica glass. The condensation reaction can be catalyzed by either acid or base with differing results for the pore structure of the

gel (see below). Drying under ambient conditions yields a "xerogel" that retains some moisture in the interstices of the gel consisting of an amorphous polymeric net with little branching. The drying of a "xerogel" monolith typically causes the volume of the glass to drop to 12.5% of the original volume of the gel. A concomitant collapse of many internal pores occurs with a significant loss of internal surface area and pore volume. Drying the gel with supercritical carbon dioxide or other solvents produces a glass called an "aerogel" of high porosity, greater network branching and very low density but extraordinary mechanical strength.

Cobalt is introduced into the sol before drying begins as a salt such as cobalt nitrate hexahydrate dissolved in water. The resulting gel is dried at room temperature, is calcined in air at a temperature of ~550°C and is finally reduced under a flowing hydrogen atmosphere at an even higher temperature. The result is a catalyst with well dispersed cobalt metal particles which appear to have an average diameter of about 7 nanometers based on experiments carried out by Seehra and Punnoose.

The resulting supported cobalt metal catalyst resembles one prepared from a zeolite except that the sol-gel support lacks the very regular channel network architecture of a molecular sieve. Potential advantages of the sol-gel catalyst support include the tunability of pore sizes and the greater possible porosity and internal surface area of the material. It remains to be seen whether sol-gel F-T yields are as large as those reported for other cobalt catalyst supports, whether the production costs and durability of the sol-gel catalysts are favorable, and whether or not the hydrocarbon distribution is suitable for diesel range fuels.

Ernst and coworkers[1] drew a number of interesting conclusions from their F-T study that have not been confirmed or challenged by the later F-T papers.[2-5] Acid catalysis of the TEOS polymerization reaction gives a nanoporous (pore diameter under 4 nm) catalyst support whereas base catalysis yields an intermediate average diameter pore catalyst support that Ernst and coworkers call mesoporous. In the mesoporous catalyst transport of primary products is more efficient favoring lower molecular weight products ($C_5 - C_{13}$ fraction, mainly gasoline). In the nanoporous catalysts (pore diameters under 4 nm) residence time of primary products is longer and hydrocarbon chain growth is favored (C_{22} and higher, waxes). The duration of the gel ripening process affects BET surface area but not cobalt metal crystallite size. The degree to which the cobalt has been reduced to the metal is also an important variable. Ernst et al.[1] conclude that to produce waxes with high selectivity one must prepare supported catalysts with large specific surface areas and with cobalt particle sizes greater than 30 nm to limit support interactions. Our recent success with much smaller cobalt particles contradicts this claim.

The "xerogel" and "aerogel" forms of these catalyst supports represent the two extremes of what is feasible. It may be possible to control the pore structure on an F-T catalyst, therefore exerting better control of the F-T product distribution. One method of pore control is by controlled ambient drying followed by supercritical CO_2 or liquid CO_2 drying which "locks in" the pore structure. By controlling the duration and extent of ambient drying, complete control over the resulting pore structure can be achieved.

So far, we have prepared and characterized one Fischer-Tropsch cobalt metal catalyst supported by a nanoporous TMOS xerogel. The catalytic material is a black powder that has a BET surface

area of 300 m^2g^{-1}. Figure 4 presents the distribution of hydrocarbons obtained when syngas was passed through a continuous flow reactor containing this catalyst at a temperature of 225 ^oC, a pressure of 30 psi, and a CO:H_2 mole ratio of 0.5. From XRD measurements Seehra and Punnoose have determined (unpublished) that cobalt metal and cobalt oxide are present in this catalyst in particles with an average apparent size of 7 nm with the oxide layered on the outside of the particles and cobalt metal segregated to the core of the particles. We have assembled an apparatus for drying gels with CO_2 and soon will have enough aerogel catalyst to test in our Fischer-Tropsch flow-through reactor to see whether the expected larger pore size does indeed give rise to lower molecular weight Fischer-Tropsch reaction product as suggested by Ernst and coworkers. The next stage in this study will be a comparison of the F-T product distribution and yields when a xerogel with the same cobalt loading is prepared by impregnation from aqueous solution.

We have recently made significant improvements in our flow reactor to facilitate study of F-T reactions. A cold trap has been added immediately downstream from the catalyst bed to trap very large ($>C_{22}$) products and prevent them from condensing further downstream in the heated system. Risk of fouling the GC column is also minimized. A pressure gauge has been added upstream from the catalyst bed in order to quantify the pressure drop across the bed and a high temperature diaphragm gauge replaced the gauge in the heated zone to improve safety, accuracy and eliminate the dead volume of the bourdon tube.

Future work

Our experiments will address the following questions:

1) How long does a cobalt catalyst continue to give reasonable yields of hydrocarbons from a fully automated continuous flow reactor loaded with a cobalt/xerogel catalyst and how does the distribution of product hydrocarbons change with catalyst time spent in the reactor bed?
2) Does a nanoporous support structure (pore diameter < 4 nm) favor F-T wax production as claimed by Ernst et al.?
3) What roles do cobalt metal particle size, presence of cobalt oxide, pore size, support morphology and BET surface area play in the product hydrocarbon distribution?
4) Does a trace amount of some other noble metal promoter dramatically alter the yield and/or product distribution of a sol-gel supported cobalt catalyst?
5) Can a quantitative comparison be made by diffuse reflectance FTIR spectroscopy of the number of CO molecules adsorbed on xerogel and aerogel cobalt catalysts at elevated temperatures and pressures? (We have preliminary xerogel infrared spectra obtained at 200°C through a zinc selenide window at pressures ranging from 50 to 300 psi using a Spectra Tech DRIFTS high temperature, high pressure cell.)

Summary of results

Conditions for making diethylcarbonate (DEC) an oxygenated diesel fuel additive, from syngas have been optimized. Selectivity for DEC is good but product yields from the oxidative carbonylation of ethanol over a $CuCl_2/PdCl_2$/activated carbon-KOH catalyst are typically less than 20% without recycling of reactants.

The porosity of xerogel and aerogel supports for cobalt nanoparticle Fischer-Tropsch catalysts can be adjusted by a judicious combination of ambient drying conditions and supercritical CO_2

drying of the sol-gels. A nanoporous (pores under 4 nm diameter) xerogel containing 7 nm diameter cobalt particles yields an product which contains diesel fuel range hydrocarbons from the Fischer-Tropsch reaction of syngas at 225°C and 30 psi.

References

1. B. Ernst, S. Libs, P. Chaumette, and A. Kiennemann, "Preparation and characterization of Fischer-Tropsch active Co/SiO_2 catalysts," Applied Catalysis A: General 186 (1999) 145-168.
2. L. Guczi, Z. Schay, G. Stefler, and F. Mizukami, "Bimetallic catalysis: CO hydrogeneration over palladium-cobalt catalysts prepared by sol/gel method," Journal of Molecular Catalysis A: Chemical 141 (1999) 177-185.
3. K. Okabe, X. Li, T. Matsuzaki, H. Arakawa, and K. Fujimoto, "Application of sol-gel method to preparation of ultra-uniform Co-based catalysts for Fischer-Tropsch reaction," J. Sol-Gel Science and Technology 19 (2000) 519-523.
4. C. L. Bianchi, F. Martini, and P. Moggi, "Co/SiO_2 sol-gel catalysts for Fischer-Tropsch synthesis," Catalysis Letters 76 (2001) 65-69.
5. K. Okabe, X. Li, T. Matsuzaki, H. Arakawa, and K. Fujimoto, "Fischer-Tropsch synthesis over $Co\text{-}Ir\text{-}SiO_2$ catalysts prepared by the alkoxide method," Journal of the Japan Petroleum Institute 44 (2001) 135-139.

Publications

1. B. C. Dunn, C. Guenneau, S. Hilton, E. M. Eyring, J. Dworzanski, H. L. C. Meuzelaar, J. Z. Hu, and R. J. Pugmire, "Production of Diethyl Carbonate from Ethanol and Carbon Monoxide over a Heterogeneous Catalyst," *Fuel Chemistry Div. Preprints* **46** (2001) 236.
2. B. C. Dunn, C. Guenneau, S. Hilton, N. S. Roh, E. M. Eyring, J. Dworzanski, H. L. C. Meuzelaar, J. Z. Hu, and R. J. Pugmire, "Diethyl Carbonate Production from Ethanol and Carbon Monoxide," *Fuel Chemistry Div. Preprints* **46** (2001) 390.
3. Brian C. Dunn, Catherine Guenneau, Steven A. Hilton, Jorg Pahnke, Edward M. Eyring, Jacek Dworzanski, Henk L. C. Meuzelaar, J. Z. Hu, Mark S. Solum, and Ronald J. Pugmire, "Production of Diethyl Carbonate from Ethanol and Carbon Monoxide over a Heterogeneous Catalyst," *Energy & Fuels* **16** (2002) 177-181.
4. A. Punnoose, M. S. Seehra, B. C. Dunn, and E. M. Eyring, "Characterization of $CuCl_2/PdCl_2$/Activated Carbon Catalysts for the Synthesis of Diethyl Carbonate," *Energy & Fuels* **16** (2002) 182-188.
5. N. S. Roh, B. C. Dunn, E. M. Eyring, J. Dworzanski, H. L. C. Meuzelaar, J. Z. Hu, M. S. Solum and R. J. Pugmire, "Continuous Production of Diethyl Carbonate over a Supported $CuCl_2/PdCl_2$/KOH Catalyst," *Fuel Chemistry Division Preprints* **47** (2002) 142.
6. Nam-Sun Roh, Brian C. Dunn, Edward M. Eyring, R. J. Pugmire and H. L. C. Meuzelaar, "Production of Diethyl Carbonate from Ethanol and Carbon Monoxide over a Heterogeneous Catalytic Flow Reactor," to be submitted to *Fuel Processing Technology*.

Personnel

People participating in this team effort (listed in alphabetical order) are:
Paul Cole, Daniel J. Covington, Brian C. Dunn, Edward M. Eyring, Jennifer Gasser, Emily Hieder, Henk L. C. Meuzelaar, Ronald J. Pugmire, Alex Punnoose, N. S. Roh, and Mohindar Seehra.

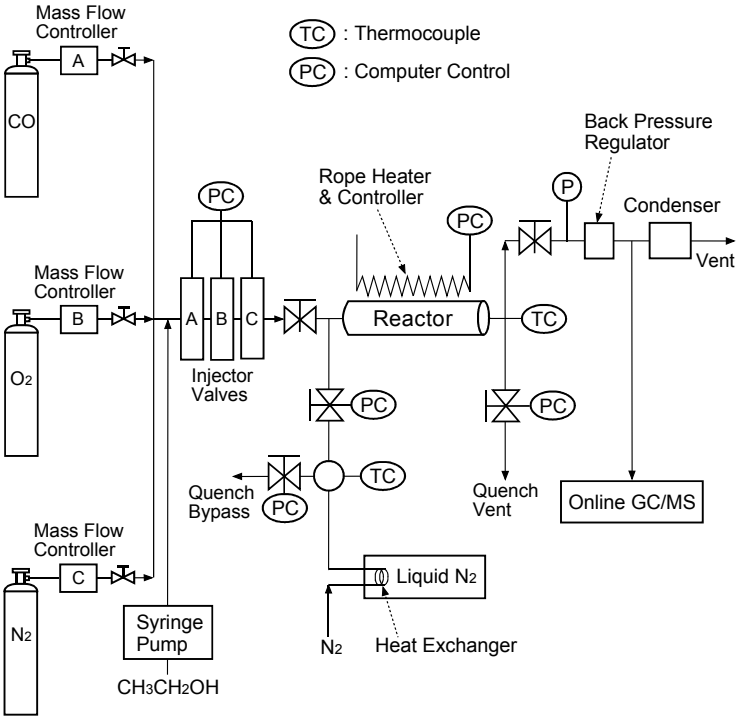

Figure 1. Schematic diagram of the experimental apparatus for DEC synthesis.

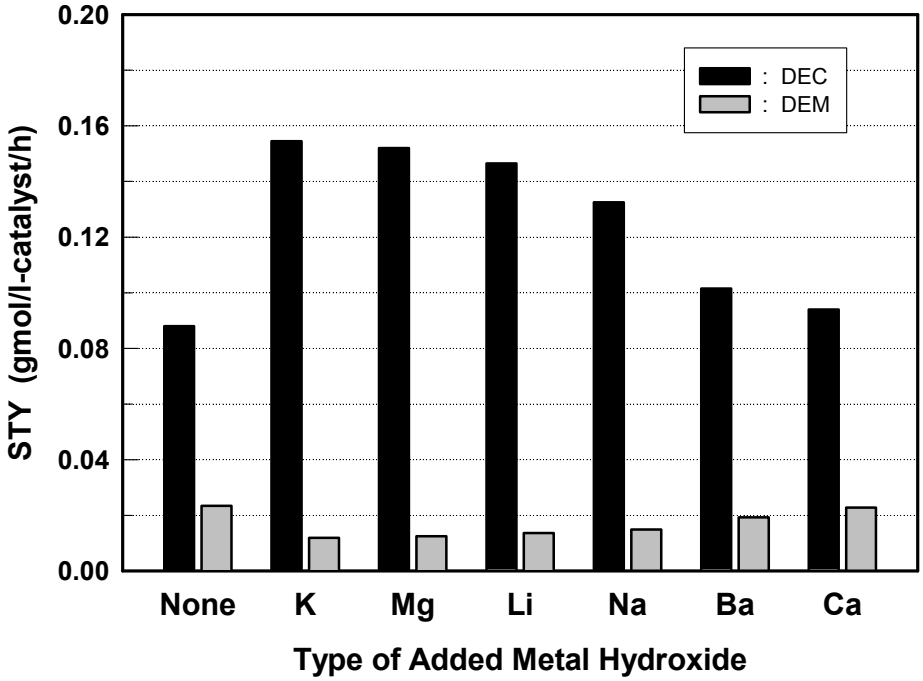

Figure 2. Influence of treating an activated carbon supported $CuCl_2/PdCl_2$ catalyst with various metal hydroxides on the STY(space time yield) of DEC and DEM. Conditions: 2.0 g catalyst, OH:Cu mole ratio = 1.0, 2.0 sccm O_2, 6.0 sccm CO, 3.6 mL/hr ethanol (as liquid), 150 ^oC, 100 psig, τ = 9.61 sec.

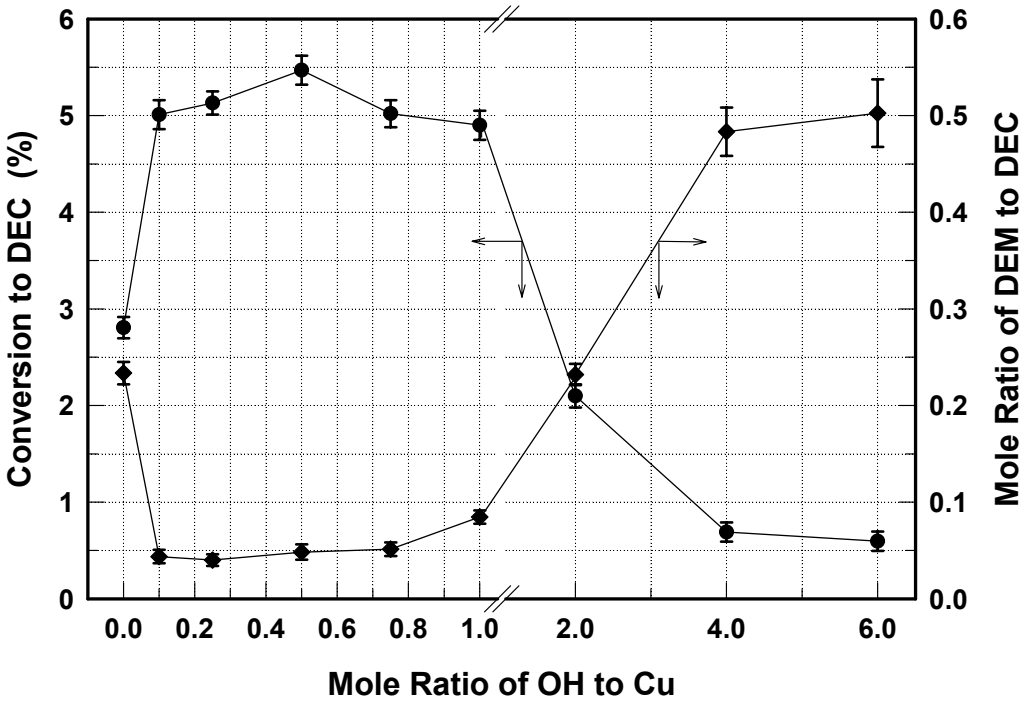

Figure 3. Change in yield of DEC and DEM depending on OH:Cu mole ratio. Conditions: 2.0 g catalyst, 3.0 sccm O_2, 6.0 sccm CO, 3.6 mL/hr ethanol (as liquid), 150 ^oC, 100 psig, τ = 9.61 sec.

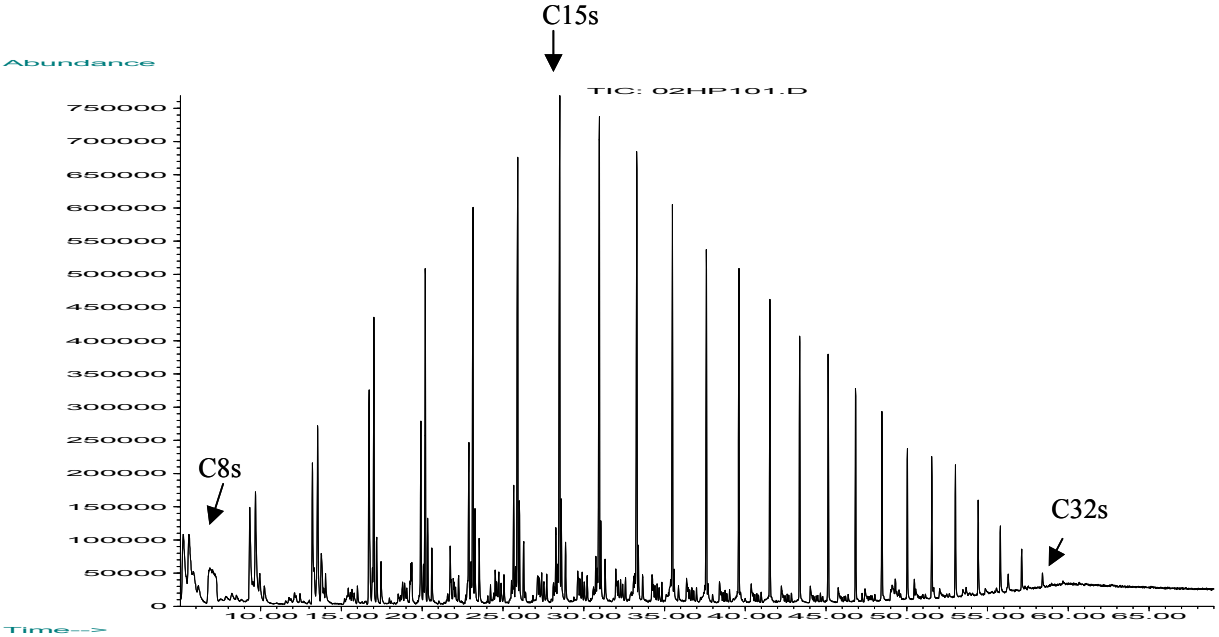

Figure 4. GC/MS chromatogram of F-T products collected in *n*-pentane colled in dry ice/ethanol bath. Reactor conditions: 225 ^oC, 30 psi. Flow rates: H_2 at 90 sccm, CO at 45 sccm, N_2 at 135 sccm. Vertical axis is total ion current (TIC). Horizontal axis is time in minutes. "Solvent delay" excludes the possibility of observing species below C8. Eack peak group is a mixture of alkanes and alkenes. The largest peak in each group is the normal alkane.

Hydroisomerization of Fischer-Tropsch Products to Environmentally Clean Transportation Fuels

Zhou Zhang, Yulong Zhang, G.D. Holder, J.W. Tierney and I. Wender
University of Pittsburgh

The acid-catalyzed isomerization of alkanes is of growing important in determining the nature of transportation fuels, including environmentally clean high octane gasoline, high cetane diesel fuel, low pour point jet fuel and lubricant base stocks. However, isomerization of long-chain paraffins, C_7+ is generally followed by cracking, which tends to limit catalytic paraffin isomerization to C_4-C_6 alkanes. It is highly desirable to obtain catalytic systems that can be used to isomerize long-chain paraffins with optimal cracking. Catalysts that function under mild reaction conditions are needed to achieve high selectivity to desired transportation fuels from long-chain paraffins. Work is directed chiefly to obtaining these fuels from the large amounts of wax produced in the Fischer-Tropsch (F-T) synthesis.

Research in this laboratory first investigated the activity of platinum-promoted sulfate-modified zirconia ($Pt/SO_4/ZrO_2$) catalyst, for the isomerization of n-heptane ($n\text{-}C_7H_{16}$) and n-hexadecane ($n\text{-}C_{16}H_{34}$)
[1]. Zirconium oxide was modified by doping with sulfuric acid. Platinum, as $H_2PtCl_6 \cdot 6H_2O$, was then loaded by incipient wetness impregnation. After being dried and calcined, the prepared catalyst had 0.5 wt% Pt and about 6 wt% SO_4^{2-}. This catalyst was found to be a highly active cracking catalyst, easily converting hexadecane and longer chains into C_5-C_9 hydrocarbons, albeit with high normal to isomer (n/iso) ratios. However, this catalyst declined in activity due to the loss of sulfur from the catalyst[2].

An objective of this research was to combine high activity at low temperature and pressure with catalyst stability and regenerability. We found that the substitution of tungsten trioxide (WO_3) for sulfate (SO_4^{2-}) resulted in a more stable and selective catalyst for the hydroisomerization of *n*-hexadecane. Platinum-promoted tungstate-modified zirconia ($Pt/WO_3/ZrO_2$) is a weaker acid than $Pt/SO_4/ZrO_2$ which may reduce its activity for cracking. $Pt/WO_3/ZrO_2$ is an active and selective catalyst for the isomerization of n-alkanes, partly as the result of increased hydride transfer rates, which limit the lifetime of adsorbed carbenium ions[3]. The state of Pt on the surface of these catalysts is still being debated[4,5].

A continuous trickle-bed reactor was used to compare the activities and selectivities of three $Pt/WO_3/ZrO_2$ catalysts prepared by different methods and to investigate the effects of tungsten loading and of reaction conditions for hydroisomerization of n-hexadecane. A run of 93.5 hr was conducted using the most highly active $Pt/WO_3/ZrO_2$ catalyst which contains 0.5 wt% well-dispersed Pt and 6.5 wt% W. Reaction conditions were manipulated and five shutdown (feed stopped, reactor temperature lowered but H_2 flow rate maintained) and restart operations were carried out. This catalyst showed high activity and stability (Figure 1).

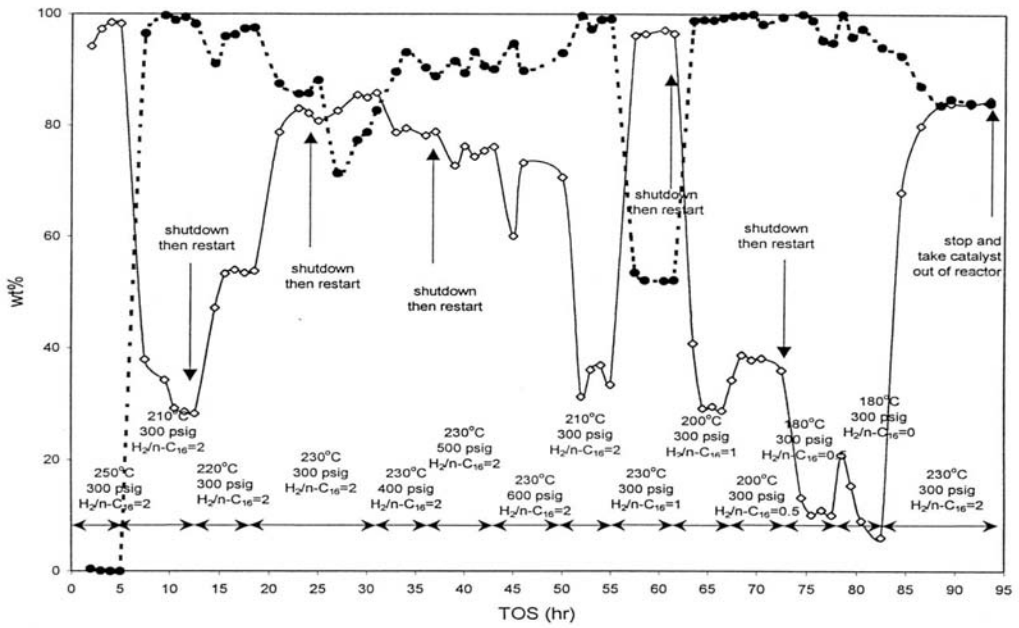

Figure 1. Effects of reaction variables on hydroisomerization of nC_{16}: T, P and H_2/nC_{16} mole ratio. WHSV= $1h^{-1}$ nC_{16} conversion (——) and iC_{16} selectivity (----)[6]

Considerable success has also been achieved in converting n-hexadecane to iso-hexadecanes for 100 h at temperatures of about 220°C and under H_2 pressure as low as 160psig. Our best results (highest i-C_{16} yield) are a 79.1 wt% n-C_{16} conversion and 89.9 wt% i-C_{16} selectivity. The $Pt/WO_3/ZrO_2$ catalyst is rugged and has properties which allow one to propose that it may attain commercial use after further study. A typical GC-MS spectrum of hexadecane isomers in the products of n-C_{16} hydroisomerization is shown in Figure 2[6].

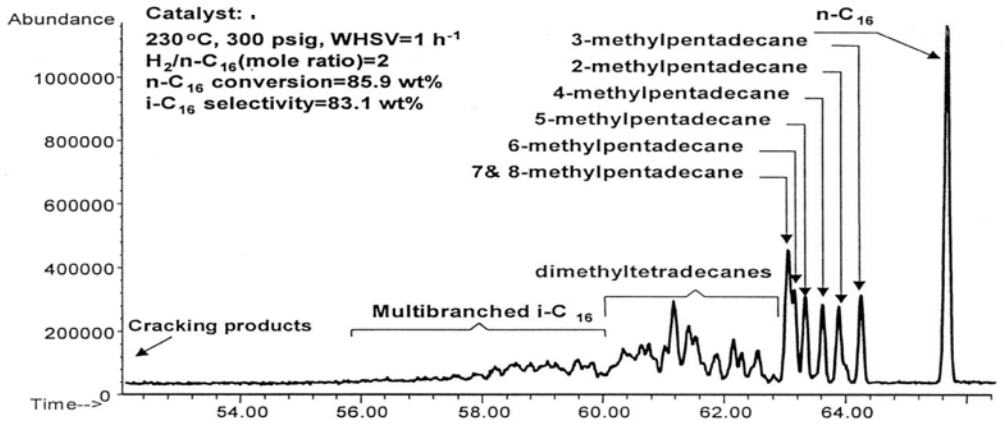

Figure 2. A typical GC-MS spectrum of hexadecane isomers in the products of n-C_{16} hydroisomerization

An objective in the past year has been to extend research to the conversion of straight chain alkanes longer than hexadecane, such as those produced in the F-T synthesis process, to a variety

of clean transportation fuels. This was carried out using the stable and selective $Pt/WO_3/ZrO_2$ catalyst to hydroisomerize and hydrocrack n-C_{24} and n-C_{36}[7,8].

Catalytic activity tests were then carried out in a 27ml microautoclave system. In a typical reaction, 0.25 g of the catalyst was activated at 500°C for 90 minutes in air and then charged into the microreactor, which was pre-dried overnight. After loading the catalyst, the reactant, typically 1.0 g, was charged. The initial hydrogen pressure was 500 psig (at room temperature). Reaction temperatures varied from 180 to 230°C. The reactor was shaken horizontally at 180 rpm during reaction. A computer was used to record the reaction pressure, temperature and time during the run. The reaction was terminated by cooling the reactor to room temperature. The reaction variables were reaction time, reaction temperature, hydrocarbon/catalyst ratios and, importantly, hydrogen pressure.

Product ranges for this work were arbitrarily taken as follows (considerable overlap is recognized):

Gasoline	C4-C9
Diesel Fuel	C10-C20
Lube-base Oil	C21-C32

A comparison of $Pt/WO_3/ZrO_2$ and $Pt/SO_4/ZrO_2$ in the activity and selectivity of n-C_{24} at similar levels of conversion is shown in Table1.

Table 1. Comparison of $Pt/WO_3/ZrO_2$ and $Pt/SO_4/ZrO_2$

				Selectivity, wt%		
Catalyst	n-C_{24}	reaction time	conversion	to gasoline	to diesel	to lube-base oil
$Pt/WO_3/ZrO_2$, 0.125g	1.5 g	15 min	33 wt%	52.8	30.0	17.2
$Pt/SO_4/ZrO_2$, 0.25g	1.0 g	25 min	32 wt%	2.2	2.4	95.4

220°C, initial H_2 pressure =500psig

$Pt/SO_4/ZrO_2$ showed much higher activity by achieving a similar conversion with a much lower catalyst/reactant ratio and a shorter reaction time than did $Pt/WO_3/ZrO_2$. Moreover, with conversion as low as 33 wt%, $Pt/SO_4/ZrO_2$ cracked the reactant to gasoline as the main product. For conversions higher than 50 wt%, $Pt/SO_4/ZrO_2$ would readily yield very short chain hydrocarbons. With $Pt/WO_3/ZrO_2$, the main reaction that occurred was the hydroisomerization of n-C_{24} to iso-C_{24} products.

At 220°C, $Pt/WO_3/ZrO_2$ catalyzes some cracking of the n-C_{24} molecule, but significant hydroisomerization to gasoline, diesel fuel and lube-base oils takes place (Figure3)[8].

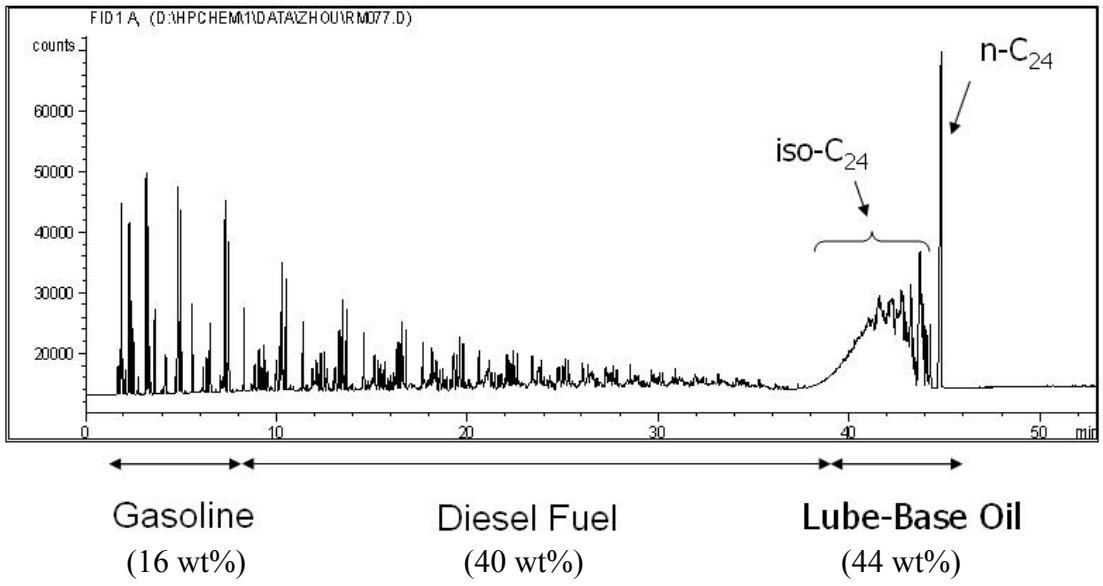

Fig.3. GC analysis of product from reaction of n-C_{24} over Pt/WO_3/ZrO_2 Catalyst: (0.5 wt%) Pt/WO_3/ZrO_2 (12.5 wt% W). 0.25 g, 1.0 g n-C_{24}, 25 min, 220°C, initial H_2 pressure =500psig. Conversion = 96 wt%.

Pt/WO_3/ZrO_2 catalysts demonstrated good performance in converting a real F-T wax, SASOL H1 wax, that has an average carbon number of 58 and consists of normal paraffins from C_{28} to $C_{80,}$ to transportation fuel products under appropriate conditions. The result is shown in Figure 4. The. products are chiefly branched hydrocarbons. For gasoline, this gives a good high octane number product; similarly the highly branched lube-base oil product has good low pour points. Our GC columns are not suitable for the analysis of very heavy wax hydrocarbons, and we are now using a simulated distillation method to obtain the distribution of products from the heavy waxes.

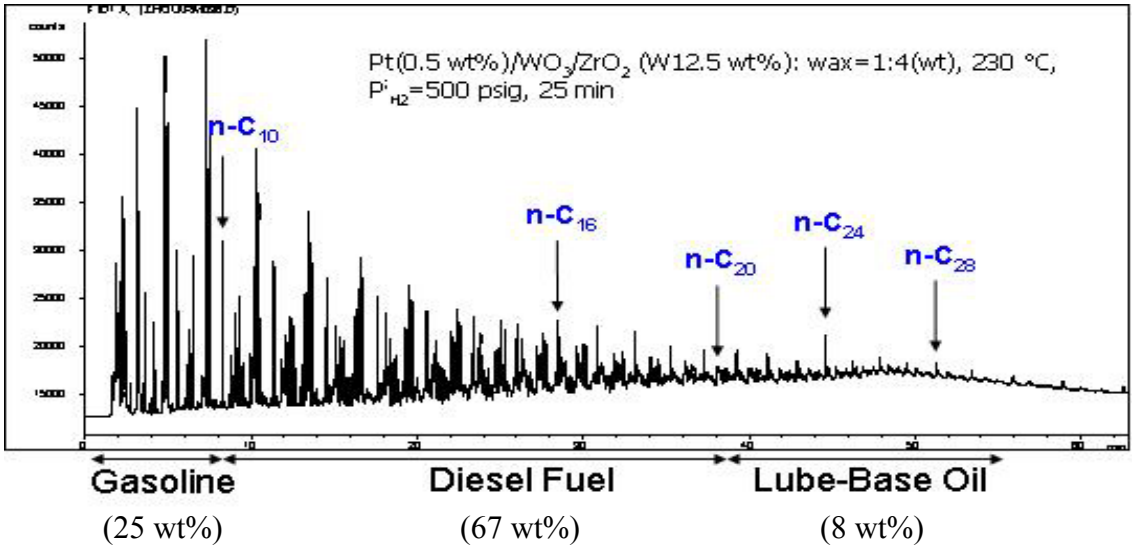

Fig.4 GC analysis of products from Sasol H1 wax over Pt/WO_3/ZrO_2

We next directed our efforts to improve $Pt/WO_3/ZrO_2$ as a hydroisomerization catalyst. Combination catalysts were made by physically mixing $Pt/WO_3/ZrO_2$ and other components in different ratios. This was investigated in several ways:

a) Addition of sulfated zirconia (SO_4/ZrO_2) to $Pt/WO_3/ZrO_2$ (PtWZr)

While $Pt/SO_4/ZrO_2$ catalyst possesses a very high cracking function in converting long-chain paraffins, SO_4/ZrO_2 (SZr) without Pt demonstrates very little activity at the same conditions. However, a very small amount of SO_4/ZrO_2 combined with $Pt/WO_3/ZrO_2$ greatly affects the performance of $Pt/WO_3/ZrO_2$. As shown in Figure 5, at 200°C, only 33 wt% conversion was obtained with 0.25 g Pt/WO3/ZrO2; most products were isomers of n-C_{24}. After mixing 0.008 g of SO_4/ZrO_2 with 0.242 g of $Pt/WO_3/ZrO_2$, the combination catalyst PtWZr/SZr (30:1) increased the conversion to 96 wt%. At the same time, product selectivities to C_4-C_9 and C_{10}-C_{20} increased by more than 20 times While SO_4/ZrO_2 alone has hardly any activity at 200°C, adding it to $Pt/WO_3/ZrO_2$ greatly increased cracking. A significant interaction between the two components is evident so that the hydroisomerization and hydrocracking reactions reached higher levels.

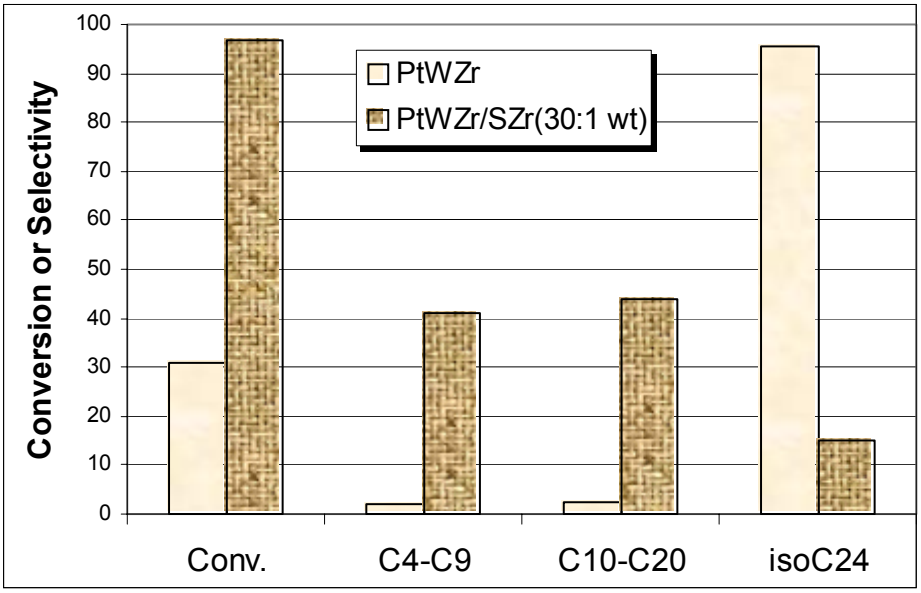

Fig.5 Comparison of products from reaction of PtWZr and PtWZr/SZr(30:1) with n-C_{24}. Catalyst: (0.5 wt% Pt) PtWZr. 0.25 g, 1.0 g n-C_{24}, 25 min, 200°C, initial H_2 pressure = 500psig.

b) Addition of WO_3/ZrO_2 to $Pt/WO_3/ZrO_2$

In investigating the effect of adding WO_3/ZrO_2 to $Pt/WO_3/ZrO_2$, we realized that the Pt distribution over WO_3/ZrO_2 could affect the activity and selectivity. Figure 6 compares the results of 0.25 g $Pt/WO_3/ZrO_2$ with 0.25 wt% Pt loading and a combination catalyst (PtWZr/WZr 1:1) made of 0.125 g $Pt/WO_3/ZrO_2$ with 0.5 wt% Pt loading and 0.125 g WO_3/ZrO_2. Since the overall Pt content in the two catalysts is the same, the difference in their performance should be due to Pt distribution.

c) $Pt/WO_3/ZrO_2$ with various zeolites

Zeolites were also tested in combination with $Pt/WO_3/ZrO_2$. Different product distributions were obtained with each zeolite. With the same ratio of zeolite to PtWZr significant differences in product distribution were observed. Figure 7 compares results of $Pt/WO_3/ZrO_2$ (PtWZr) used alone, and PtWZr modified by Y zeolite (Y720), Beta zeolite (H-BEA814) and mordenite

(Mor21A). With a 1:1 ratio, Pt/WO_3/ZrO_2 modified with mordenite had the highest reactivity for converting n-C_{24} and the product has the highest selectivity to the diesel fuel range (C_{10}-C_{20}) and gasoline range (C_4-C_9).

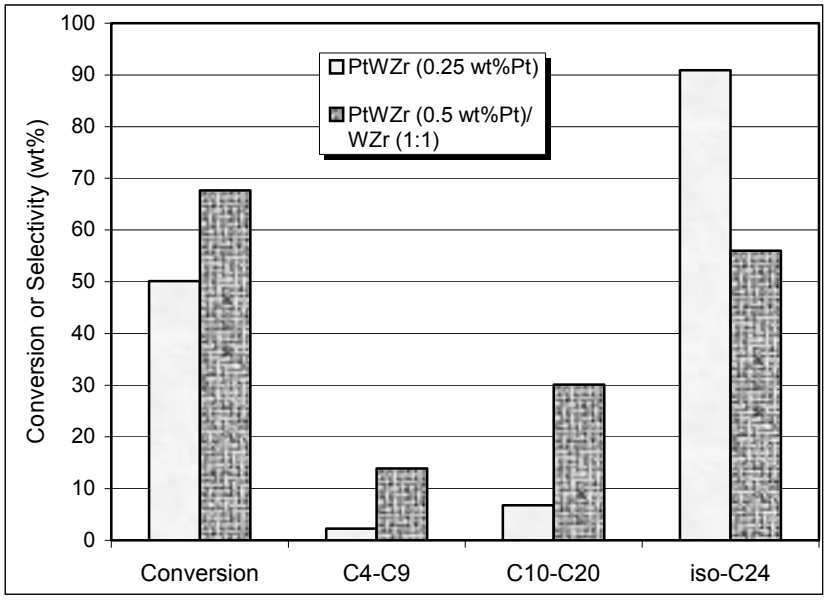

Fig.6 Comparison of PtWZr and PtWZr/WZr(1:1) with the same overall compositions. Catalyst: n-C_{24}= 0.25 g/1.0g, P_{H2}=500psi, T= 200°C

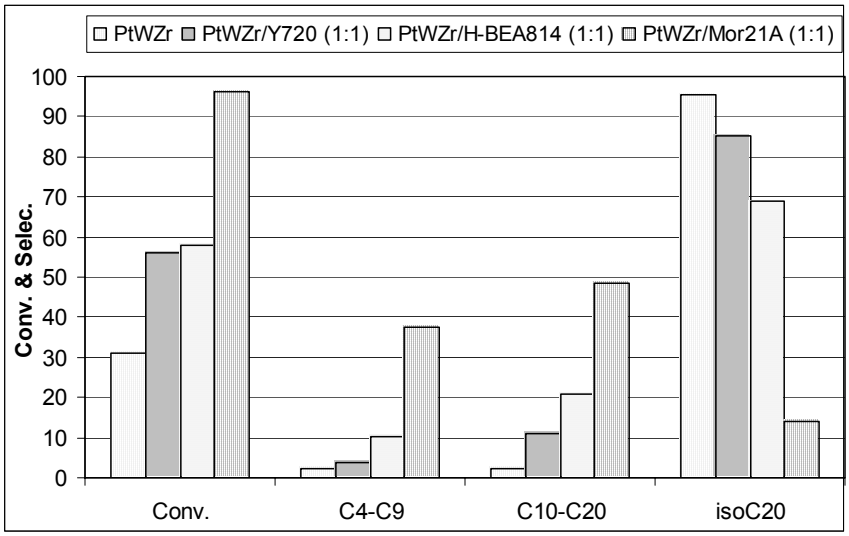

Figure 7. Products obtained using PtWZr and PtWZr modified by Y, Beta and Mordenite Reaction conditions: 200°C, nC_{24} /catalyst = 1.0 g/ 0.25g , 25 min, initial H_2 pressure = 500 psi

An extended investigation was made using combinations of Pt/WO_3/ZrO_2 and mordenite (Mor21A) in treating n-C_{24}. As shown in Figure 8, the conversion varied from zero to almost 100%. The presence of a maximum at about 50wt% was unexpected and indicates that the interactions between the catalysts are not simple. We are continuing to investigate these interactions.

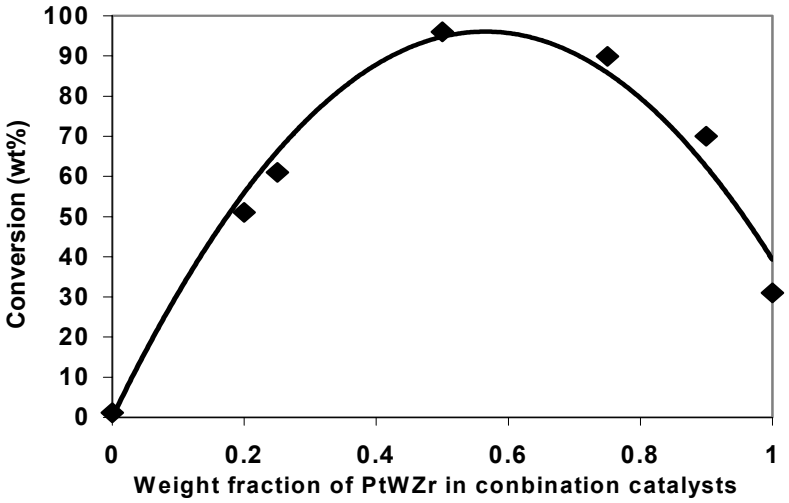

Figure 8. PtWZr/Mor21A with different ratios. Reaction conditions: 200 °C, nC_{24} /catalyst = 1.0 g/ 0.25g , 25 min, initial H_2 pressure = 500 psi

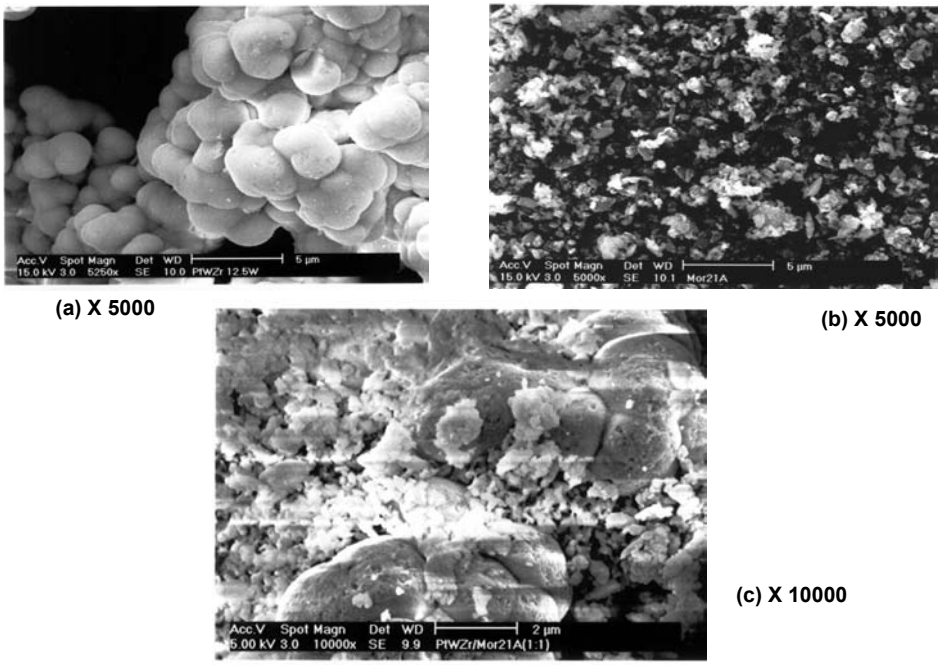

Fig.9 SEM of (a)PtWZr, (b)Mor21A and (c)PtWZr/Mor21A(1:1)

From characterization tests using SEM and XRD, we have determined that the combination catalysts are basically physical mixtures. . Comparing the SEM images of PtWZr, Mor21A and PtWZr/Mor21A (1:1) in Figure 9, we see that in the combination catalysts, although particles of two components are very close to one other, they basically keep their original shapes. XRD patterns of these three samples show that no new crystal structures were formed after the two components were combined, Figure 10.

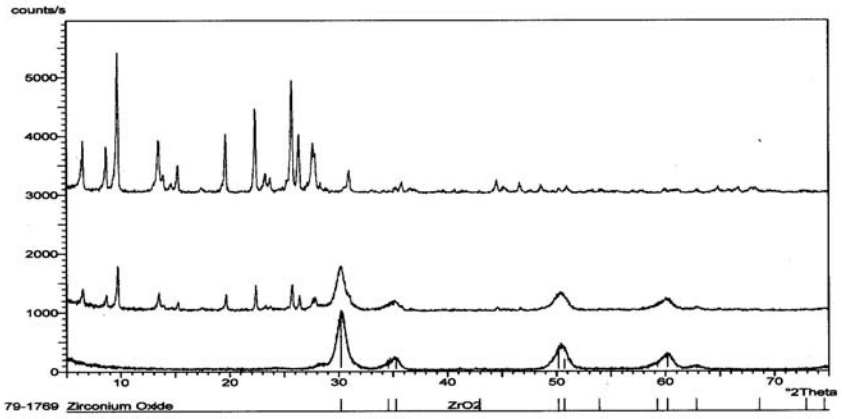

Fig.10 XRD Patterns of Mor21A (top), PtWZr/Mor21A (1:1) (middle) and PtWZr (bottom)

It is difficult to understand the mechanism involved in a physical mixture where components work interactively to facilitate reactions; but we have found interesting beneficial interactions using these combination catalysts, and we believe that using such mixtures is a promising route to obtain desirable transportation fuels at mild conditions.

d) Effect of hydrogen pressure

Initial hydrogen pressure is a factor that has a great effect on conversion and selectivity. Experiments with initial hydrogen pressures of 180, 300 and 500 psig were carried out with PtWZr catalysts while keeping other conditions the same. The results are shown in Table 2. It can be seen that lower hydrogen pressures result in much higher conversions and selectivities to cracked products. Lower hydrogen pressure results in more cracking. Experiment with a combination catalyst, PtWZr/Mor21A (1:1), led to similar conclusions.

Table 2. Effect of Initial Hydrogen Pressures

Initial hydrogen Pressure (psig)	Conversion (wt %)	C_4-C_9 (wt%)	C_{10}-C_{20} (wt%)	isoC_{24} (wt%)
500	31	2	2	96
300	93	11	33	56
180	99	37	56	7

Catalyst: Pt(0.5 wt.%)/WO_3/ZrO_2 (12.5 wt.% W). Reaction conditions: 200°C, nC_{24} /catalyst = 1.0 g/ 0.25g , 25 min

Preliminary studies using normal paraffins longer than n-C_{24} are being carried out. n-C_{36} somewhat better resembles the heavier hydrocarbons found in F-T waxes. Extra cracking is required to convert n-C_{36} to acceptable product ranges. Table 3 shows the results from experiments with pure PtWZr and with PtWZr/Mor21A(1:1) catalysts with n-C_{36}.

Table 3. Comparison of product distributions (weight %) with n-C_{36} as the reactant.

Catalyst	Conversion	Gasoline	Diesel	Lube-base oil	isoC_{36}
PtWZr	93.0	4.1	16.3	3.4	76.2
PtWZr/Mor21(1:1)	86.6	25.1	60.6	5.5	8.8

Reaction conditions: 200°C, nC_{36} /catalyst = 1.0 g/ 0.25g, 25 min., Initial H_2 Pressure = 300psig

After being modified by mordenite, selectivity to transportation fuels, especially diesel fuels, has been greatly increased. A diesel selectivity of about 60 wt% was achieved. With the PtWZr/Mor21(1:1) catalyst the overall conversion was slightly lower. This may due to the fact that longer chain hydrocarbon reactants, such as n-C_{36}, experience more difficulties in entering and exiting the pore structures of the zeolite component in the combination catalysts.

Conclusions:

- ★ $Pt/WO_3/ZrO_2$ catalysts are good hydroisomerization catalysts for converting long chain paraffins, such as n-C_{24} and n-C_{36}, and an F-T wax, into branched products which are suitable for transportation fuels such as gasoline, diesel fuel and lube-base oils.
- ★ $Pt/WO_3/ZrO_2$ functions less as a cracking catalyst than $Pt/SO_4/ZrO_2$ at 200°C. The strong cracking ability of sulfated zirconia catalysts reduces the yield to middle range transportation fuels.
- ★ Physical mixtures of $Pt/WO_3/ZrO_2$ and small amounts of SO_4/ZrO_2 or zeolites exhibit catalytic properties significantly different than those of the pure materials. A possible explanation is that $Pt/WO_3/ZrO_2$ is a good initiator for generating carbenium ions and interacts with acidic components, such as SO_4/ZrO_2, WO_3/ZrO_2 and zeolites.
- ★ The $Pt/WO_3/ZrO_2$/mordenite mixtures exhibited a maximum conversion at an intermediate composition. This raises the possibility that mixtures of platinum-promoted anion-modified catalysts and certain zeolites may give high selectivies to desired transportation fuels.
- ★ Small amounts of $Pt/WO_3/ZrO_2$ may, when added to zeolites, provide a means of activating the zeolites at lower temperatures and pressures.
- ★ Lower hydrogen pressure results in higher conversion and higher cracking rate.

References:

[1] M. Y. Wen, I. Wender and J. W. Tierney, *Energy & Fuels*, **4**, 372 (1990).

[2] K. R. Venkatesh, J. Hu, W. Wang, G.D Holder, J. W. Tierney and I. Wender, *Energy & Fuels*, **10**, 1163 (1996).

[3] D.G. Barton, S. L. Soled, J. D. Meitzner, J. A. Fuentes and E. Iglesia, *Journal of Catalysis,* **181**, 57 (1999).

[4] A. Sayari and J. Dicko, *Journal of Catalysis*, **145**, 561 (1994).

[5] T. Shishido, T. Tanaka and H. Hattori, *Journal of Catalysis*,**172**, 24 (1997).

[6] S. Zhang, Y. Zhang, J.W. Tierney and I. Wender, *Applied Catalysis A: General*,**193**,155 (2000).

[7] S. Zhang, Y. Zhang, J.W. Tierney and I. Wender, *Fuel Processing Technology*, **69** (2001).

[8] Z. Zhou, Y. Zhang, J.W. Tierney and I. Wender, "Conversion of Fischer Tropsch Waxes over Modified Zirconia Catalysts," Pittsburgh-Cleveland Catalysis Society Spring Meeting, May 10 (2002).

Synthesis of Hydrocarbons and Alcohols From Syngas

Lawrence Norcio, Andrew O'Palko, Edwin L. Kugler, and Dady B. Dadyburjor
West Virginia University

Introduction

The synthesis of mixed alcohols has drawn considerable attention due to the phase-out of lead antiknock compounds from gasoline fuels. With the recent restrictions on using methyl-*tert* – butyl-ether as a fuel additive, research on the development of active and selective catalysts is now geared toward the synthesis of high-molecular-weight alcohols (higher alcohols, C_{2+} OH). These alcohols are viewed as desirable fuel additives because they improve octane and reduce engine emissions. Moreover, mixtures of higher alcohols are preferable because of their low volatility, necessary for the fuel to meet gasoline vapor-pressure specifications.

Molybdenum-based catalysts have been found to be active for the production of higher alcohols. The Dow Chemical and the Union Carbide research groups discovered that molybdenum sulfide catalysts promoted by alkali metal compounds are active for the production of C_1 to C_5 alcohols [1-3]. Klier and co-workers had also studied alcohol synthesis with alkali-metal-doped unsupported molybdenum sulfide catalysts [4]. However, alkali-promoted sulfide catalysts form products that contain 15-20% hydrocarbons [5]. Liu *et al*. [6] screened a series of vapor-phase-synthesized molybdenum sulfide catalysts for the production of alcohols from syngas. These materials were found to have high activity for higher alcohols when promoted with alkali. Liu *et al*. also discovered that increasing the reaction temperature not only changes the selectivity toward higher alcohols but also changes the selectivity toward hydrocarbons.

The earlier studies on molybdenum-based catalysts were mostly focused on unsupported materials. The catalytic performance of a series of supported molybdenum-based catalysts was investigated by Li *et al*. [7]. They reported that, when promoted with potassium, these supported catalysts increase the space-time yield of total alcohols. Furthermore, the addition of potassium suppresses the production of methanol and favors the production of higher alcohols.

Our laboratory has shown that good alcohol synthesis performance can be obtained with molybdenum-based catalysts. The addition of Ni and K to these catalysts improves their performance considerably for higher alcohol synthesis. These catalysts generally need to be reduced prior to reaction. The effects of impregnation order as well as the effects of calcination were also found to be significant. Results from previous study [8] show that the calcined Mo-Ni-K/C catalyst should be a superior higher-alcohol synthesis catalyst.

More recently, the benefits of synthesizing both hydrocarbons and alcohols in one step have been observed. This will result in better Fischer-Tropsch diesel fuel. By careful manipulation of catalyst formulation, this should be achieved.

The work described in this report focuses on the parametric study performed on the calcined Mo-Ni-K/C catalyst. The effects of reaction temperature, H_2/CO ratio, and contact time on the productivity of alcohols have been examined. The preliminary results from the screening of tungsten-based catalysts prepared in our laboratory are also presented.

Methodology

The incipient-wetness technique of Ref. 8 was used in the preparation of the Mo-Ni-K/C catalyst. Mo was impregnated first onto the carbon, followed by Ni and then K. Each impregnation procedure was followed by drying in air at 95°C overnight, and calcining in flowing nitrogen for two hours. The calcination temperatures used were: 500°C for Mo, and Ni, and 300°C for K. Typically, 0.5 g of catalyst was used for catalyst testing.

Reactivity studies were carried out in a computer-controlled reactor system. Catalysts were reduced in flowing H_2 at atmospheric pressure and 400°C for 12-15 hours. The gas flows were maintained at 750 psig. Gas products were analyzed on-line every two hours using gas chromatography (GC). The liquid product is collected every 24 hours and is analyzed separately for water and alcohols.

Results

Effect of Reaction Temperature

The effect of reaction temperature on the performance of calcined Mo-Ni-K/C (18wt.% Mo loading) catalyst has been investigated. The reactor was run isothermally at reaction temperatures 250, 300, and 350°C. The operating conditions were set at H_2 = 25 scc/min, CO = 25 scc/min (H_2/CO = 1), P = 750 psig, and gas hourly space velocity (GHSV) = 6 sm^3/h/kg-catalyst. The increase in alcohol productivity is accompanied by an increase in hydrocarbon productivity. Figure 1 shows that increasing the reaction temperature increases the space-time yields of both total alcohols and hydrocarbons. Thus, the selectivity to total alcohols decreases as the reaction temperature increases.

Effect of Contact Time

The effect of contact time was investigated by increasing the amount of catalyst to 9 grams while maintaining the hydrogen and carbon monoxide flow at 25 scc/min each. The GHSV significantly decreased to 0.3 sm^3/h/kg-cat. The reactor was run isothermally at 250, 300, and 350°C at a reactor pressure of 750 psig. At the highest temperature tested (350°C), the liquid product collected contains two phases. GC analysis revealed that the water phase contains mostly water and small amounts of alcohols. The organic phase contains many unidentifiable peaks and some alcohols. This implies that, given a very long retention time and a very high reaction temperature, side reactions are taking place.

At lower reaction temperatures (250° and 300°C), single-phase liquid products are collected. Figure 2 shows that the space-time yield of total alcohols decreases when the GHSV is decreased. The selectivity to total alcohols also decreases with decreasing GHSV. The results indicate that short contact times (or high GHSVs) favor production of alcohols while long contact times (or low GHSVs) favor formation of hydrocarbons and other side reactions.

Effect of H_2/CO ratio

A series of experiments was performed to investigate the effect of H_2/CO ratio on alcohol synthesis. The intermediate reactor temperature of 300°C was selected for this series, so as to have significant amounts of both total alcohols and hydrocarbons.

There is a slight decrease in the selectivity to C_2-C_6 alcohols with increasing partial pressure of hydrogen. The selectivities are all less than 50% -- the space-time yield of hydrocarbons is greater than the space-time yield of total alcohols. Figure 3 shows that increasing the partial pressure of hydrogen increase both the space-time yield of total alcohols and the space-time yield of hydrocarbons.

There is a significant increase in the selectivity to total alcohols, as well as selectivities of C_2-C_6 alcohols, with increasing partial pressure of carbon monoxide. The selectivities to alcohols are all greater than 50% when the partial pressure of carbon monoxide is greater that 200 psig. This is true because the space-time yield of hydrocarbons is less than the space-time yield of alcohols as shown in Figure 4.

The results presented above demonstrate the strong effect of H_2/CO ratio on higher- alcohol synthesis. Figure 5 reveals that higher H_2/CO ratios will increase the formation of methanol and will decrease the formation of higher alcohols. The formation of higher alcohols is inhibited by the increase in partial pressure of hydrogen.

Tungsten on Carbon Catalyst

A series of carbon-supported tungsten-based catalysts was prepared in our laboratory and tested for hydrocarbon and alcohol synthesis activity from syngas. An activated-carbon support containing 18 wt-% tungsten was prepared by incipient wetness technique from sodium metatungstate. The catalysts were normally reduced with flowing hydrogen at 400°, 500°, and 600°C. The reactor was run from 200°C to 400°C at the rate of 10°C/h. Temperature-programmed reduction (TPR) and X-ray diffraction (XRD) were used to characterize the prepared catalysts.

Results show that the tungsten-on-carbon catalyst (W/C) from the sodium metatungstate source, gives the highest CO conversion when reduced at 600°C. Maximum space-time yields obtained for total hydrocarbons and total alcohols are 1953 g/h/kg-catalyst and 98 g/h/kg-catalyst, respectively. Figure 6 shows the characteristic activity of a W/C catalyst as the temperature is progressively increased. Typically, the catalytic activity is highest at 400°C, which is the maximum reaction temperature tested.

It was felt that presence of sodium could be holding back the performance of the catalyst. Accordingly, two modifications were made. In one, the catalyst prepared from the sodium metatungstate was washed with distilled water. This would remove any residual sodium left after its preparation. In the other modification, ammonium tungstate was used as the source of tungsten.

Table 1 shows the summary of results of the W/C catalyst. The washed W/C catalyst from the sodium metatungstate source has significantly lower catalytic activity than that of the unwashed catalyst. Maximum space-time yields obtained for total hydrocarbons and total alcohols are 184 g/h/kg-catalyst and 105 g/h/kg-catalyst, respectively.

The W/C catalyst from the ammonium tungstate source, when reduced at 600°C gives a very low CO conversion. Maximum space-time yields obtained for total hydrocarbons and total alcohols are 180 g/h/kg-catalyst and 104 g/h/kg-catalyst, respectively. Since the catalytic activity observed when reduced at 600°C is very low, it was felt that no benefit would accrue from reducing at 400° or 500°C. Hence data at those reduction temperatures were not obtained.

The W/C catalyst from both the sodium metatungstate and the ammonium tungstate sources, when doped with potassium, gives low CO conversion. The addition of potassium to the catalyst decreases its catalytic activity compared to that without potassium.

Summary of Results

The production of mixed alcohols from synthesis gas was studied over Mo-Ni-K/C catalysts. The effect of reaction temperature, H_2/CO ratio, and contact time has been investigated. Increasing the reaction temperature increases the space-time yield of total alcohols. However, the increase in reaction temperature also increases the production of hydrocarbons.

Decreasing the GHSV decreases the space-time yield of total alcohols and increases the space-time yield of hydrocarbons. It is concluded that short contact times (or high GHSVs) favor production of alcohols, while long contact times (or low GHSVs) favor formation of hydrocarbons and other side reactions.

The H_2/CO ratio is a key- parameter to control the productivity of higher alcohols. Increasing the H_2/CO ratio increases production of methanol and decreases production of higher alcohols. Increasing the H_2/CO ratio also increases the space-time yield of hydrocarbons. Conversely, the increase in carbon monoxide concentration on the feed stream decreases the space-time yield of hydrocarbons and increases the productivity of total alcohols.

W/C from the sodium metatungstate source shows very high catalytic activity while W/C from the ammonium tungstate source shows very low catalytic activity. The addition of potassium to the catalyst decreases its catalytic activity compared to that without potassium.

References

1. G. J. Quarderer, K. A. Cochran, European Patent 0,119,609 (1984).
2. R.R. Stevens, European Patent 0,172,431 (1986).
3. N.E. Kinkade, European Patents 0,149,255 and 0,149,256 (1985).
4. K. Klier, R. G. Herman, G. W. Simmons, C. E. Lyman, J. G. Santiesteban, M. Najbar, R. Bastian, Final Technical Report DOE/PC/80014-T1, Contract No. DE-AC22-85PC80014 (1988).
5. R. G. Herman, Catalysis Today 55 (2000) 233.
6. Z. Liu, X. Li, M. R. Close, E. L. Kugler, J. L. Petersen, D. B. Dadyburjor, Ind. Eng. Chem. Res. 36 (1997) 3085.
7. X. Li, L. Feng, Z. Liu, B. Zhong, D. B. Dadyburjor, E. L. Kugler, Ind. Eng. Chem. Res. 37 (1998) 3853.
8. E. L. Kugler, D. B. Dadyburjor, L. Feng, and X. Li., Studies in Surface Science and Catalysis, 130 (2000), 299.

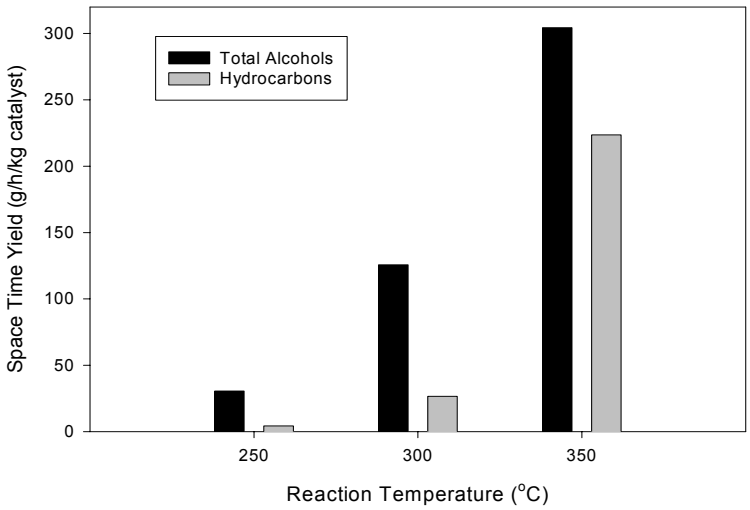

Figure 1. Effect of Reaction Temperature on the Space Time Yield of Total Alcohols and Hydrocarbons Observed over Mo-Ni-K/C Catalyst. Operating Conditions: H_2/CO=1; P=750psig; GHSV=6sm^3/h/kg catalyst.

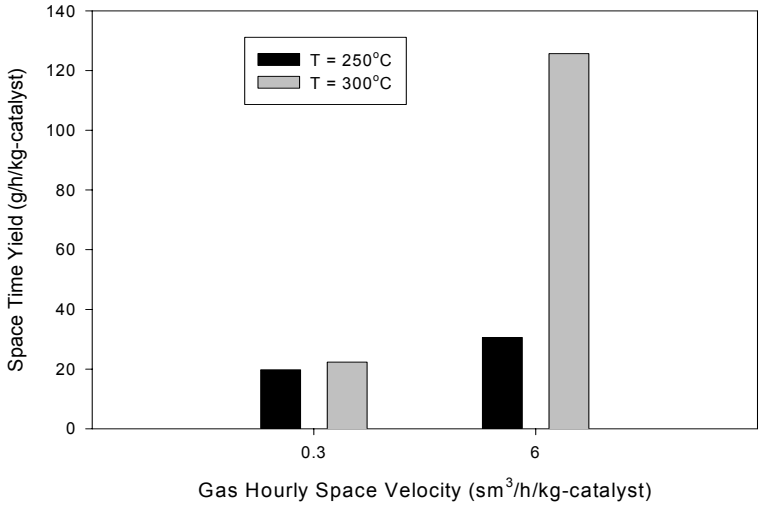

Figure 2. Effect of GHSV on the Space-Time Yield of Total Alcohols over Mo-Ni-K/C Catalyst. Operating Conditions: H_2/CO=1; P=750psig.

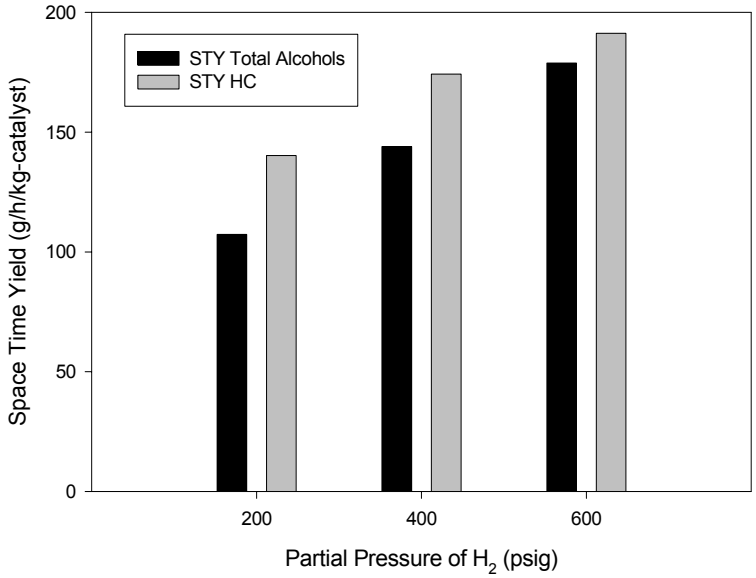

Figure 3. Effects of Partial Pressure of Hydrogen on the Space Time Yield of Alcohols and Hydrocarbons (P_{CO}=200psig).

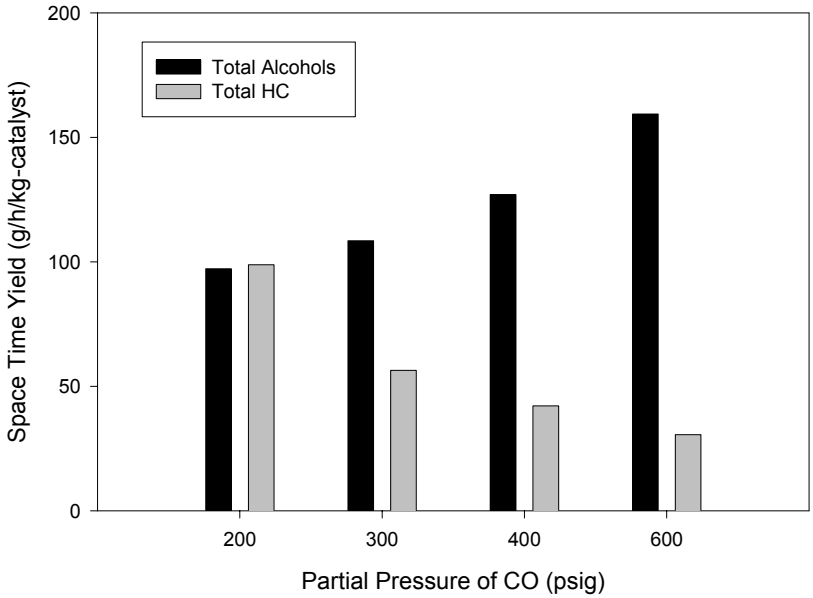

Figure 4. Effects of Partial Pressure of CO on the Space Time Yield of Alcohols and Hydrocarbons (P_{H2}=200psig).

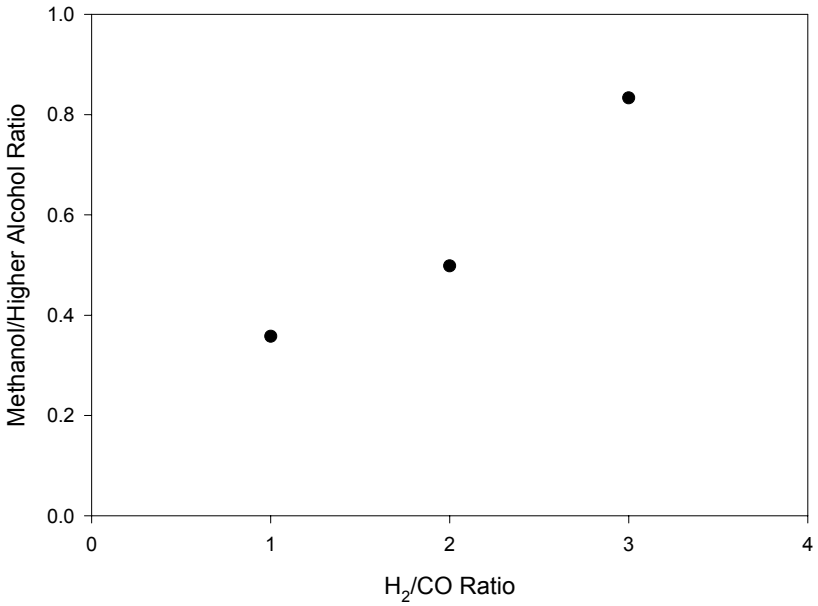

Figure 5. Effects of H_2/CO Ratio on Methanol/Higher Alcohol Ratio

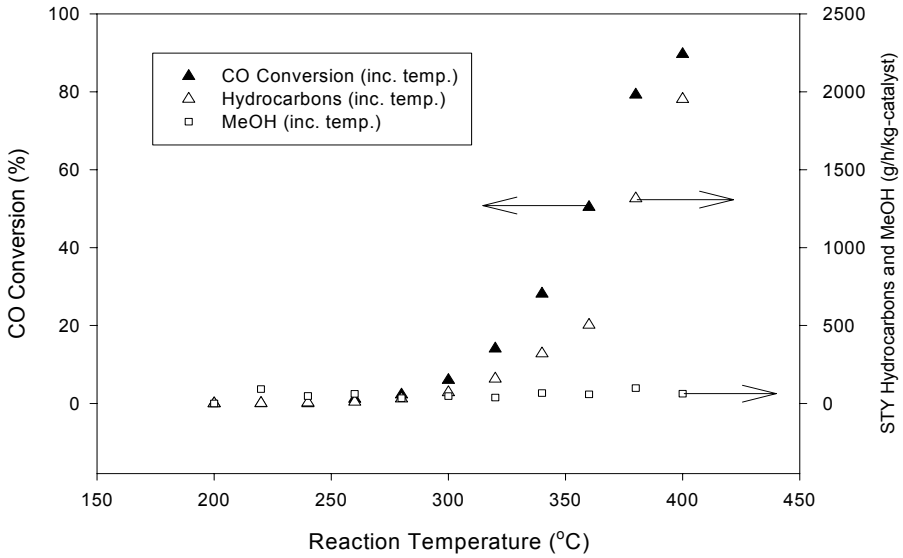

Figure 6. Activity of Calcined W/C Catalyst (18% wt. W; source: Sodium Metatungstate). Reaction Conditions: 0.51g of catalyst; P = 750 psig; flow rate of CO and H_2 = 25 cm^3 (STP)/min each. Pre-treatment: H_2= 50 cm^3 (STP)/min; temp-prog. to 600°C.

Table 1. Summary of Catalytic Experiments and Results of Tungsten-on-Carbon Catalyst (18 wt.% W Loading).

Run No.	Catalyst	Source*	Reduction Temperature (°C)	CO Conversion (%)	STY Hydrocarbons (g/h/kg-cat.)	STY MeOH (g/h/kg-cat.)
23	W/C (calcined)	SM	400	18	160	0
24	W/C (calcined)	SM	500	84	1017	80
25	W/C (calcined)	SM	600	90	1953	98
26	W-K/C (calcined)	SM	400	24	233	75
27	W-K/C (calcined)	SM	500	20	105	80
29	W-K/C (calcined)	SM	600	20	100	120
31	W/C (calcined)	AT	600	27	180	104
33	W-K/C (calcined)	AT	600	9	30	56
34	Washed W/C (calcined)	SM	600	29	184	105

*SM – sodium metatungstate
AT – ammonium tungstate

Hydrogen and Nanotube Production by Catalytic Decomposition of Ethane

Naresh Shah[1], Devadas Panjala[2], and Gerald P. Huffman[1]
[1]University of Kentucky, [2]Conoco-Phillips Research Laboratory

Introduction

The demand for hydrogen is expected to increase significantly over the next several years. This is due both to EPA regulations requiring more severe hydro-desulfurization of petroleum-based fuels in refineries and to the need for pure hydrogen to power fuel cells in automotive and power generation applications. Traditionally, hydrogen has been produced by reforming or partial oxidation of hydrocarbons to produce synthesis gas, followed by the water-gas shift reaction to convert CO to CO_2 and produce more hydrogen, followed by further purification reactions and/or separation procedures to reduce CO to levels tolerable by the catalysts used in fuel cells (~10 ppm or less). Non-oxidative, catalytic decomposition of hydrocarbons is an alternative, single-step process to produce pure hydrogen.

In our previous research in the CFFS C1 chemistry program, nanoscale, binary Fe-based catalysts supported on high surface area alumina (Fe-M/Al_2O_3, M=Mo, Pd or Ni) were shown to have high activity for the catalytic decomposition of undiluted methane into pure hydrogen and carbon nanotubes [(1)]. In continuing work on this project we are investigating the catalytic dehydrogenation of a variety of higher hydrocarbons. Ethane, a constituent of natural gas, a byproduct of cracking and fractional distillation of petroleum, and one of the light products of Fischer-Tropsch synthesis can also serve as a hydrocarbon feed stock to produce pure hydrogen. In work conducted in the past year (2001-2002) on this project, the activity of the same binary catalysts for the catalytic cracking of undiluted ethane was investigated.

Experimental Section

Supported catalysts were prepared by first adding an aqueous solution of appropriate catalyst metal salts ($Fe(NO_3)_3 \cdot 9H_2O$, $(NH_4)_6Mo_7O_{24} \cdot 4H_2O$, $Pd(NO_3)_2 \cdot xH2O$ and $Ni(NO_3)_2 \cdot 6H_2O$) in the desired proportions to a slurry of γ-alumina (150 m^2/g) and then precipitating the metal oxyhydroxide on alumina by raising the pH of the slurry with ammonia. The slurry was washed with distilled water, dewatered to form a paste, and extruded. The composition of the binary metal catalysts, M-Fe (M = Mo, Pd or Ni) was 0.5 wt % M and 4.5 wt % Fe with respect to the alumina support.

The reactions were carried out in a fixed-bed, plug-flow quartz reactor [(1)]. Prior to reaction, the catalysts were reduced in flowing hydrogen (50 mL/min) for 2 h at 700 ^oC. After reduction, the reactor was flushed with an inert gas until the GC showed no residual hydrogen peak (~15 min). Undiluted ethane was then fed to the reactor and the reaction products were measured as a function of temperature and time.

Results and Discussion

The product distributions of thermal and catalytic cracking of ethane using a (0.5%Pd-4.5%Fe)/γ-Al_2O_3 catalyst are shown in Figures 1 and 2, respectively. It can be seen that the catalytic route leads to increased hydrogen production and a significant decrease in ethane decomposition temperature relative to thermal decomposition. High methane formation at

relatively low temperatures (450-500 ^{o}C) precedes high hydrogen production, which plateaus at ~650-825 °C. Similar trends were observed for the other bimetallic catalysts (0.5%Ni or Mo-4.5%Fe)/γ-Al_2O_3. Thermal cracking, on the other hand, produces a significant amount of ethylene compared to catalytic cracking, where it is practically non-existent.

Figure 3 compares the observed hydrogen concentrations as a function of temperature for the different catalysts used, each subjected to a reduction pre-treatment at 700 ^{o}C. It is evident that the catalysts lower the temperature of ethane cracking significantly compared to thermal cracking over the alumina support. The three bimetallic catalysts show similar trends and are all more active for hydrogen production than the monometallic iron catalyst.

Time on stream studies were carried out to determine the loss of activity of the various catalysts over time. Figure 4 shows the observed behavior at a temperature of 650 ^{o}C. The activities of the bimetallic catalysts at 650 ^{o}C did not show any appreciable decay out to a reaction time of 4 hours.

HRTEM showed that multi-walled carbon nanotubes were grown by catalytically decomposing undiluted ethane. At 650°C, the multi-walled nanotubes (MWNT's) were predominantly concentric parallel-walled cylinders. However, at 500 °C, the MWNT's grown over the 0.5%Mo4.5%Fe/γ-Al_2O_3 catalyst exhibit an interesting nested cone structure that resembles stacked traffic cones (Figure 5).

Summary and Future Work

Binary Fe-M/Al_2O_3 (M = Mo, Ni, and Pd) catalysts have been shown to very active effective for the decomposition of ethane, just as they are for methane. Catalytic decomposition of ethane to both methane and hydrogen begins at a temperature of only about 400 °C. Methane production peaks at about 80% at ~475 °C, then decreases to 10-15% at ~650 °C, while hydrogen production rises to ~ 80-90% and maintains that level out to about 850 °C (Figures 2 and 3). The open structure of these "traffic cone" nanotubes appears promising for hydrogen storage and this will be investigated in collaboration with Dr. Brad Bockrath of the NETL. These results were presented at the 2002 fall meeting of the American Chemistry Society in Boston [(2)]. A detailed paper is in preparation.

Other work planned for the future includes catalytic dehydrogenation of several higher hydrocarbons, including cycloalkanes, isoalkanes, and Fischer-Tropsch fuels.

References

1. Shah, N.; Panjala, D.; Huffman G. P. *Energy & Fuels,* **2001***, 15(6),* 1528-34.
2. Shah, N.; Panjala, D.; Huffman G. P. *ACS Fuel Chemistry Division Preprints,* **47(2)** (2002) 782-783.

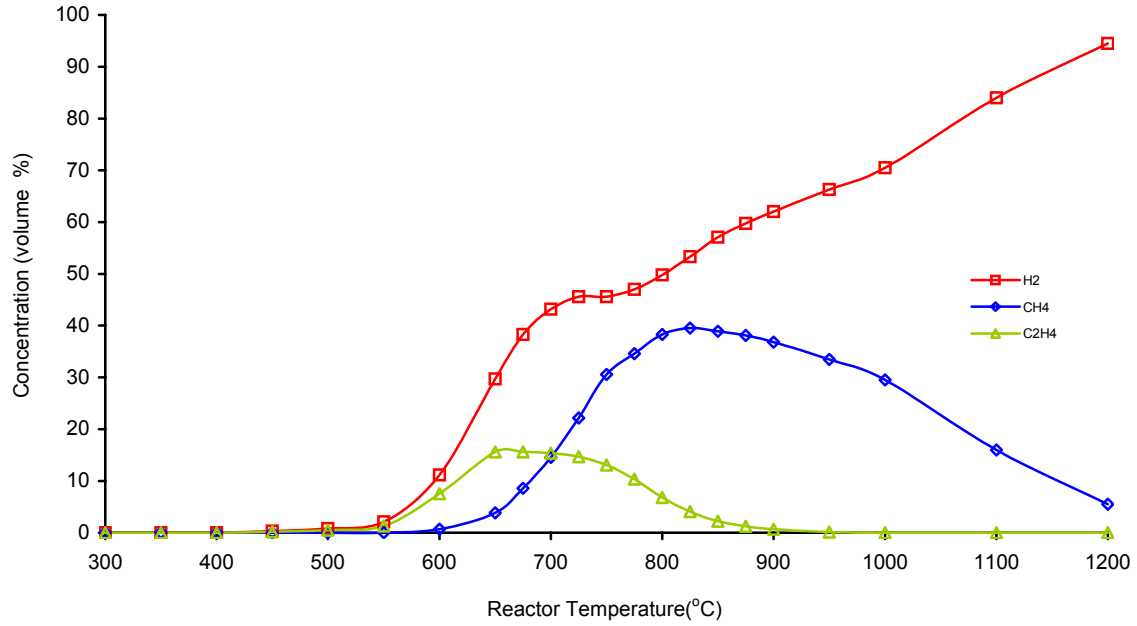

Figure 1. Product distribution of thermal cracking of ethane.

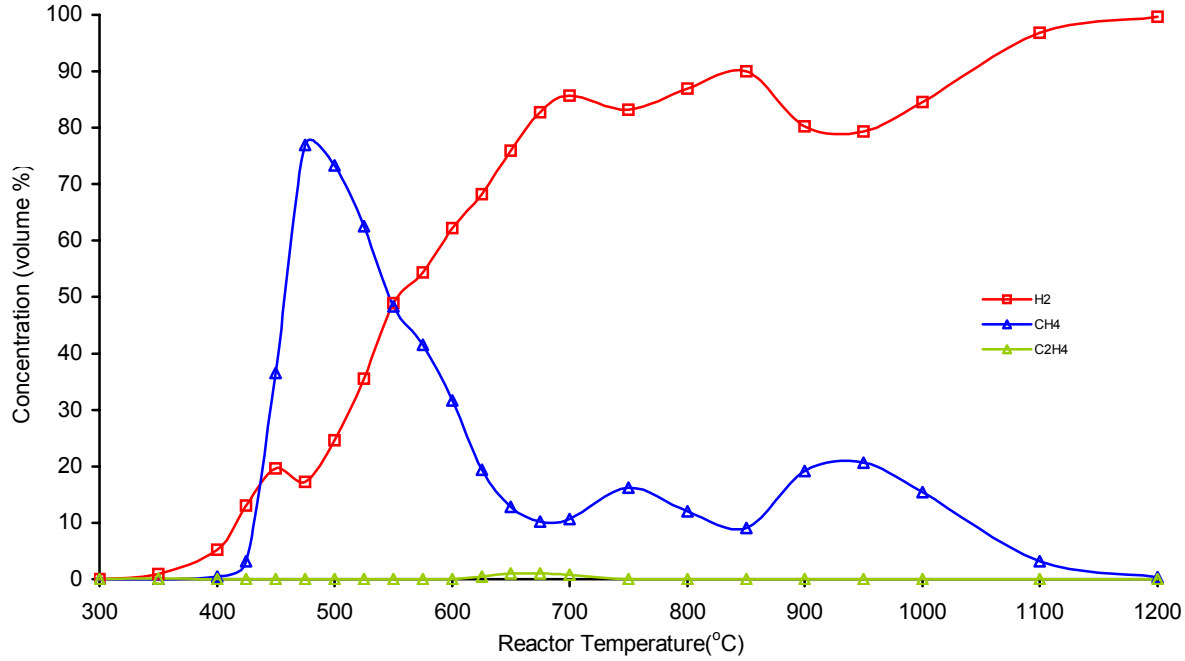

Figure 2. Product distribution of catalytic cracking of ethane, 0.5%Pd4.5%Fe/γ-Al2O3.

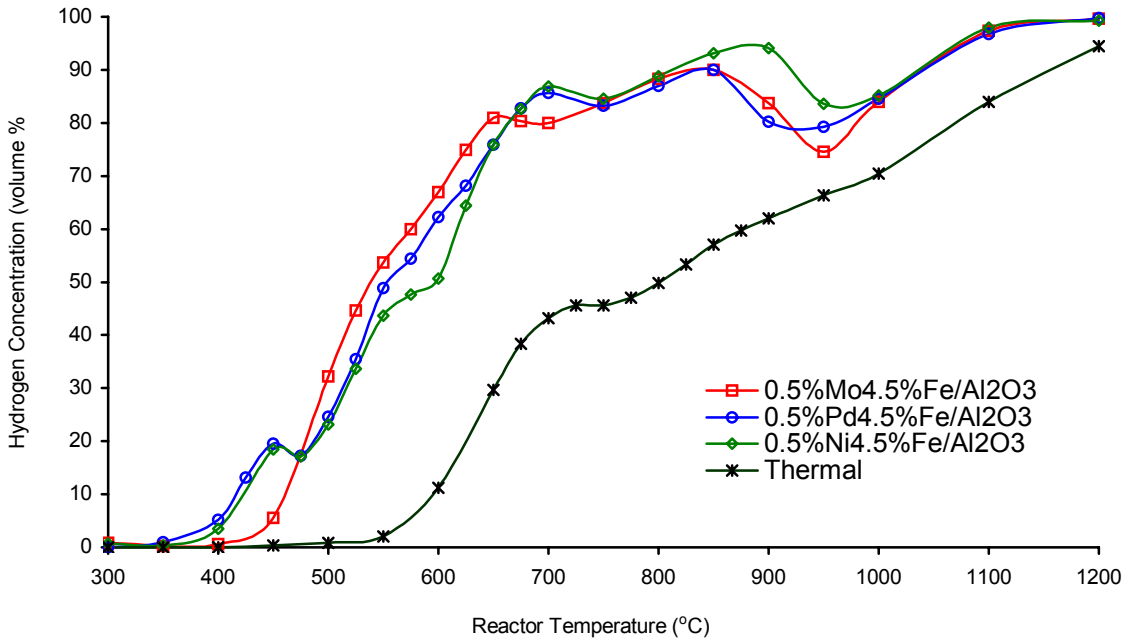

Figure 3. Comparison of hydrogen production by catalytic cracking of ethane using several binary catalysts to hydrogen production by thermal decomposition of ethane.

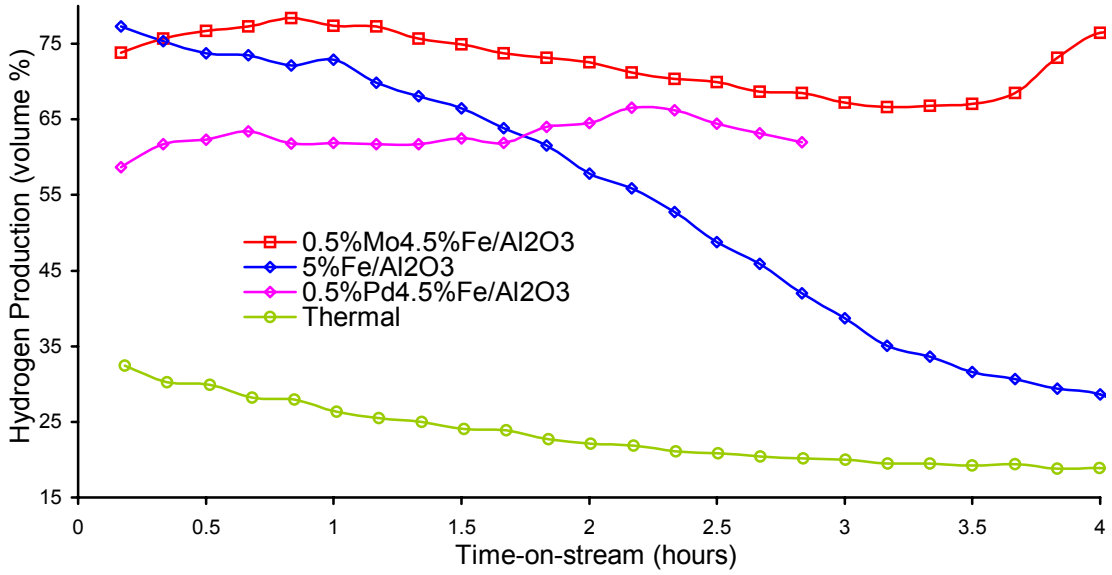

Figure 4. Time-on-Stream at a reactor temperature of 650 oC.

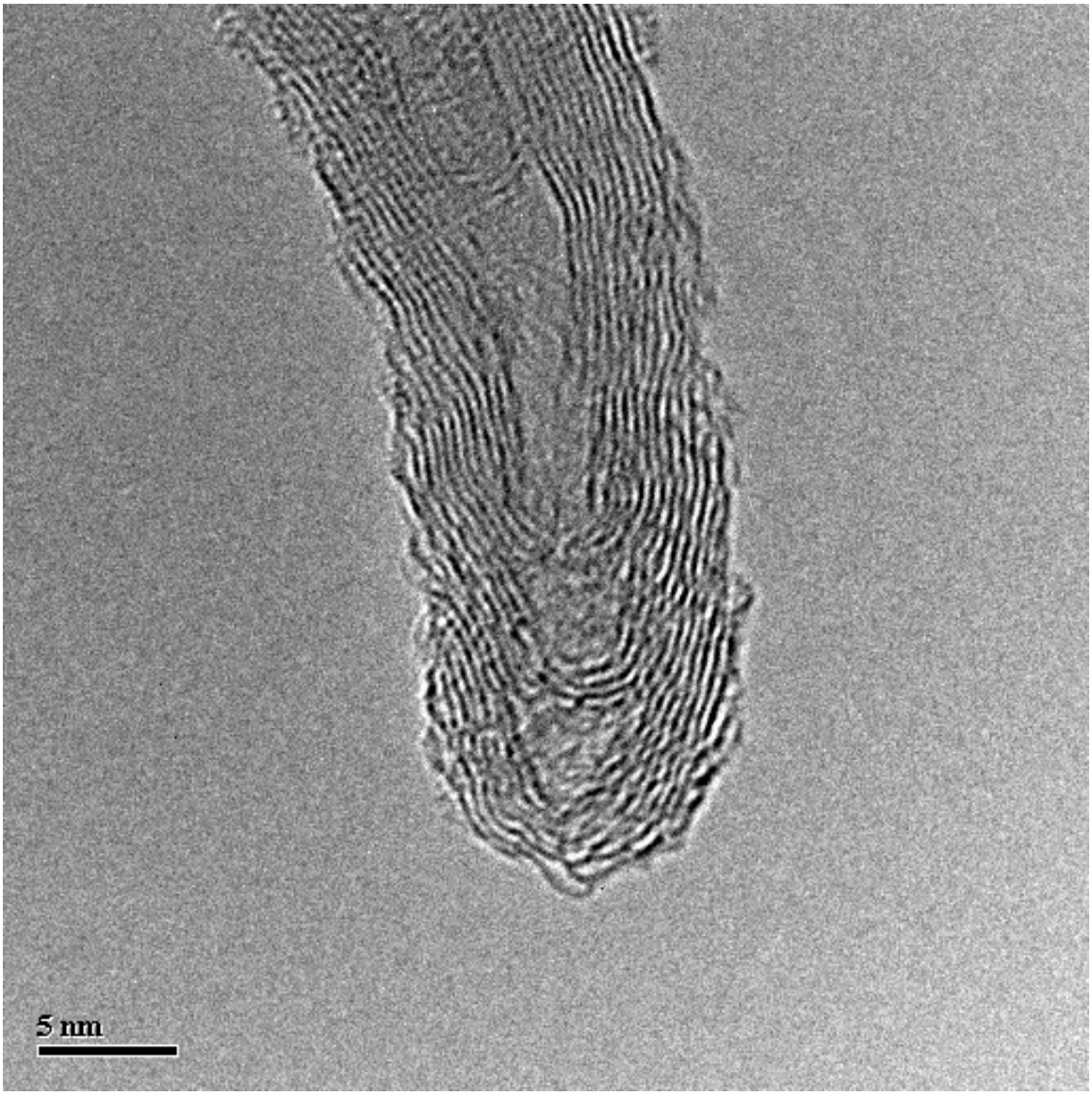

Figure 5. HRTEM image of multiwalled carbon nanotubes grown by decomposing undiluted ethane at 500 °C over 0.5%Mo4.5%Fe/γ-Al_2O_3 pre-reduced at 700 ^oC.

Structure of Supported Binary Fe-Based Catalysts Used for Non-Oxidative Dehydrogenation of Methane and Other Hydrocarbons

Naresh Shah[1], Frank E. Huggins[1], Devadas Panjala[2], S. Pattanaik[3], and Gerald P. Huffman[1]
[1]University of Kentucky, [2]Conoco-Phillips Research Laboratory, [3]Eastern Kentucky University

Introduction

As discussed elsewhere in this report, nanoscale, binary Fe-based catalysts supported on high surface area alumina (Fe-M/Al_2O_3, M=Mo, Pd or Ni) have been shown to have high activity for the catalytic decomposition of undiluted methane and ethane into pure hydrogen and carbon nanotubes [(1,2)]. The current report focuses on the structure of these catalysts and the catalytic mechanisms responsible for their activity. The analytical techniques employed for this investigation included x-ray absorption fine structure (XAFS) spectroscopy, Mössbauer spectroscopy, and scanning transmission electron microscopy (STEM).

Results and Discussion

A complete summary of the results and experimental procedures used in this part of the investigation has been given in a forthcoming paper [(3)]. Therefore, in this report we will present only a brief summary of our results on catalyst structure. This should be sufficient to present our principal conclusions regarding catalytic mechanisms.

As discussed elsewhere in this report and in the literature [(1, 2)], the catalysts were prepared by precipitating the metals from solution onto gamma-alumina in an oxyhydroxide form, dewatering, extruding and drying the resulting paste, pre-reducing at 700 °C in flowing hydrogen, than carrying out the decomposition of either methane or ethane over a range of temperatures. To investigate the catalyst structures, XAFS spectroscopy, Mössbauer spectroscopy, and STEM measurements were made on all three supported binary catalysts in their as-prepared state, after pre-reduction, and after time on stream (TOS) in methane for several hours at 700 °C.

Figures 1 shows STEM images and x-ray maps of an (0.5% Mo – 4.5% Fe)/Al_2O_3) catalyst after approximately seven hours TOS. From the images and maps, it is evident that the catalyst particles are indeed binary, since the Fe and Mo are clearly shown by the maps to be in the same places on the alumina support. It is also seen that the particles remain quite small after reaction, with mean diameters of ~20-30 nm.

Radial structure functions (RSF) derived from the Ni K-edge XAFS spectra for the (0.5%Ni-4.5%Fe)/Al_2O_3 catalyst in the as-prepared, pre-reduced, and TOS states are shown in Figure 2. The peaks in the RSF represent shells of atoms surrounding the absorbing atoms. In the as-prepared catalyst, the strongest RSF peak is due to the nearest-neighbor (nn) oxygen shell. After pre-reduction, this peak is somewhat weakened and new peaks corresponding to metal shells begin to appear. Finally, after several hours TOS, the RSF strongly resembles the RSF of Ni metal, which is a fcc structure. The ^{57}Fe Mössbauer spectrum of this sample, however, reveals that the fcc structure is not Ni metal, but an Fe-Ni austenite. On the basis of the percentage of Fe contained in this phase, we conclude that the approximate composition of this phase is 75% Fe – 25% Ni. This places the phase squarely in the Fe-Ni γ-field [(4)]. However, since C has good solubility in austenite [(5)], it is likely that the phase is an Fe-Ni(C) austenite containing several

percent of C. As discussed in detail in a forthcoming paper, similar results were obtained for the supported Fe-Pd and Fe-Mo catalysts.

Summary and Conclusions

Binary nanoscale Fe-M/Al_2O_3 (4.5%Fe-0.5%M, M=Mo, Ni, or Pd) catalysts have been shown to be much more effective in producing hydrogen by non-oxidative decomposition of methane than the individual metal catalysts [(1)]. STEM clearly established that the catalysts are binary in nature. To understand the synergistic behavior of the two metals in these supported catalysts, they were analyzed using XAFS and Mössbauer spectroscopy in their as-prepared, pre-reduced and after reaction (TOS) states. The results of these catalyst characterization studies are briefly summarized below.

1. Following pre-reduction in hydrogen at 700 ºC, most of the Fe (60-70%) is present as hercynite ($FeAl_2O_4$).
2. The secondary element significantly enhances the reducibility of the catalysts in the approximate order: Fe < Fe-Mo < Fe-Ni < Fe-Pd.
3. For both the Fe-Ni and Fe-Pd catalysts, the dominant metallic phase is an austenitic alloy containing approximately 70-75% of Fe and 25-30% of Ni or Pd. It is likely that several percent of C are incorporated into the austenite in interstitial positions during reaction in methane. For Fe-Mo, an intermetallic Fe_2Mo phase is formed during reduction that probably becomes mixed with an Fe-Mo-C austenite during reaction. These nonmagnetic* alloys are believed to be the active phases.

These conclusions suggest that the key factors that account for the high activity and comparatively long lifetimes of these catalysts are:

★ Binding of the catalyst particles to the alumina support by the formation of hercynite, preventing deactivation by demetallization.

★ Dehydrogenation of methane with simultaneous formation of carbon nanotubes, which grow away from the surfaces of the bound, nonmagnetic, Fe-M-C alloy catalyst nanoparticles, preventing deactivation by coking.

References:

1. N. Shah, D. Panjala, G.P. Huffman, *Energy & Fuels,* **15(6)**, (2001), 1528-34.
2. A Makuni, N. Shah, D. Panjala, and G. P. Huffman, *ACS Fuel Chem. Div. Preprints,* **47(2)** (2002) 782-783.
3. N. Shah, F. E. Huggins, Sidharta Pattanaik, D. Panjala, and G. P. Huffman "XAFS and Mössbauer spectroscopy characterization of supported binary catalysts for non-oxidative dehydrogenation of methane", to be published in a special issue of *Fuel Processing Technology* on C1 chemistry, edited by Christopher Roberts.
4. Max Hansen and Kurt Anderko, Constitution of Binary Alloys (McGraw-Hill Book Co., 1958).
5. Lawrence S. Darken and Robert W. Gurry, Physical Chemistry of Metals (McGraw-Hill Book Co., Inc., 1953).

* Nonmagnetic means "not magnetically ordered". These phases are probably paramagnetic.

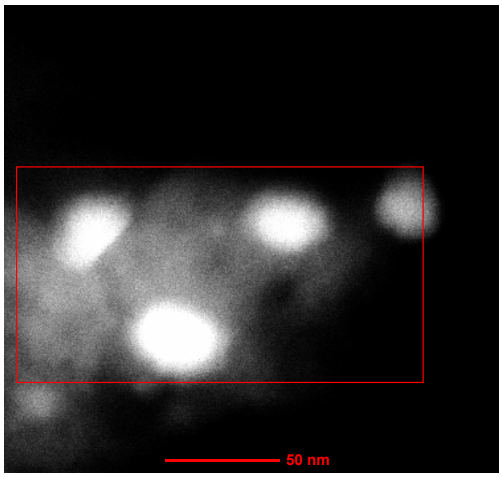

STEM Image

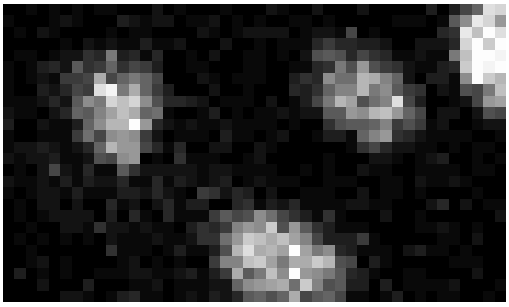

Fe K map

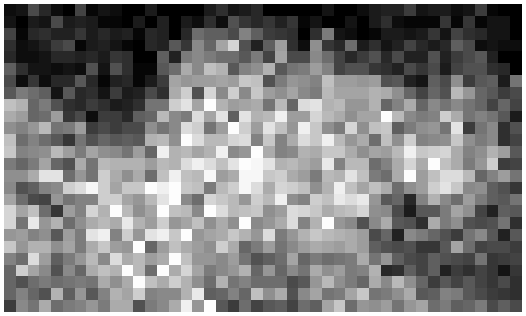

Al K map

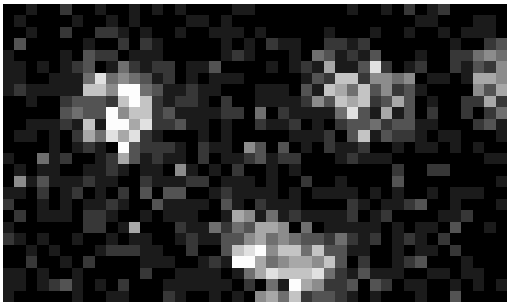

Mo K map

Figure 1. STEM images and x-ray maps for Al, Fe, and Mo clearly show that Fe-Mo alloy catalyst phases are formed.

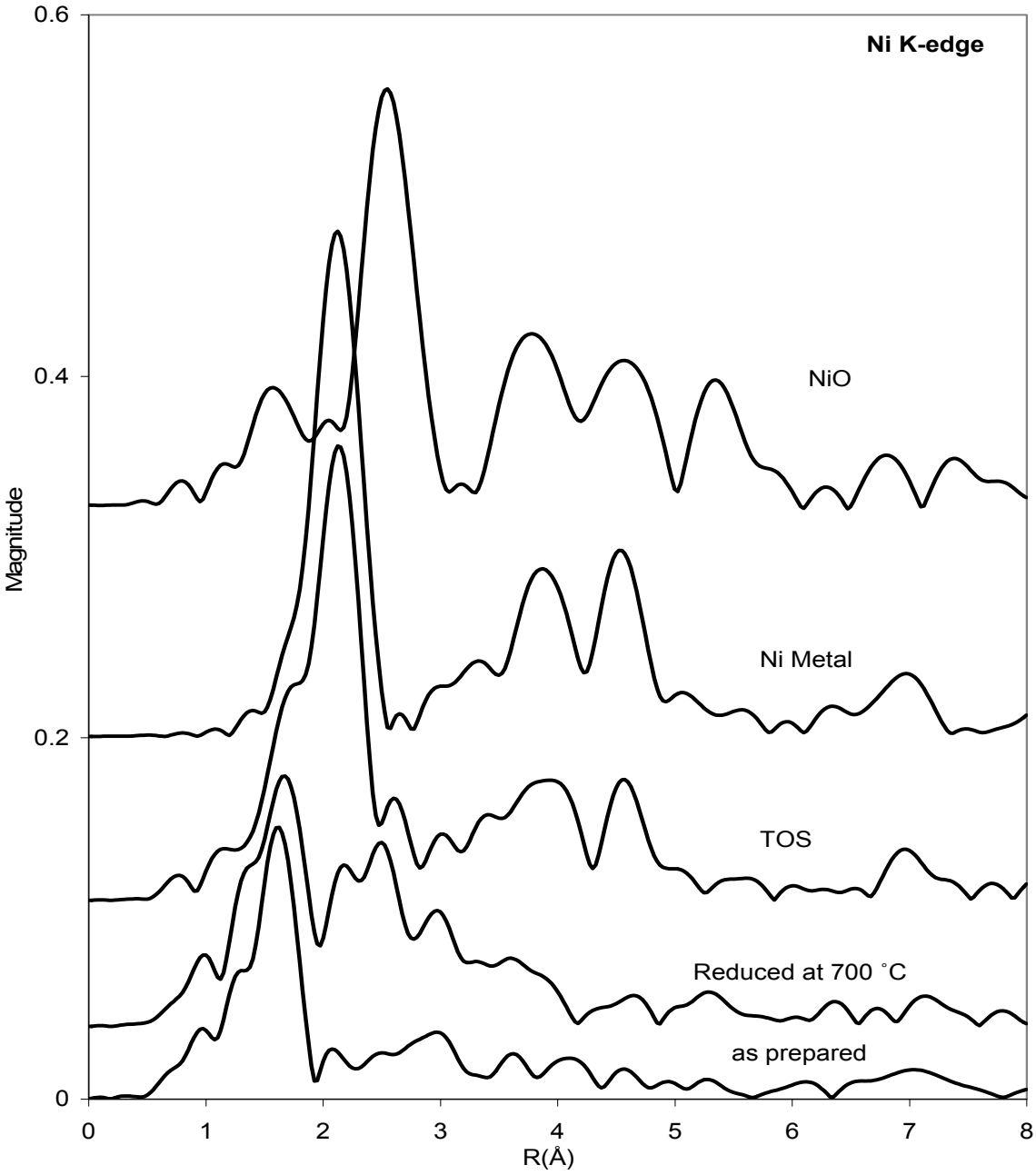

Figure 2. Ni K-edge radial structure functions of 0.5%Ni-4.5%Fe/ Al_2O_3 catalysts before and after various treatments.

Dry Reforming of Methane To Synthesis Gas With Tungsten Carbide Catalyst

Mahesh V. Iyer, Lawrence Norcio, Huifang Shao, Edwin L. Kugler, and Dady B. Dadyburjor
West Virginia University

Introduction

Reserves of natural gas exceed those of crude oil by a considerable margin (1). Natural gas contains 70 to 98 % methane. Existing industrial processes use methane as a primary feedstock for producing a mixture of carbon monoxide and hydrogen, called synthesis gas (syngas). Syngas serves as the feedstock for a variety of downstream processes, such as methanol synthesis, Fischer-Tropsch synthesis or ammonia synthesis (2-5). Reducing the cost of syngas would play a significant role in the economics of the production of synthetic liquid fuels by, for example, the Mobil gas-to-liquids (GTL) process (4,6). Reforming of methane to syngas can be carried out in four different ways (2-4,7): steam reforming, dry reforming using carbon dioxide in place of water, partial oxidation using oxygen, and autothermal reforming using air. Of these, steam reforming:

$$CH_4 + H_2O \rightarrow CO + 3H_2$$

is the conventional process and produces syngas with high H_2/CO ratios. Dry reforming:

$$CH_4 + CO_2 \rightarrow 2\,CO + 2\,H_2$$

has been proposed as a promising technology due to the use of the greenhouse gas CO_2. Besides, dry reforming can be employed in those natural-gas fields where there is an abundance of CO_2 (7,8). Finally, dry reforming has been evaluated (4) to have the lowest operating costs, about 20 % lower than those of the other reforming processes.

Metal catalysts are suitable for methane reforming, with nickel-based catalysts preferred commercially over noble metals, due to the inherent availability and low costs of the former. However, nickel also catalyzes the formation of coke, unsaturated polyaromatic hydrocarbons with H/C ratios less than unity, via methane decomposition and/or CO disproportionation (2-4,7). Coke may form on the catalyst surface and/or the tubes of the reformer, and leads to deactivation of the catalyst and plugging of the tubes. Hence coke formation is one of the major problems associated with dry reforming using these catalysts (4,6).

There has been considerable interest in the catalytic properties of metal carbides. Metal carbides are abundant and may be effective enough to replace noble metals as catalysts. Carbides of molybdenum and tungsten, in particular, have been identified as “magic catalysts” for this millennium (8). Recently, there have been reports of application of these metal carbide catalysts for dry reforming of methane (8-13). These carbides are stable at elevated pressures and are moderately resistant to carbon deposition. However, addition of a second metal could result in improvements in activity and stability.

We have investigated the performance of cobalt tungsten carbide [Co_6W_6C] as a potential bimetallic carbide catalyst for the dry reforming of methane. The unsupported material was obtained from Nanodyne Inc. The performance of this catalyst is presented in this report. We are currently in the process of developing methods to prepare this unsupported Co_6W_6C catalyst. Preliminary results of this catalyst prepared in our laboratory are also presented.

Methodology

The unsupported cobalt tungsten carbide [Co_6W_6C] catalyst was obtained from Nanodyne Inc. and has a surface area of about 5 m^2/g. The differential reactor consists of a silica-lined stainless-steel tube placed in a single-zone furnace. The silica lining on the stainless tubes was applied at Restek Corp. The catalyst is placed in the center of the reactor, with the quartz chips placed upstream and downstream of the catalyst. The weight of the catalyst used was 0.3 g and the size was less than 38 μm. The product stream is sampled immediately downstream using a gas-sampling valve. There is a cooling system between the reactor outlet and the sampling valve. The products are analyzed on-line by a gas chromatograph (GC), which provides quantitative analysis for He, H_2, CO, CH_4, CO_2 and H_2O. Helium is used as the internal standard while argon serves as the carrier gas. The GC feed line from the sample loop is maintained at a temperature of 150 ^{0}C by wrapping the line with heating tapes. This prevents the water in the product stream from condensing before reaching the GC inlet. The reactor effluent (vapor phase) that is not passed through the GC is vented after passing through a scrubber.

The Co_6W_6C was first heated *in-situ* by flowing H_2 at a rate of 62 standard cc (scc)/min at 400 ^{o}C and atmospheric pressure for 1 hour. (One scc is the amount corresponding to a volume of 1cc of gas at standard temperature and pressure, 0°C and 1 atm.) The system was then flushed with Ar (190 scc/min) at 400°C and atmospheric pressure for 1 hour. The feed mixture was then introduced into the system (at a weight-hourly space velocity, WHSV, of 11,200 scc/hr/g catalyst) with the feed ratio maintained at $CH_4/CO_2/Ar = 1/1/3$ and under a total pressure of 5 atm. The reaction temperature was raised from 400°C to 850°C over 1.5 hours and was then maintained at 850°C in the flowing reactant mixture.

Results

Lifetime Study

The results of a catalyst-lifetime study at 850°C are shown in Figure 1. Here t = 0 corresponds to the time when the temperature reaches 850°C in the presence of the feed mixture. The CH_4 and CO_2 conversions increase steadily during the first 20 hours at 850°C and then level off at 82% and 78% respectively, giving rates of consumption of 1.3 and 1.25 mmol/min/g catalyst respectively. The H_2/CO ratio obtained is close to unity and the CO yield is about 76 %. The catalyst is found to be very stable at 850°C for a period of over 90 h in Figure 1.

In a second set of experiments, the reaction temperature was progressively decreased. As expected, yield and H_2/CO ratio values were found to decrease with decreasing temperatures. After approximately 150 h, the temperature was again brought up to 850°C. The catalyst performed as it had after 90 h on stream. (These data can be found in Ref 14.) Hence the catalyst is actually stable for over 150 h.

Characterization of the cobalt tungsten carbide [Co_6W_6C] catalyst is achieved by X-ray diffraction (XRD) analysis in Prof. Seehra's laboratory. The XRD patterns of the fresh and stabilized catalyst are given in Figure 2. ("Fresh catalyst" is the material as received. The "stabilized catalyst" consists of fresh catalyst subjected to a two-stage *in-situ* pretreatment. The first stage of pretreatment consists of flowing H_2 (62 scc/min) at 400 ^{o}C for 1 hour and then flushing the system with Ar (190 scc/min) at 400 ^{o}C for 1 hour. The second stage of pretreatment is performed in a $CH_4/CO_2/Ar = 1/1/3$ flow at 850 ^{o}C and 5 bar total pressure for

about 20 hours, at which time Figure 1 indicates that the catalyst is active and stable.) The XRD patterns for the stabilized catalyst reveal a phase transformation of the catalyst from Co_6W_6C to a mixture of WC + Co + C. The details of this phase transformation can be explained from a Co-W-C ternary phase diagram (15). These results are consistent with those reported in the literature (2,9) for carbide catalysts. The stability of these metal carbide catalysts, is due to the carbide phase formed (10). Hence, coking is not a problem for these catalysts. The macroscopic carbon deposits could be due to the presence of Co in the catalyst, which is known to enhance carbon formation (16).

It should be noted that the overall carbon balances obtained at various times during these continuous experiments range from 98 to 103 %. This implies that we have accounted for virtually all of the reaction products.

Kinetic Expression

Until recent times, there have been only a few reports on kinetic studies of methane dry reforming cited in the literature. A list of the rate expressions derived so far by various investigators is tabulated in Table 1. These researchers proposed Langmuir-Hinshelwood, Eley-Rideal and Hougen-Watson type of reaction models.

In this study, a kinetic model for the carbon dioxide reforming of methane with the cobalt tungsten carbide [Co_6W_6C] precursor has been developed from the results of a set of designed experiments. The experiments were performed under differential reaction conditions over a temperature range of 500-600 ^{o}C. The initial modeling was based on a simple power-law model. This was followed by a Langmuir-Hinshelwood type of reaction model, based on a simple reaction mechanism proposed for the system. The following simple reaction mechanism is proposed for this study:

$$CH_4 + * \underset{}{\overset{K_1}{\rightleftharpoons}} CH_X* + (x/2)\,H_2$$

$$CO_2 + * \overset{K_2}{\rightleftharpoons} CO + O*$$

$$CH_X* + O* \xrightarrow{k_3} CO + (x/2)\,H_2 + 2*$$

$$CH_X* \overset{K_4}{\rightleftharpoons} C* + (x/2)\,H_2$$

$$H_2 + O* \underset{k_{-5}}{\overset{k_5}{\rightleftharpoons}} H_2O + *$$

$$C* + O* \xrightarrow{k_6} CO + 2*$$

The mechanism incorporates carbon deposition as well as carbon removal occurring in the reaction system, both of which are generally disregarded in most of the reported kinetic models. From the above reaction mechanism, the expressions for the rate of formation of the products were derived (14):

$$r_{CO} = \frac{K_1 K_2}{(den)^2}\left(\frac{P_{CH_4} P_{CO_2}}{P_{CO} P_{H_2}}\right)\left(k_3 + \frac{k_6 K_4}{P_{H_2}}\right)$$

$$r_{H_2} = \frac{k_3 K_1 K_2}{(den)^2}\left(\frac{P_{CH_4} P_{CO_2}}{P_{CO} P_{H_2}}\right) - \frac{k_5 K_2}{(den)}\left(\frac{P_{H_2} P_{CO_2}}{P_{CO}}\right) + \frac{k_{-5} P_{H_2O}}{(den)}$$

$$r_{H_2O} = \frac{k_5 K_2}{(den)}\left(\frac{P_{H_2} P_{CO_2}}{P_{CO}}\right) - \frac{k_{-5} P_{H_2O}}{(den)}$$

where:

$$den = 1 + K_1\left(\frac{P_{CH_4}}{P_{H_2}}\right) + K_2\left(\frac{P_{CO_2}}{P_{CO}}\right) + K_1 K_4\left(\frac{P_{CH_4}}{P_{H_2}^2}\right)$$

A comparison of the experimental data with the predicted values from the Langmuir-Hinshelwood model for all the product species is given in Figure 3. The model gives a reasonably good fit to the observed experimental data. Other models did not work as well. For details, see Iyer (14).

Validation of Catalyst Prepared in Laboratory

We are currently in the process of developing methods to prepare this unsupported Co_6W_6C catalyst. The procedure described in the original patent (15) is used as a starting point. About 14.5 g of H_2WO_4 in 400 mL of 1:1 mixture of NH_4OH and H_2O was mixed with 300mL of ethylenediamine. This is followed by heating and stirring until a clear solution is obtained. On a separate container, 13.8 g of $CoCl_2$. $6H_2O$ was dissolved in distilled water. This cobalt solution is mixed with the first solution. The resulting mixture is evaporated until $CoWO_4$ precursor is precipitated. The mixture is filtrated, washed and dried. The solid product is treated in flowing CO and CO_2. The Co_6W_6C catalyst is prepared in a thermodynamically controlled way by varying the ratio of CO and CO_2 in the feed stream.

The initial XRD pattern from the unsupported Co_6W_6C catalyst (CO_2: CO = 0.75:1) prepared in our laboratory is shown in Figure 4. Figure 4 confirms that the material prepared in our laboratory is Co_6W_6C. Efforts to study the performance of Co_6W_6C catalyst prepared in our laboratory are currently in progress.

Summary of Results

The cobalt tungsten carbide material used as catalyst for CO_2 reforming of CH_4 was found to be very stable for more than 150 hours at elevated pressures and high temperatures. The catalyst shows stabilization with increasing activity when heated at 850 ^oC in the presence of the feed mixture at 850^oC and 5 atm. total pressure, for over 20 hours. The stabilized catalyst gives CH_4 and CO_2 conversions of 82 and 78 % respectively, with CO yields of 76 % and H_2/CO ratio close to unity at 850^oC and 5 atm total pressure. XRD patterns of the transformed catalyst suggest a phase transformation, at 850 ^oC, from Co_6W_6C to a mixture of WC + Co + C. Hence coke is not a factor in the performance of these catalysts, unlike that of conventional catalysts.

The kinetics of CO_2 reforming of methane with Co_6W_6C catalyst were studied under differential conditions over a temperature range of 500-600^oC, based on a detailed experimental design. The rates of formation of the products H_2, CO and H_2O were used for the kinetic analysis. The observed rates seem to follow a Langmuir-Hinshelwood type of reaction mechanism. Hence, this type of kinetic model has been proposed based on a simplified reaction mechanism. The mechanism incorporates carbon deposition as well as carbon removal occurring in the reaction system, both of which are generally disregarded in most of the reported kinetic models. The parameters of the model were successfully estimated for all the experimental data. The comparison plot of the observed data and the predicted model show generally a good fit for all the product species.

The preparation of the unsupported Co_6W_6C catalyst in our laboratory has been successful. Refining the methods of preparation as well as studying the performance of this catalyst is still in progress.

References

1. K. Otsuka, T. Ushiyama, I. Yamanaka, *Chem. Lett.* 9, 1517 (1993).
2. J. B. Claridge, A. P. E. York, A. J. Brungs, C. Marquez-Alvarez, J. Sloan, S. C. Tsang, M. L. H. Green, *J. Catal.* 180, 85 (1998).
3. K. Seshan, T. H. W. Barge, W. Hally, A. N. J. van Keulen, J. R. H. Ross, *Stud. Surf. Sci. Catal*. *Natural Gas Conversion II*, H. E. Curry-Hyde, R. F. Howe, Eds. (Elsevier, Amsterdam) 81, 285 (1994).
4. J. R. H. Ross, A. N. J. van Keulen, M. E. S. Hegarty, K. Seshan, *Catal. Today* 30, 193 (1996).
5. S. Wang, G. Q. Lu, G. J. Millar, *Energy Fuels* 10, 896 (1996).
6. J. R. Rostrup-Neilsen, J. H. Bak-Hansen, *J. Catal*. 144, 38 (1993).
7. M. C. J. Bradford, M. A. Vannice, *Catal. Rev.- Sci. Eng.* 41, 1 (1999).
8. A. P. E. York, *Chem. Brit.* 35, 25 (August 1999).
9. A. J. Brungs, A. P. E. York, J. B. Claridge, C. Marquez-Alvarez, M. L. H. Green, *Catal. Lett*. 70, 117 (2000).
10. A. J. Brungs, A. P. E. York, M. L. H. Green, *Catal. Lett*. 57, 65 (1999).
11. A. Shamsi, D. Lyons, *Prepr. Symp. - Am. Chem. Soc., Div. Fuel Chem.* 45, 132 (2001).
12. M. Tsuji, T. Miyao, T., S. Naito, *Catal. Lett*. 69, 195 (2000).
13. K. Oshikawa, M. Nagai, S. Omi, *Chem. Lett*. 9, 1086 (2000).
14. M Iyer, MSChE Thesis, West Virginia University, December 2001.

15. A. Guerrero-Ruiz, I. Rodriquez-Ramos, A. Sepulveda-Escribano, *Catal. Today*. 21, 545 (1994).
16. R. S. Polizzotti, L. E. McCandlish, & E. L. Kugler, Multiphase Composite Particle Containing a Distribution of Nonmetallic Compound Particles. *US Patent* 5,338,330 August 16, 1994.
17. W. K. Lewis, E. R. Gilliland, and W. A. Reed, *Ind. Eng. Chem.,* 41, 1227 (1949).
18. I. M. Bodrov and L. O. Apel'baum, *Kinet. Catal.*, 8, 326 (1967).
19. J. T. Richardson, and S. A. Paripatyadar, *Appl. Catal*., 61, 293-309 (1990).
20. Z. L. Zhang and X. E. Verykios, *Catal. Today*, 21, 589 (1994).
21. M. F. Mark, and W. F. Maier, *J. Catal.*, 164, 122 (1996).
22. M. F. Mark, F. Mark, and W. F. Maier, *Chem. Eng. Technol.*, 20, 361 (1997).
23. U. Olsbye, T. Wurzel, and L. Mleczko, *Ind. Eng. Chem. Res.,* 36, 5180 (1997).
24. T. Osaki, T. Horiuchi, Suzuki K. and T. Mori, *Appl. Catal. A: General*, 155, 229 (1997).
25. V. C. H. Kroll, G. J. Tjatjopoulos and C. Mirodatos, *Natural Gas Conversion V. (Stud. Surf. Sci. Catal.)*, 119, 753 (1998).

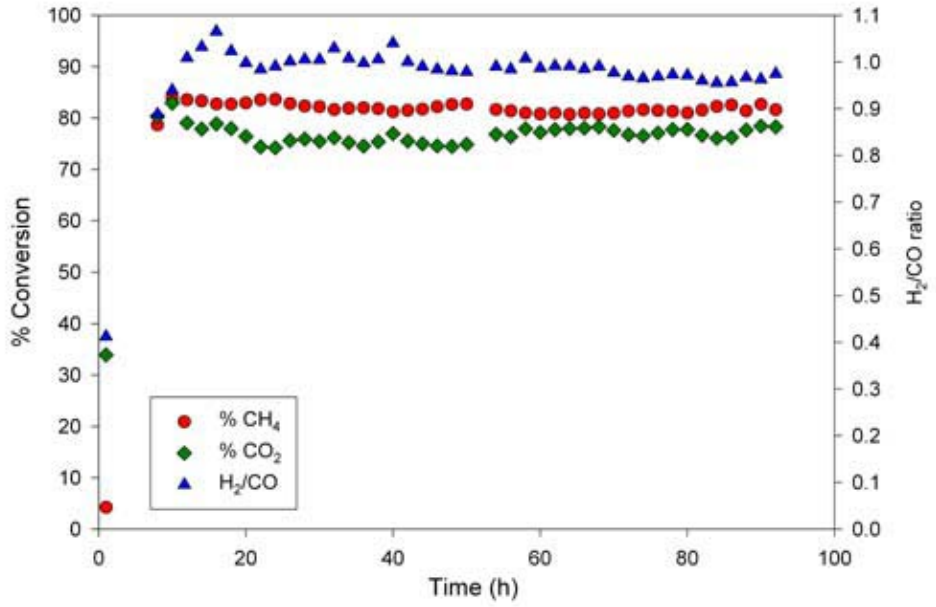

Figure 1. Conversions during the lifetime study of the Co_6W_6C catalyst for the CO_2 reforming of CH_4 (T = 850 ^oC, particle size < 38 μm, $CH_4/CO_2/Ar$ = 1/1/3, P_{total} = 5 atm., Total feed WHSV = 11,200 scc/hr/$g_{catalyst}$).

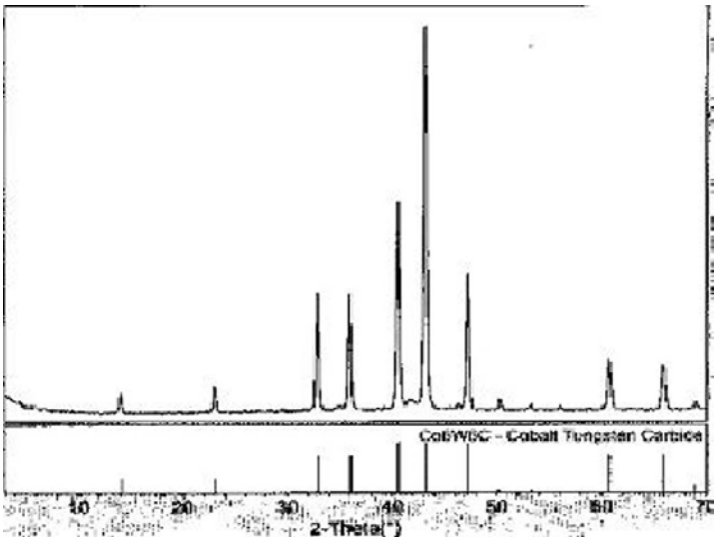

fresh Co_6W_6C catalyst (before stabilization)

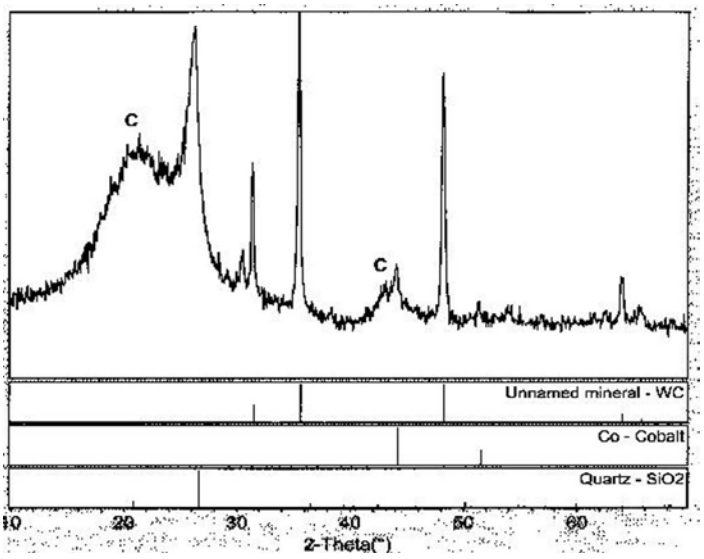

after stabilization

Figure 2. XRD patterns of: (a) fresh Co_6W_6C catalyst and (b) after stabilization; during CH_4/CO_2 reforming at 850°C. (Particle size < 38 μm, $CH_4/CO_2/Ar$ = 1/1/3, P_{total} = 5 atm., Total feed WHSV = 11,200 scc/hr/$g_{catalyst}$).

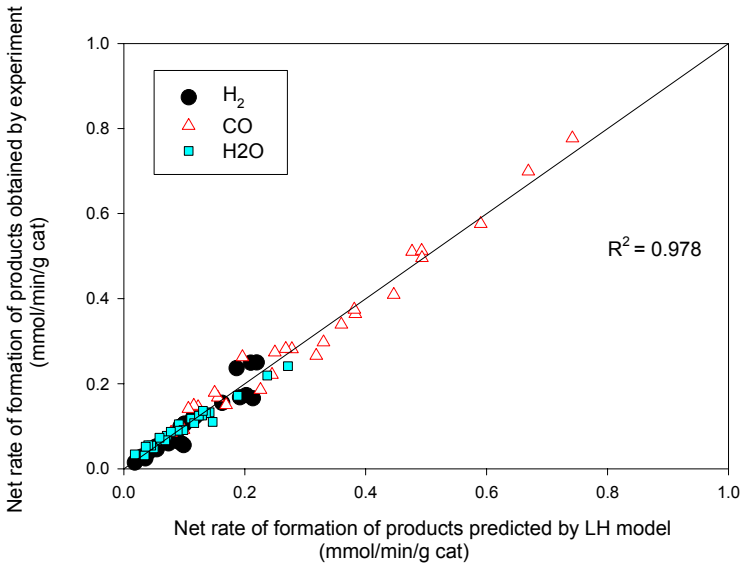

Figure 3. Comparison Plot for the Net Rates of Formation for Each of the Species.

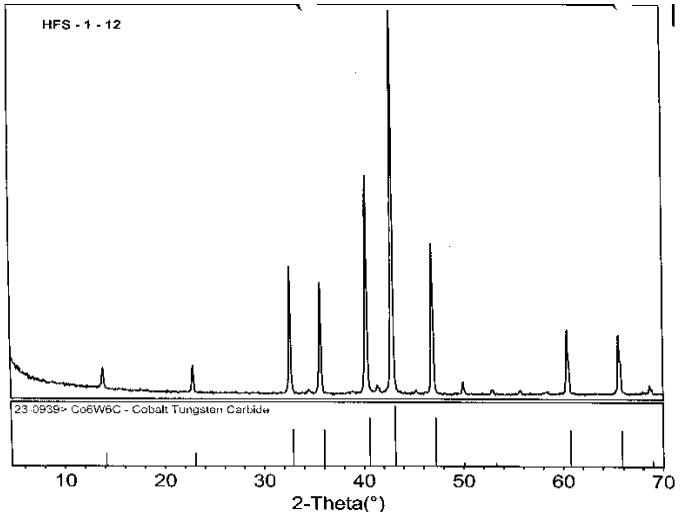

Figure 4. XRD pattern of fresh Co_6W_6C catalyst prepared in our laboratory (CO_2: CO = 0.75:1).

Table 1. Proposed Rate Expressions for Dry Reforming of Methane with Carbon Dioxide.

Rate model	Catalyst	Reference
$r_{ref} = \frac{k_{ref} P_{CH_4} (P_{CO_2} + P_{H_2O})}{[1 + 24 (P_{CO_2} + P_{H_2O}) + 8 P_{H_2}]^2}$	Cu/SiO_2	17
$r_{ref} = \frac{k_{ref} P_{CH_4}}{1 + a \frac{P_{H_2O}}{P_{H_2}} + bP_{CO}}$	Ni foil	18
$r_{ref} = \frac{k_{ref} K_{CH_4} K_{CO_2} P_{CH_4} P_{CO_2}}{(1 + K_{CH_4} P_{CH_4} + K_{CO_2} P_{CO_2})^2}$	Rh/Al_2O_3	19
$r_{ref} = \frac{aP_{CH_4} P_{CO_2}^2}{(a + bP_{CO_2}^2 + cP_{CH_4})^2}$	Ni/Al_2O_3 $Ni/CaO\text{-}Al_2O_3$	20
$r_{ref} = \frac{k_{ref} \left(P_{CH_4} - \frac{P_{H_2}^2 P_{CO}^2}{K_{ref} P_{CO_2}} \right)}{1 + \frac{P_{CO}^2}{K \quad P}$	Ir/Al_2O_3	21
$r_{ref} = \frac{k_{ref} K_{CH_4} \left(P_{CH_4} P_{CO_2} - \frac{P_{H_2}^2 P_{CO}^2}{K_{ref}} \right)}{1 + K_{CH_4} P_{CH_4}}$	Ir/Al_2O_3	22
$r_{ref} = \frac{k_{ref} K_{CO_2} \left(P_{CH_4} P_{CO_2} - \frac{P_{H_2}^2 P_{CO}^2}{K_{ref}} \right)}{1 + K_{CO_2} P_{CO_2}}$	Ir/Al_2O_3	22
$r_{ref} = \frac{k_{ref} K_{CH_4} K_{CO_2} \left(P_{CH_4} P_{CO_2} - \frac{P_{H_2}^2 P_{CO}^2}{K_{ref}} \right)}{(1 + K_{CH_4} P_{CH_4} + K_{CO_2} P_{CO_2})^2}$	Ir/Al_2O_3	22
$r_{ref} = \frac{k_{ref} P_{CH_4} P_{CO_2}}{(1 + K_1 P_{CH_4} + K_2 P_{CO})(1 + K_3 P_{CO_2})}$	$Ni/La/Al_2O_3$	23
$r_{ref} = \frac{k_{ref} \sqrt{K_1 K_2 P_{CH_4} P_{CO_2}}}{\left(1 + \sqrt{K_1 P_{CH_4}} + \sqrt{K_2 P_{CO_2}}\right)^2}$	Ni/Al_2O_3, Ni/SiO_2 $Ni/CaO\text{-}Al_2O_3$	24
$r_{CH_4} = \frac{k_3 K_1 K_2 P_{CH_4} P_{CO_2} P_{CO} P_{H_2}^2}{(P_{CO} P_{H_2}^2 + K_1 P_{CH_4} P_{CO} + K_2 P_{CO_2} P_{H_2}^2)^2}$	Ni/SiO_2	25

Development of Microporous Shape-Selective Catalysts for Ethylene, Propylene and other Value-Added Products via C-1 Chemistry

Delphine Dubois, Daniel Obrzut, T. M. Jyothi, Jing Liu, A. M. Prakash and James A. Guin
Auburn University

Abstract
Due to uncertainties of petroleum supplies and the increasing costs of oil imports (balance of trade), there is considerable interest in producing value-added products from coal and other secure U. S. energy resources. Examples of such products are ethylene and propylene, as well as higher olefins and other hydrocarbons. The first two products are particularly interesting since light olefins can be easily converted to premium clean liquid transportation fuels as well as a vast array of other value-added products including fuel additives, lubricants, and chemicals which are currently available only via a petroleum route.

We are studying the development of microporous molecular sieve (shape-selective) catalysts, such as silicoaluminophosphates (SAPO's), to produce these value added products from syngas. Both direct and indirect routes, via methanol, are being explored. The overall catalytic process is designed to produce a narrow range of products very selectively, e. g. very high selectivity to ethylene, rather than a broad range of products such as obtained by the conventional F-T chemistry. Several types of modified SAPO catalysts have been prepared via hydrothermal crystallization and tested in a continuous flow reactor with product analysis by GC. Variables explored in the catalyst development and testing program include catalyst synthesis variables, along with process variables such as temperature, reactor types, and feed composition. Metals addition, e. g., Me-SAPO's also has been explored using both impregnation, and incorporation during the hydrothermal synthesis itself. The effects of these variables on parameters such as catalyst lifetime and product selectivity have been studied. Some catalyst characterization also has been done in cooperation with other consortium members such as Mohindar Seehra's group at West Virginia University.

Catalyst Preparation

Several microporous catalysts were successfully prepared for testing during the year. There are many variables in the hydrothermal synthesis of microporous catalysts, including amounts of various reagents, sources of silica, alumina, templating molecule, order of mixing, synthesis time and temperature, pH, degree of agitation, etc. Coupled with this wide array of variables is the fact that some of the desired crystal forms are actually metastable states, which due to their instability, are difficult to achieve. All of these variables make the synthesis of a particular catalyst somewhat tenuous when a particular crystal form is desired. Sometimes it is necessary to try several formulations in order to achieve a desired result, and sometimes even apparently similar formulations can yield different crystal phases, or mixtures of phases. Nonetheless, we have been successful in synthesizing several pure SAPO catalysts, including SAPO-34 and SAPO-11. In addition, several composites of SAPO-5 and 34 with varying ratios were prepared during initial attempts at SAPO-34 preparation.

SAPO-34

15.1 g aluminum isopropoxide (AIP) (99.99%) was combined with 31.1 g of an aqueous solution of 35 wt % tetraethylammonium hydroxide (TEAOH) and stirred 1.5 hours. Then 0.666 g fumed

silica (99.8%) was added, and stirred until homogeneous. 8.52 g of 85 wt % phosphoric acid in 12.2 g of water was added slowly, then stirred for 2 hours. The mixture final pH was 7~8 and the molar composition was: $Al_2O_3 : P_2O_5 : 2.0TEAOH : 0.3SiO_2 : 50H_2O$. Synthesis was performed at 200°C for 48 hours in a teflon lined stainless steel autoclave. The product was washed with deionized water by repeated centrifuging dried overnight at 100°C, and calcined at 550 °C with flowing air for 10 hours to remove the template.

SAPO-34:SAPO-5 1:1.3 composite

15.1 g AIP (99.99%) plus 27.2 g of 20 wt % TEAOH was stirred 1.5 hours until homogeneous. 0.666 g fumed silica (99.8%) was added, and stirred until homogeneous. 8.52 g of 85 wt % phosphoric acid in 10.25 g of water was added slowly and stirred for 2 hours. The mixture final pH was 3 ~ 4 with molar composition: $Al_2O_3 : P_2O_5 : 1.0TEAOH : 0.3SiO_2 : 50H_2O$. The mixture was treated the same as SAPO-34 to produce the final catalyst.

SAPO-11

15.1 g AIP (99.99%) in 22.3 g water and 8.52 g of 85 wt % phosphoric acid in 10 g water was mixed 30 minutes until homogeneous. 0.222 g fumed silica (99.8%) was added, and stirred for 20 minutes until homogeneous. 3.75 g dipropylamine (DPA) was added slowly, then stirred for 1.5 hours. The final pH was ~ 6 with molar composition: $Al_2O_3 : P_2O_5 : 1.0DPA : 0.1SiO_2 : 50H_2O$. The homogeneous mixture was treated the same as SAPO-34 to produce the final catalyst except the synthesis time was only 24 h and calcination was at 600°C.

Ni-SAPO-34 hydrothermal synthesis

15.1 g AIP (99.99%) plus 31.1 g of 35 wt % TEAOH was stirred 1.5 hours until homogeneous. 0.666 g fumed silica (99.8%) and a solution of 0.08 g nickel (II) nitrate hexahydrate (99.999%) in 2 g of water were added, and stirred until homogeneous. 8.52 g of 85 wt % phosphoric acid in 10.2 g water was added and stirred for 2 hours. The final pH was 7 ~ 8 with molar composition of: $Al_2O_3 : P_2O_5 : 2.0TEAOH : 0.3SiO_2 : 0.0075NiO : 50H_2O$. The mixture was treated as for SAPO-34 to produce the catalyst

Impregnation method (4% Ca-SAPO-34)

SAPO-34 was added to a solution of 0.18 g calcium acetate monohydrate (99%) in 30 mL water and stirred for 1 hour, then heated until all water evaporated. The powder was dried at 100°C oven, and calcined at 450°C for 10 hours.

$CuO/ZnO/Al_2O_3$ Methanol Synthesis Catalyst

2.42 g aluminium nitrate, 9.55 g zinc nitrate and 9.37 g copper nitrate were diluted in 200 mL water. 1M NaOH solution (8 g in 200 mL water) was added with stirring. The final pH was 8-9. The solution was held at 70° C for 1 hr and was allowed to settle. It was then washed with 2.5 liters of water by decantation, filtered under vaccum, dried at 110° C, and calcined at 400° C for 5 hr. The molar ratio was 50Cu : 40Zn : 10Al.

Equipment and Procedures

Two reactor systems were used. Figure 1 shows the stainless steel (SS) reactor system consisting of a 0.5" OD SS reactor tube 18" long, a back pressure regulator to control the system pressure, Brooks mass flow meters for control of two gas flows, and an ISCO 500D syringe pump for

liquid feed. The quartz (Q) tube reactor system consists of a Kd Scientific syringe pump, Lindberg tube furnace, and a $^3/_8$" I.D quartz-tube reactor 32" long. Gas collecting bulbs are used for collection of product samples for GC analysis.

Reaction Procedures

Methanol conversion was conducted at atmospheric pressure using 0.5g catalyst between 2 portions of quartz wool. Liquid methanol was fed at a rate of 5 μL/min and vaporized in 60 ml/min nitrogen. Process variables tested include temperature, methanol partial pressure, and flowrate. In some cases, the catalyst was regenerated by flowing air at 500°C and used in subsequent tests.

Direct conversion of syngas (H_2/CO=2/1) was studied in the reactor system of Dr. Roberts' group using a mixed catalyst of 0.5g each of Cu/ZnO/Al_2O_3 + SAPO-34 at 280°C. The catalyst was prereduced using 2% H_2 in N_2 at 280°C overnight. In addition, runs at elevated pressures were performed using only the Cu/ZnO/Al_2O_3 catalyst.
Products were collected in gas bulbs and analyzed using two Varian chromatographs with GS-GasPro and Plot-Q capillary columns. The latter column was found to be necessary for analysis of methanol which would not elute from the GasPro column.

Results

XRD patterns

Drs. Seehra and Punnoose at West Virginia University have characterized samples of SAPO molecular sieves synthesized in our lab. Their XRD patterns of SAPO-34, mixed phase of SAPO-34 and SAPO-5, and SAPO-11 molecular sieves are shown in figures 2, 3, and 4, respectively. High intensity of the peaks and absence of any baseline drift indicates that the samples are highly crystalline. XRD patterns compare well to the literature both in intensity and line position.

SEM image/morphology

The approximate mean crystal sizes and size distribution ranges were obtained from SEM images. Figure 5 shows that the SAPO-34 crystals appear as cubic crystals ranging from 0.70 μm to 1.51 μm. These images are comparable to the literature [2]. Figure 6 shows that the SAPO-5 crystals in a mixed phase of SAPO-34/SAPO-5 are typical of SAPO-5 hexagonal morphology.

Reactor Comparisons

To ascertain whether stainless steel could have a catalytic effect on the reactions, we ran replicate catalyst screening runs in both quartz and SS reactor tubes. Figure 7 shows that the product distribution using a catalyst with a 1:2 SAPO-34 to SAPO-5 ratio with zirconium incorporated into the framework for the two reactors are very similar. Methanol conversion over SAPO-34 at 400°C and 450°C also produced similar results as seen in Figure 8. It is notable that at 450°C, SAPO-34 showed a dramatic decrease in lifetime when compared to the runs at 400°C.

Temperature Effects

Figure 9 shows the product distribution for methanol conversion over SAPO-34 at five temperatures. Effects of temperature on the product selectivity were dramatic. At 450°C, the

production of ethylene reached a maximum, while the ethylene to propylene ratio was highest at 500°C due to a large amount of methane at 500°C. As noted earlier (Fig. 8), deactivation of the catalyst is also more rapid at higher temperatures. These results indicate that a catalyst with better stability and lower propensity to produce methane than SAPO-34 could produce very interesting results. Higher ethylene production with increased selectivity might be achieved at 500°C with an improved catalyst.

Syngas Reactions

Experiments were conducted in Dr. Roberts' reactor with the objective of investigating the production of light olefins directly from syngas. Syngas flowed at 60 sccm over the mixed $Cu/ZnO/Al_2O_3$ + SAPO-34 catalyst at 280°C and atmospheric pressure. As shown in Figure 10, the major product from this reaction was methane with small amounts of olefins and paraffins. The dominance of paraffins rather than olefins in the products may result from the hydrogenation of olefins due to hydrogen in the syngas. Elevated pressure experiments were conducted with the $Cu/ZnO/Al_2O_3$ catalyst only. As shown in Figure 11, methane and methanol were the main products with a methanol concentration reaching 0.816 mol% at 21 atm.

Ethanol Production over SAPO-34

Several experiments were conducted to investigate the production of ethanol over SAPO-34 using a 95:5 water to methanol feed mixture. This mixture could promote the hydration of olefins to alcohol over the acid sites of SAPO-34. Analysis of the products revealed that at 350°C with 1g of SAPO-34 a trace amount of ethanol was produced at atmospheric pressure. Further manipulation of the reaction conditions might give a higher yield of ethanol.

Effect of Steaming on SAPO-34

Because the conversion of methanol involves the generation of significant amounts of water vapor in the reactor, it was of interest to examine the effects of this variable on the stability of the catalyst. Thus, a batch (S1) of SAPO-34 (0.5g) was treated with 0.01 mL/min of water in 60 sccm nitrogen flow at 350°C for 5 hrs. A second batch (S2) of SAPO-34 (0.5g) was treated with the same flowrate of water with the temperature increased to 500°C for 15 hrs. Following the steaming treatments, methanol conversion reactions were conducted with the results shown in Figure 12. A comparison of the product distribution showed that the selectivity to ethylene (Figure 12) and propylene was constant at around 50% and 30%, respectively, until the 21st hr of time on stream (TOS). DME appeared at 12 hr TOS for S1, and S2; while it appeared after 24 hr TOS for SAPO-34. The earlier appearance of DME for S1 and S2 is in keeping with the fact that the lifetimes of S1 and S2 are half of the lifetime of SAPO-34. From these experiments we can conclude that the initial selectivity to ethylene is not greatly affected by the steaming treatments, although the catalyst lifetime is shortened depending on the severity of the steaming.

Effect of H_2O/MeOH Feed Ratio

Since water is a co-product in the methanol conversion reaction, and because the actual raw feed from a methanol plant will likely contain some water, we have investigated the effect of the presence of water on the product distribution from methanol conversion. The results from experiments with differing percentages of water in the feed are shown in Figure 13. As the percentage of water in the feed increases, the selectivity towards ethylene increases, while the selectivity towards propylene decreases. In addition, the formation of paraffins, most notably

methane, was suppressed in the presence of 90% water, although, methane formation was unaffected by the presence of 30% or 60% water. This might be explained by the following hypothesis: water vapor facilitates the desorption of lower alkenes which terminates the chain growth and the coke formation. There was no methanol or dimethyl ether detected in the products when water was used as co-feed.

SAPO-34:SAPO-5 Composites

Several methanol conversion experiments were performed with catalyst compositions containing both SAPO-34 and SAPO-5 phases, as identified by XRD, in various ratios. For reference, Figure 14 shows the product distribution with pure SAPO-34. Figure 15 shows that when the catalyst contains SAPO34:SAPO-5 in a 1:0.5 ratio, ethylene is still the dominant product for the first 20 hrs, although the catalyst is less active with DME and MeOH breakthrough very soon after beginning the reaction. Figure 16 shows the product distribution for a composite catalyst with SAPO34:SAPO-5 in a 1:6 ratio. In this case, ethylene is no longer the preferred product, and a large amount of methane was formed, appearing as other hydrocarbons (HC) in the figure. In addition, there was a significant formation of C6+ products in this case, which condensed at the cool outlet end of the reactor. Due to the larger pore size of SAPO-5 vs. SAPO-34, viz. 0.73 vs. 0.38 nm, higher molecular weight products are allowed to exit the catalyst pores. This would explain the observation of heavier products with the catalyst having a smaller ratio of SAPO34:SAPO-5. Figure 17 shows only the ethylene distribution vs. TOS for the composite catalysts. This figure suggests that it may be possible to tailor the product composition, e. g. C2=/C3= ratio, by adjustment of the SAPO34:SAPO-5 phase ratio in the composite catalyst.

Metal modified SAPO catalysts

The incorporation of additional metals into SAPO catalysts offers interesting possibilities for modified and enhanced catalytic behaviors [3]. We modified several SAPO catalysts by: (a) impregnation and (b) hydrothermal incorporation, followed by testing in methanol conversion reactions. Impregnated metals included Ce, Cs, Mo, Ni, Pt, Ag, and Co. In general, the lifetimes of the impregnated SAPO catalysts were shortened, perhaps due to pore clogging caused by the metals themselves. Metal loading lower than the 4% level used could be beneficial in this regard. Some positive effects were realized, however. For example, the 4 wt% Ce-SAPO-34 had the longest lifetime of the impregnated catalysts: 72 hours, whereas, the methane production of 9 wt% Ce-SAPO-34 was minimal of all catalysts tested. Also the selectivity for the Ce impregnated catalyst was generally higher in propylene than neat SAPO-34. Zr impregnation appeared to generally minimize methane production, although Mo and Ni yielded significant increases in methane selectivity. In general, the impregnated metals did not appear to significantly increase ethylene selectivity, and in many cases increased the selectivity to methane. The metals Ni, Zr, Co, and Mn, as well as binary combinations of Ni-Co, and Mn-Co were introduced during hydrothermal synthesis itself. One of these metals-modified catalysts, a Co-modified SAPO-34: SAPO-5 composite, had the longest lifetime (96 hrs on-stream) of all catalysts tested to date, although the ethylene selectivity was somewhat less than the unmodified SAPO-34 (38 vs. 57 mol %).

Conclusions

Several silicoaluminophosphate (SAPO) catalysts were successfully synthesized by hydrothermal crystallization and tested in syngas and MeOH conversion reactions. Ethylene

selectivities of up to 63 mol% and overall C2-C4 olefin yields of 94% were achieved in MeOH conversion reactions. Inclusion of water in the MeOH feed increased selectivities of C2-C4 olefins to 99.6%. A 100 hr run was made with a Co modified SAPO-34:SAPO-5 composite catalyst. Metals modified SAPO's showed interesting changes in selectivities and activities based on metals incorporated. Results suggest that it may be possible to tailor the olefins product composition, e. g. C2=/C3= ratio, by adjustment of the SAPO34:SAPO-5 phase ratio in a composite catalyst.

References

1. I.M. Dahl, R. Wendelbo, A. Andersen, D. Akporiaye, H. Mostad and T. Fuglerud, Microporous Mesoporous Mater. 29 (1999) 159.
2. X. Wu, R.G. Anthony, Appl. Catal. A: Gen. 218 (2001) 241.
3. M. Hartmann, L. Kevan, Chem. Rev. 99, (1999) 635.

Publications

Shaobin Wang, J. A. Guin, "Etherification of dimethylbutene with methanol over clay-based acid catalysts" Reaction Kinetics and Catalysis Letters 75(1), (2002) 169-175.

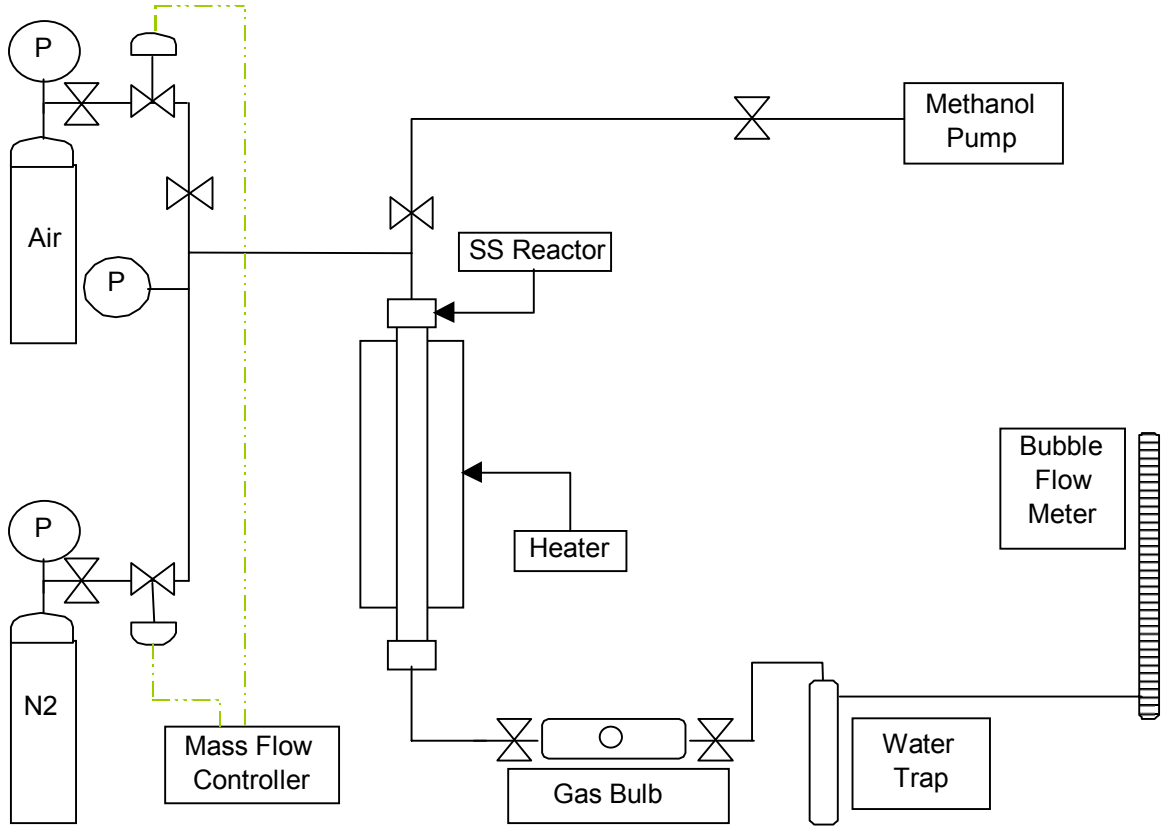

Figure 1. Diagram of the stainless steel reactor system

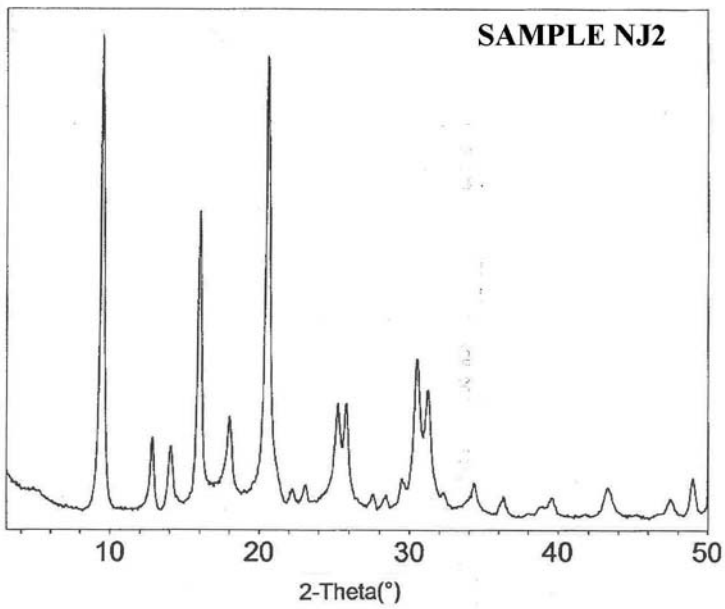

Figure 2. XRD pattern of SAPO-34

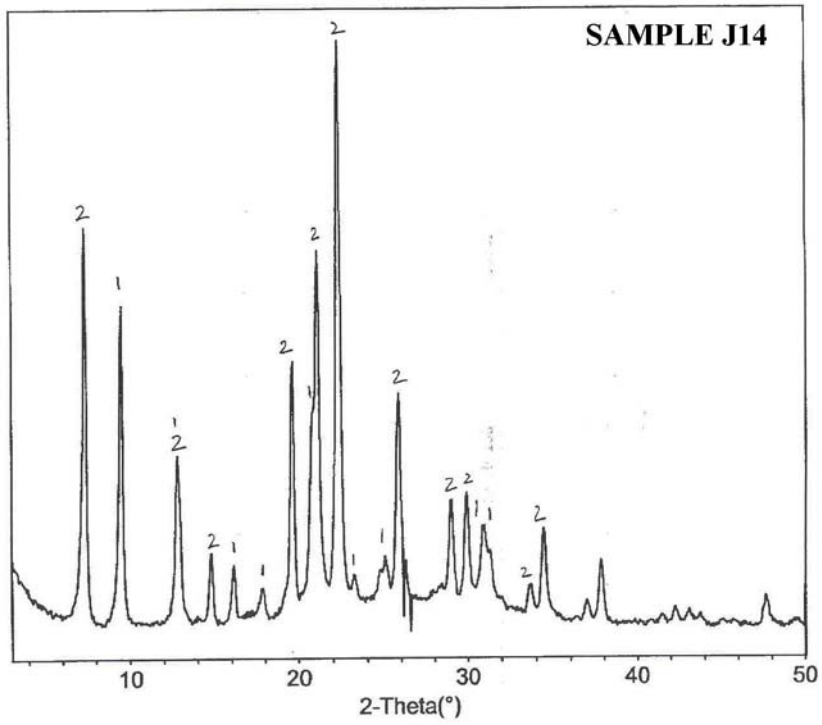

Figure 3. XRD pattern of SAPO-34 (1) and SAPO-5 (2) hybrid catalyst

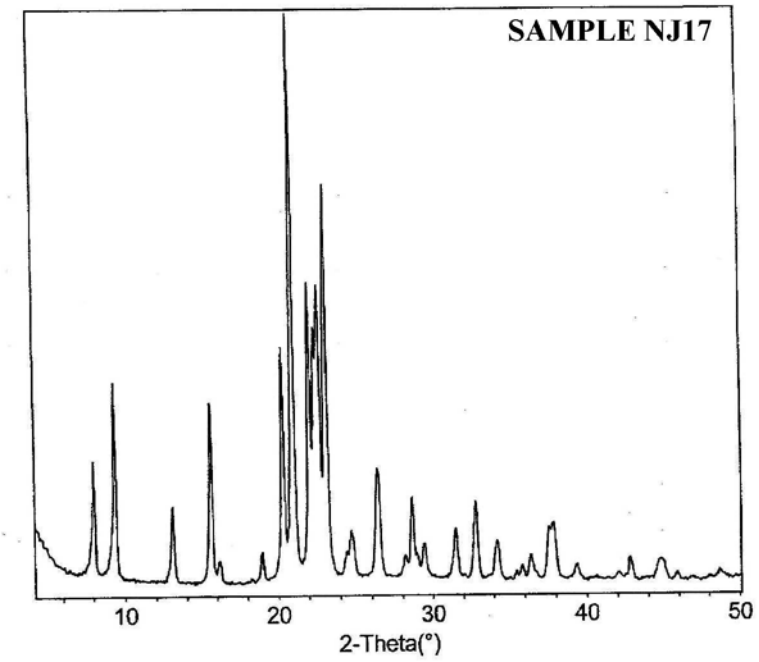

Figure 4. XRD pattern of SAPO-11

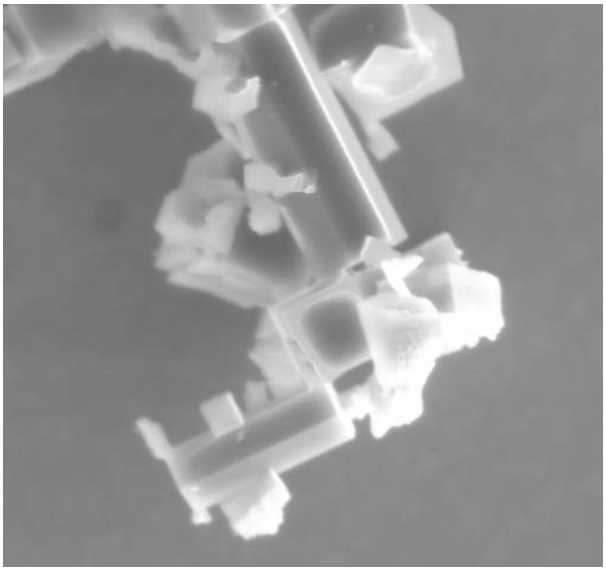

Figure 5. SEM micrographs of the SAPO-34: SAPO-5 (1:2) molecular sieves as synthesized. 10kV, 15 mm, x3000, catalyst J2.

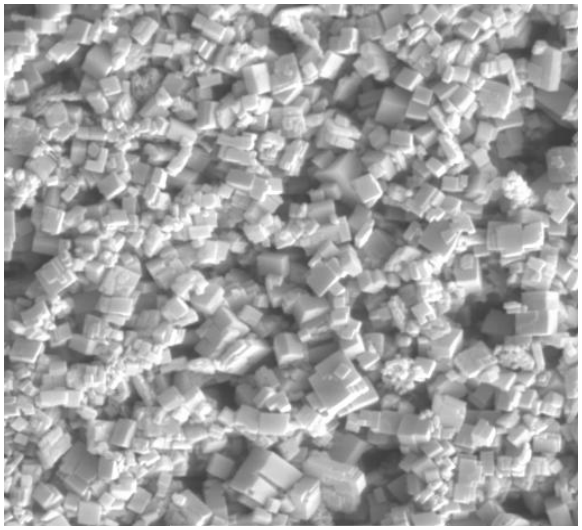

Figure 6. SEM micrographs of the SAPO-34 molecular sieves as synthesized. 10kV, 12 mm, x2500, crystal size from 0.70 μm to 1.51 μm, catalyst J15.

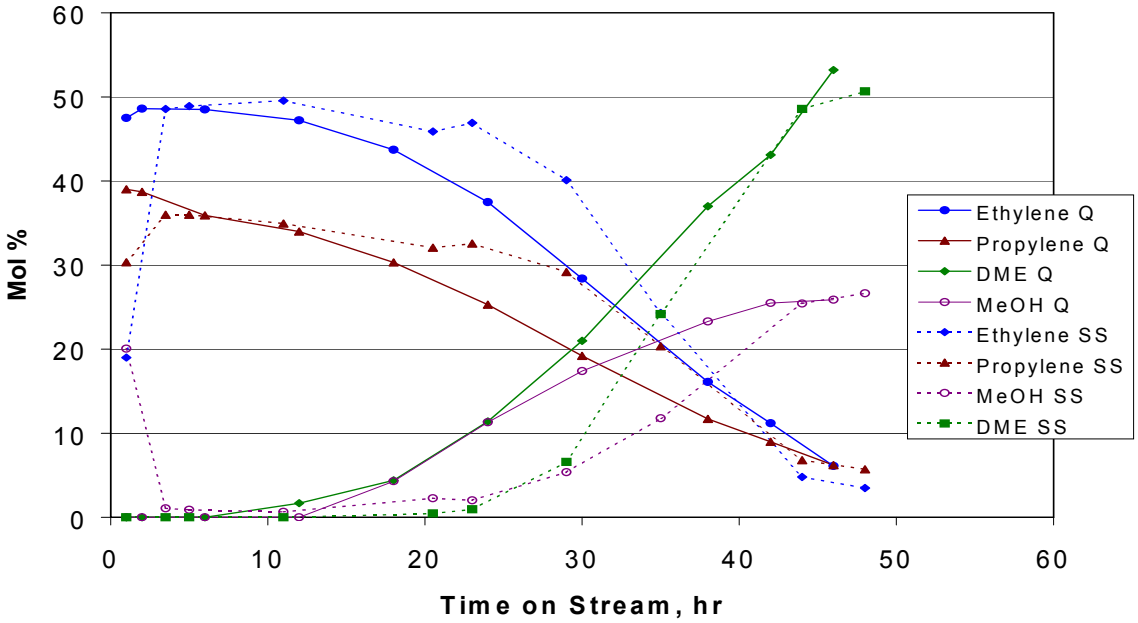

Figure 7. Distribution of ethylene, propylene, MeOH, and DME with Zr-SAPO-34:SAPO:-5 composite at 400°C in quartz (Q) and stainless steel (SS) reactors.

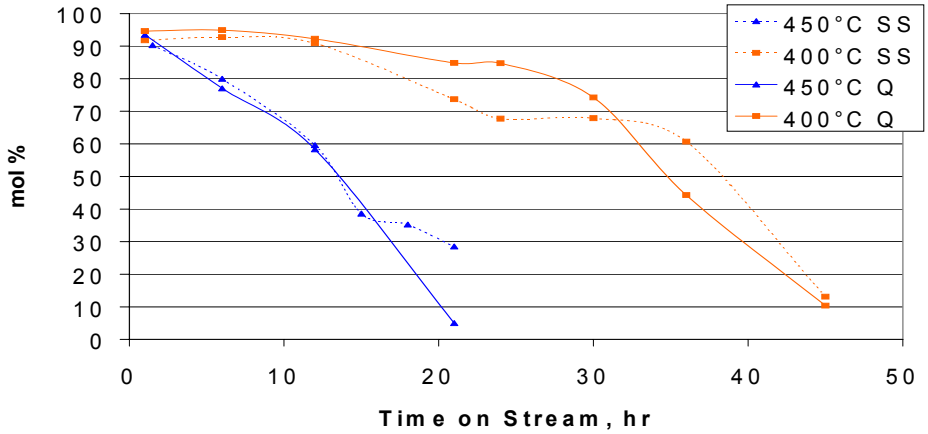

Figure 8. C2-C4 olefin selectivity at 400 and 450°C in quartz and SS reactors.

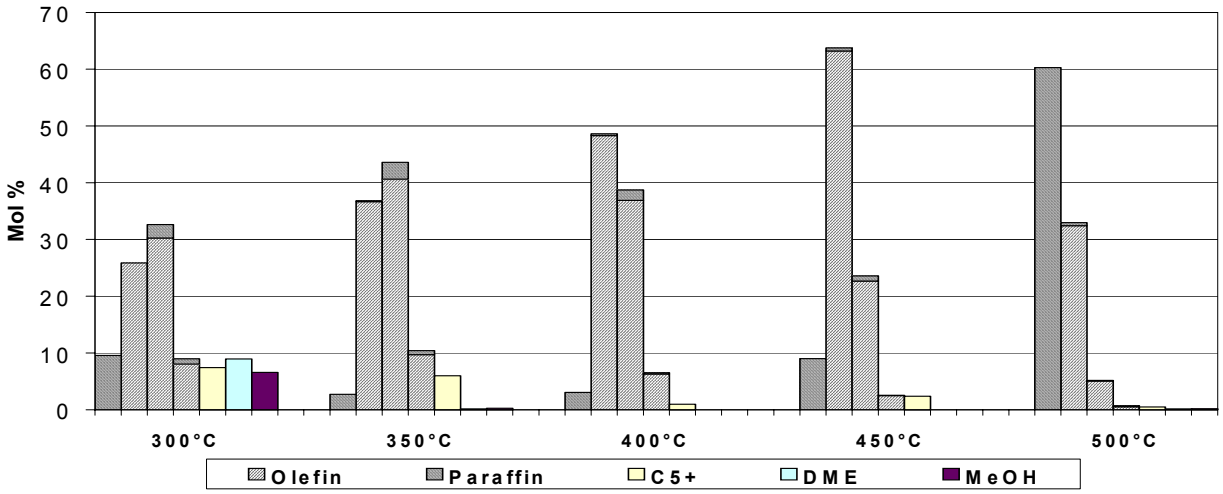

Figure 9. Product distribution over SAPO-34 at various temperatures.

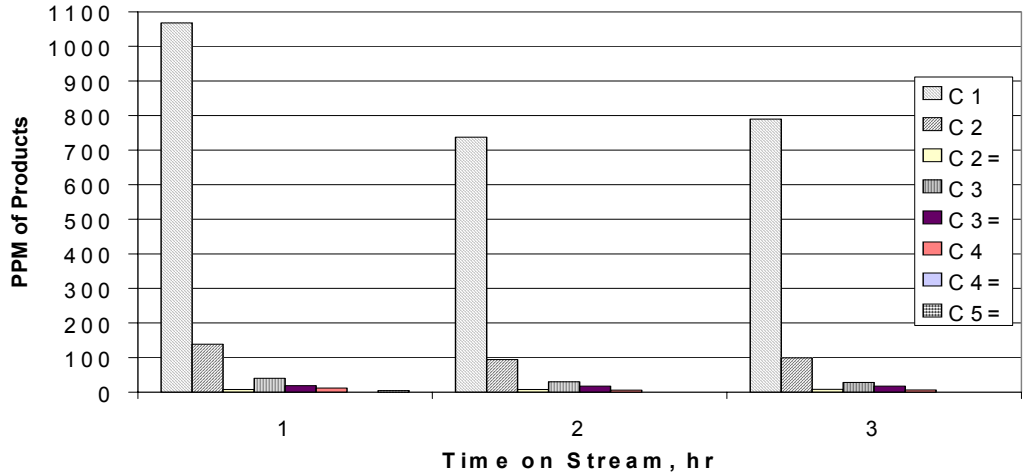

Figure 10. Products from syngas over $Cu/ZnO/Al_2O_3$ + SAPO-34, 280°C, 1atm.

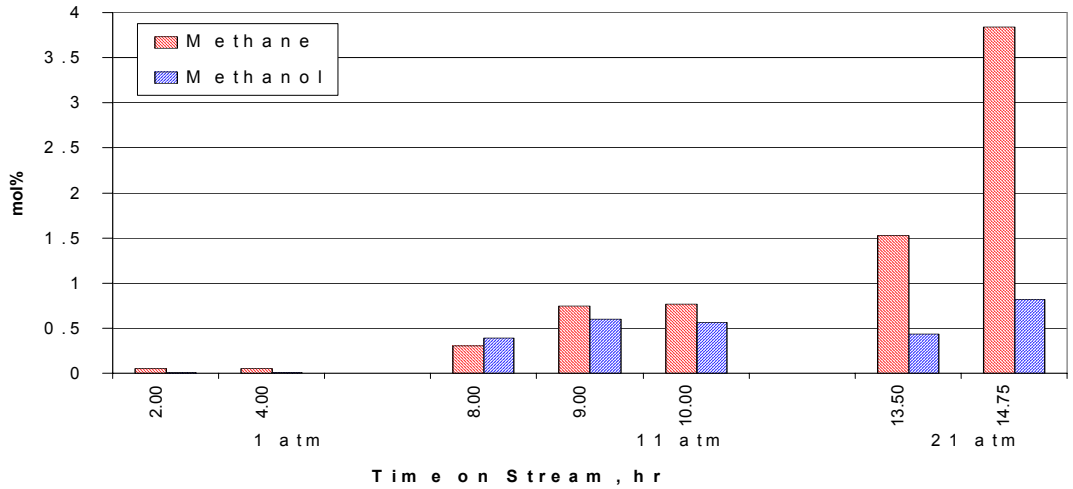

Figure 11. MeOH and methane distribution, $Cu/ZnO/Al_2O_3$, 280°C, 1-21 atm.

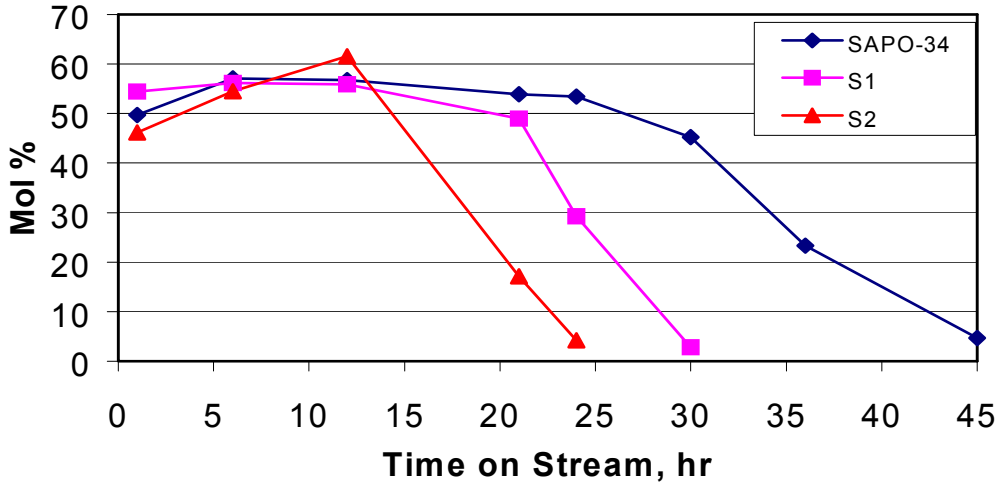

Figure 12. Effect of steaming on ethylene distribution over SAPO-34, S1-SAPO-34 and S2-SAPO-34 at 400°C.

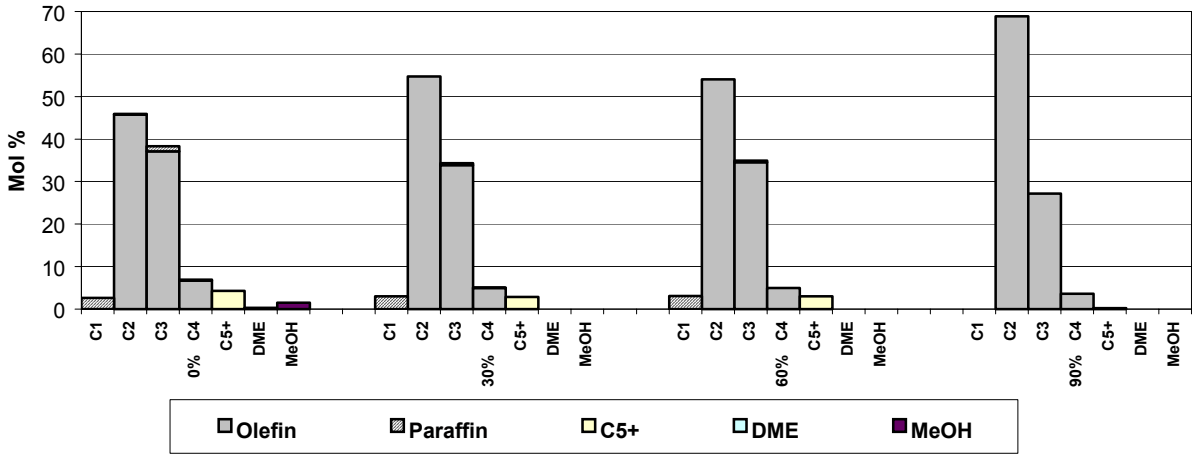

Figure 13. Effect of %.water in MeOH feed over SAPO-34 at 400°C.

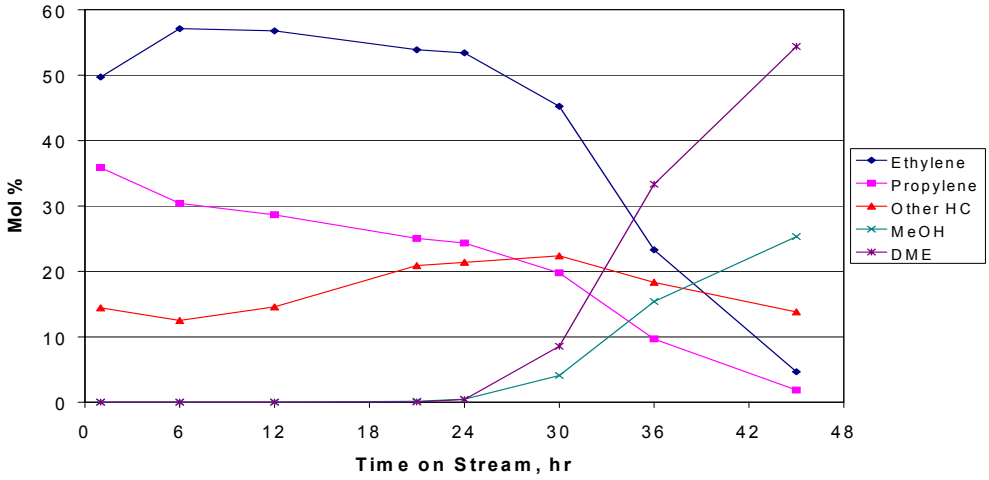

Figure 14. Product distribution over SAPO-34 at 400°C

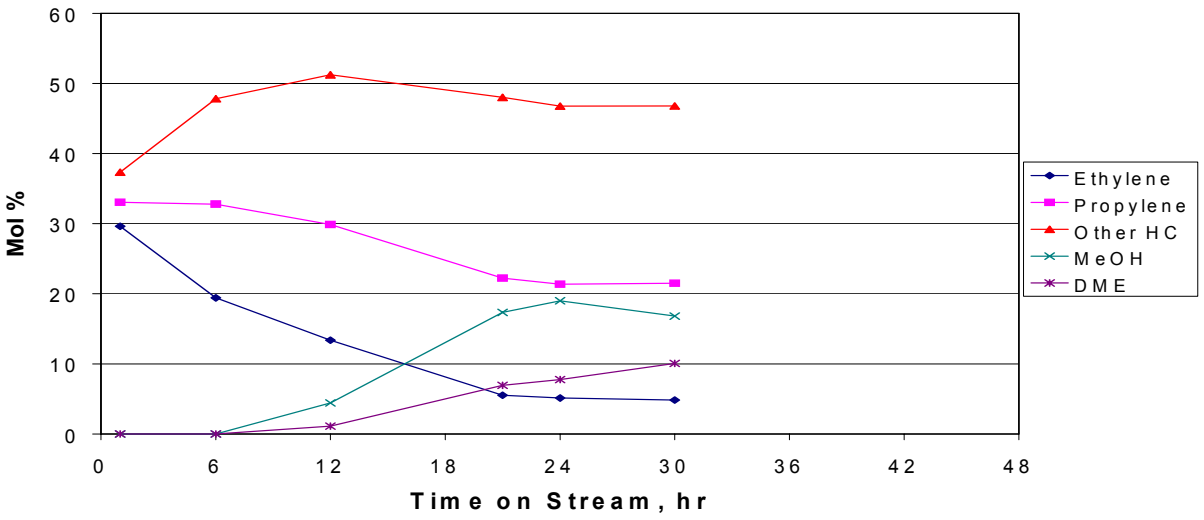

Figure 15. Product distribution over 2:1 SAPO-34:SAPO-5 composite at 400°C.

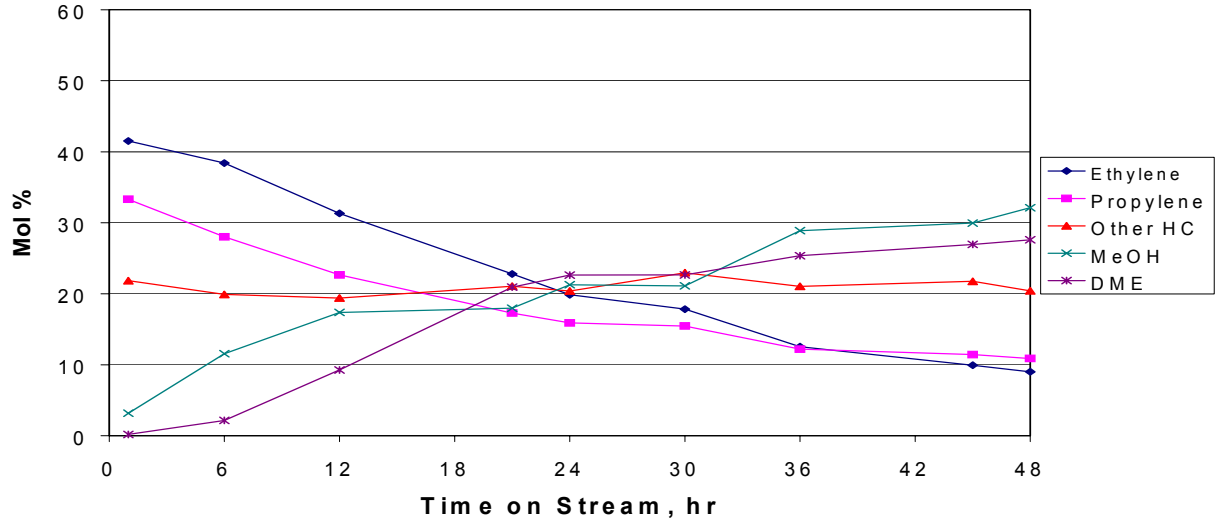

Figure 16. Product distribution over 1:6 SAPO-34:SAPO-5 composite at 400°C.

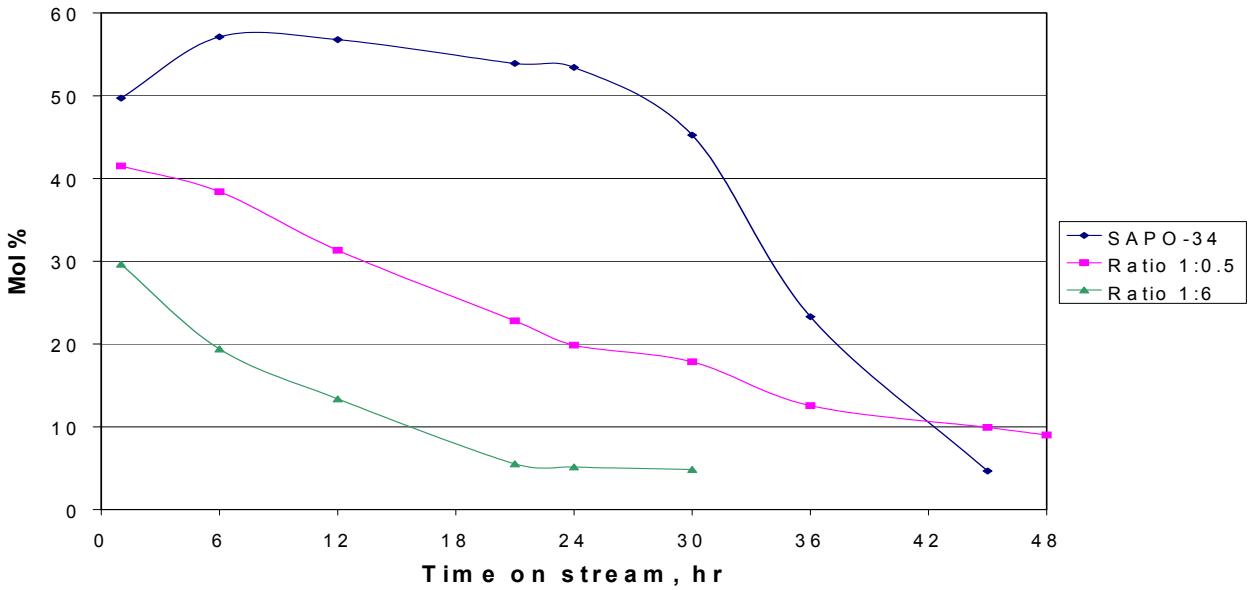

Figure 17. Ethylene distribution over SAPO-34, and 2:1, 1:6 SAPO-34:SAPO-5 composite catalysts at 400°C.

Analytical Characterization of Catalyst Structure and Product Distribution

M. S. Seehra and A. Punnoose
West Virginia University

Objectives

Our work under this task involves in-situ and ex-situ investigations of catalysts used in the C1 reactions by the CFFS researchers. Although some of these catalysts were prepared in our laboratory, most were obtained from other research groups in the Consortium, at different stages of the C1 reactions. We employ the techniques of x-ray diffraction (XRD), electron magnetic resonance (EMR) spectroscopy, SQUID magnetometry, thermogravimetric analysis (TGA) and photoacoustic/FTIR spectroscopy to determine the structural and electronic properties of the catalysts before and after the reactions. This information is then related to the product distribution in an effort to understand the reaction pathways. So working with other research groups in the Consortium is an important component of our program. During the past year, we have worked with Eyring et al at Utah, Wender et al at Pittsburgh, Huffman et al at Kentucky, Guin et al at Auburn, and Kugler et al at West Virginia University. A brief summary of some of the results from our research is given below, with details available in the publications listed at the end of this report.

Summary of Results

Results from the Kentucky Collaboration

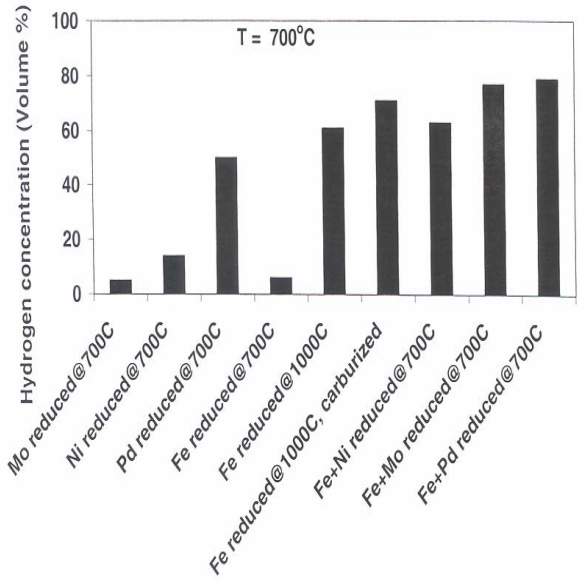

Fig. 1. Percentage conversion to H_2 for the different alumina supported catalysts.

Huffman et al [1] at Kentucky have recently achieved efficient production of hydrogen gas (H_2) from methane (CH_4) at 700°C using the reduced catalysts 0.5% M/4.5% Fe/γ-Al_2O_3 (M = Ni, Mo, Pd). The percentage conversion to H_2 for the different catalysts is shown in Fig. 1. To determine the structural and electronic properties of these catalysts, XRD at 300 K and EMR spectroscopy at 5 K and 300 K were employed, before and after the reaction with CH_4 at 700°C to produce H_2. Before the time-on-stream (TOS) reaction, catalysts reduced at 700°C contain γ–

Al_2O_3 and elemental Fe as determined by XRD (Fig. 2), and iron oxides, Fe, and Fe^{3+} substituting for Al^{3+} in Al_2O_3, as determined by EMR spectroscopy. The presence of Ni, Mo and Pd promotes the more complete reduction of iron oxides to Fe (Fig. 3). In the post reaction catalyst, the amount of elemental Fe (shown by ↓ in Fig. 2 and 3) is considerably lowered and presence of Fe_3C and graphitic nanotubes is observed (Fig. 3). However, there are no noticeable changes in the concentrations of Fe^{3+}/Al_2O_3 and iron oxides species. These results lead us to suggest that the nanoparticles of elemental Fe, produced from the reduction of iron oxides, are the primary catalysts for the efficient production of H_2 from CH_4 at 700°C. The results of these investigations were presented at a recent ACS conference [2] and a detailed paper has now been submitted for publication [3].

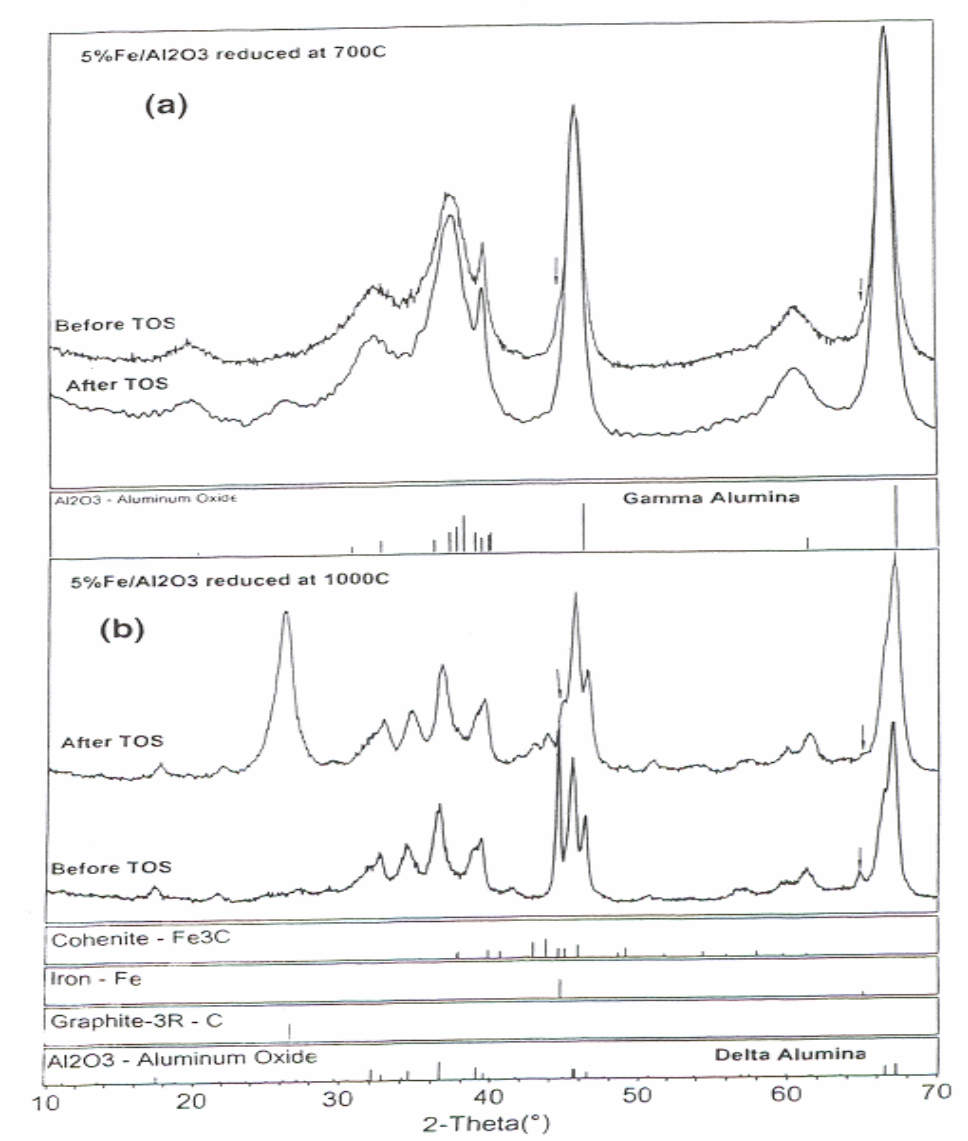

Fig. 2. XRD patterns of different 5%Fe/Al_2O_3 samples.

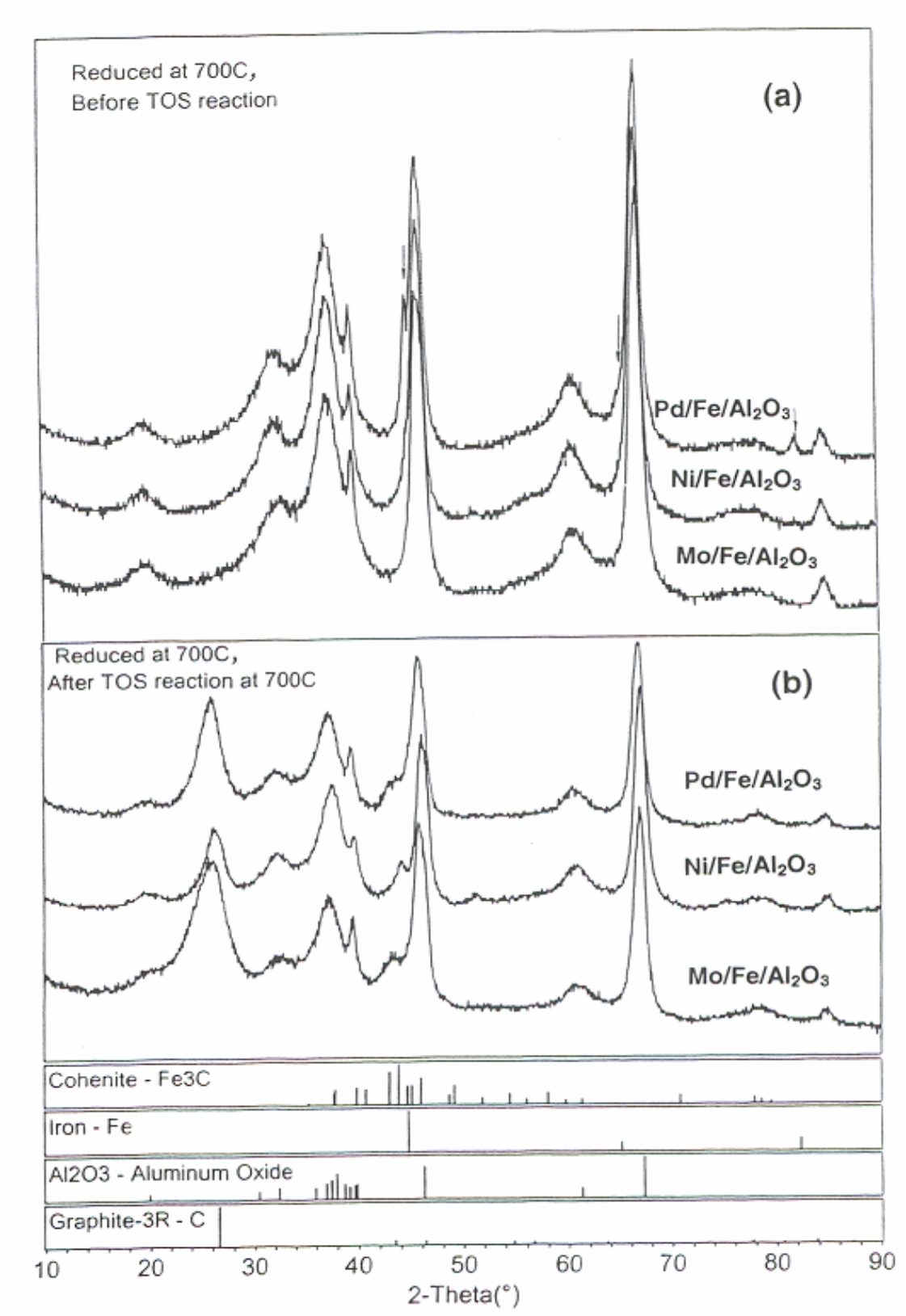

Fig. 3. XRD patterns of the 0.5% M/4.5% Fe/Al_2O_3 catalysts reduced at 700°C

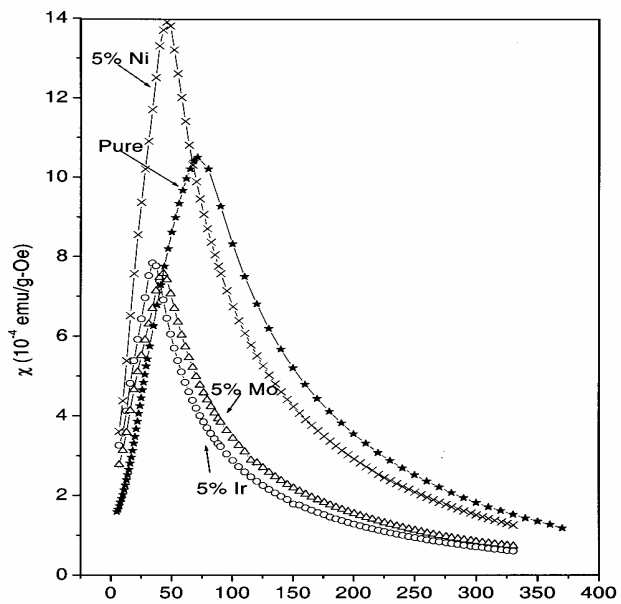

Fig. 4. Temperature variation of magnetic susceptibility of pure and doped ferrihydrites

The $M/Fe/Al_2O_3$ catalysts discussed above are prepared through the ferrihydrite route. Consequently we have also investigated the structural and magnetic properties of the ferrihydrites ($FeOOH \cdot nH_2O$). A comprehensive research paper on the magnetic properties of ferrihydrite nanoparticles doped with Ni, Mo and Ir has been submitted recently for publication [4]. Significant changes in the magnetic susceptibility χ upon doping are observed [Fig. 4] from which we have inferred that Ni substitutes for Fe throughout the nanoparticle whereas doping with Mo and Ir occurs primarily at the surface of the nanoparticle. The latter effect provides additional thermal stability to the doped ferrihydrites in catalytic reactions. Analysis of the data in Fig. 4 is based on a new theory for magnetism in nanoparticles which we published in Physical Review late last year [5].

Results from the Utah Collaboration

Eyring et al at Utah synthesized $CuCl_2/PdCl_2/AC$ (activated carbon) as catalyst for the production of diethyl carbonate (DEC). We worked with the Eyring group to investigate the $CuCl_2/PdCl_2/AC$ catalysts with different loadings of Cu. Our investigations using EMR spectroscopy of Cu^{2+} showed that DEC conversion activity (%) varies systematically with the intensity of the EMR signal due to Cu^{2+} surface species, showing the important role of Cu^{2+} in the catalytic reaction. Further, the pretreatment of $PdCl_2/CuCl_2/AC$ with KOH significantly increases the DEC yield and in these samples, using XRD we were able to show the presence of paratacamite, $Cu_2Cl(OH)_3$ whose intensity correlates well with the DEC conversion. Thus paratacamite was found to be more active than $CuCl_2$ for the regeneration of Pd(0) to $PdCl_2$ to continue the reaction. A joint paper on this work with Eyring et al has now appeared in print [6], where details of these results are available.

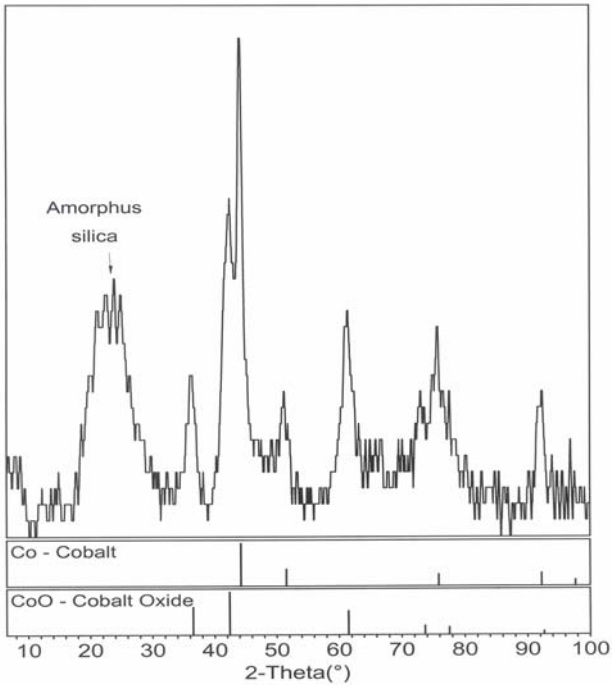

Fig. 5. XRD pattern of Co loaded aerogel sample.

A new project was initiated during the past year with Prof. Eyring whose group is synthesizing Co-loaded aerogels and xerogels for Fischer-Tropsch reactions. One of the important issues here is the electronic state of Co e.g. elemental Co vis-à-vis oxides of Co. In Fig. 5, we show the XRD pattern of an aerogel sample received from Utah. Presence of elemental Co, CoO and amorphous SiO_2 is clearly indicated. We also carried out temperature variation of the magnetization (M) of this sample in different magnetic fields (H) using our SQUID magnetometer. A hysterestic loop in M vs. H is observed, as expected for the ferromagnetic Co. However, when the sample is cooled in a magnetic field to 5 K and then the hysteresis loop is measured, the loop is no longer symmetric about the origin but shifted to negative fields [Fig. 6]. This phenomenon of exchange-bias is observed in coupled ferromagnet/antiferromagnetic systems and it is of great current interest because of its interesting physics and numerous applications currently under development in magnetic storage and magnetic sensors [7]. Regarding the status of Co in the aerogel, these studies show that CoO is only partially reduced to Co and that the sample contains antiferromagnetic CoO coupled to ferromagnetic Co. Thus the sample contains nanoparticles with a shell of Co and core of CoO (or vice-versa). This collaboration will continue during the coming year and it is expected that these results will be written up for publication in the near future.

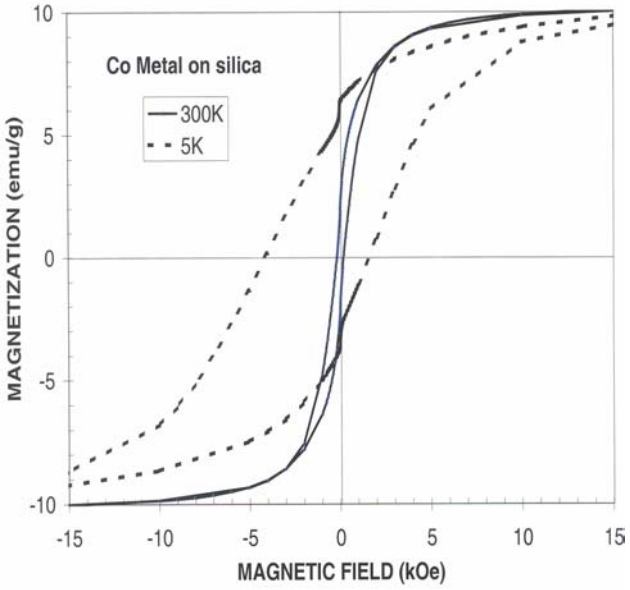

Fig. 6. Hysteresis loops from Co loaded aerogel sample illustrating exchange bias.

Results from the Pittsburgh Collaboration

We have worked with Prof. Wender's group at Pittsburgh to characterize the $Pt/WO_x/ZrO_2$ (PWZ) catalysts which they are using in a number of reactions. Our aim was to determine the structural and electronic properties of the three constituents of the PWZ catalysts, viz. Pt, WO_x and ZrO_2 under different conditions of preparation, heat treatments to 1000°C, tungsten loading and chemical reactions. The results of these investigations using XRD, EMR spectroscopy, temperature variation of magnetic susceptibility (χ) and thermogravimetric analysis have recently appeared in two comprehensive publications [8,9].

Here we briefly summarize the results on the role of Pt. From the magnitude and temperature variation of χ (Fig. 7), we concluded that Pt in fresh PWZ catalysts exists as Pt-oxides, which under the hydroisomerization reactions is reduced to metallic Pt [8]. Also, our ESR studies showed that Pt has a role in changing the oxygen stoichiometry of WO_3 and ZrO_2 to generate the observed W^{5+} and Zr^{3+} states in PWZ since in samples without Pt, these states are not observed [9]. In samples annealed at 500°C, electron transfer between the W^{5+} and Zr^{3+} states is observed since the concentration of one state increases at the expense of the other (Fig. 8). These electron transfer processes may be playing an important role in catalysis.

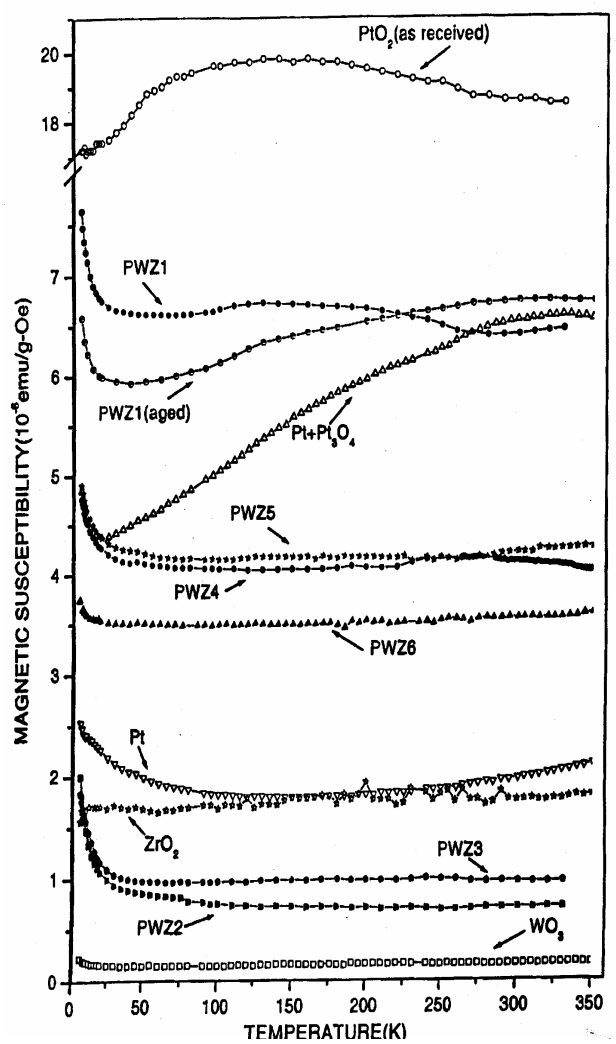

Fig. 7. Temperature variation of the magnetic susceptibility of different samples

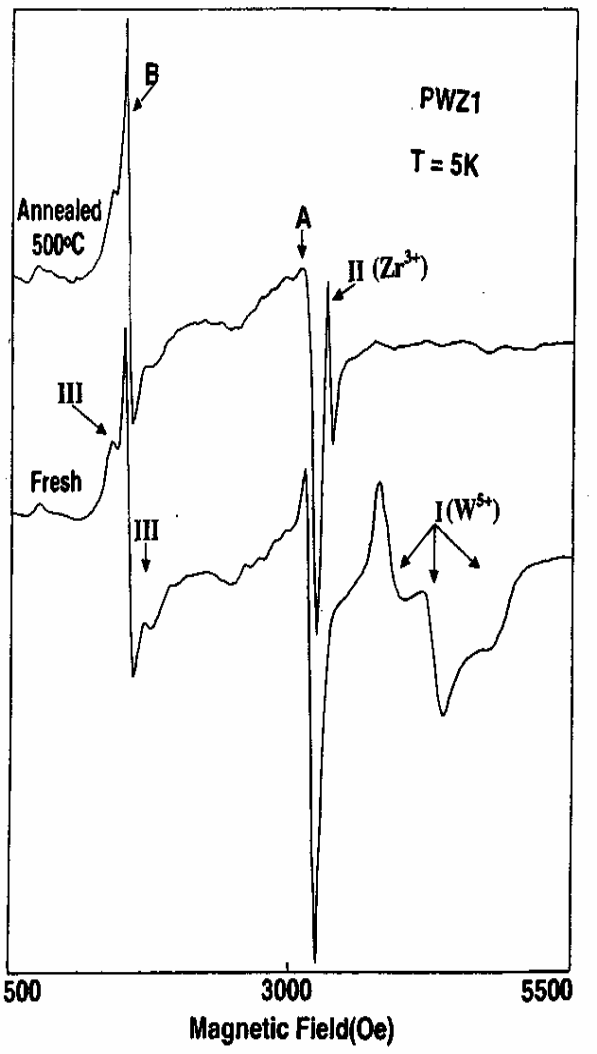

Fig. 8. ESR spectra of PWZ sample showing the W^{5+} and Zr^{3+} states

Results from the Auburn Collaboration

During the past year, a new collaboration was initiated with Prof. Guin at Auburn University whose group is synthesizing SAPO-5, SAPO-34 and SAPO-11 catalysts for use in the conversion of methanol to ethylene, propylene and other value-added products. Since the synthesis of these catalysts is not trivial, we characterized several dozen samples supplied by the Auburn group using XRD to determine whether the desired products are being formed under controlled conditions. A major result of this collaboration is that the Auburn group has nearly optimized the conditions for the controlled synthesis of SAPO-5, SAPO-34 and SAPO-11. In Fig. 9, we show the XRD patterns of the three catalysts, clearly showing significant differences in their XRD patterns, especially at lower angles.

The Auburn group has also doped the base samples with transition metal ions (Mn, Co, Ni), which are expected to provide the catalytic activity. These dopings are not detected in the XRD

spectra because of their low concentrations. However, in EMR spectroscopy and in SQUID measurements, the different dopant are distinctly detected. Analysis of this data is now underway which will allow us to determine the concentrations of each dopant and their electronic state. Then, we will attempt to correlate these characteristics with the data on the product yields provided by the Auburn group. For reference, the pore sizes of SAPO-5, SAPO-11 and SAPO-34 are 0.8 nm, 0.6 nm and 0.43 nm respectively.

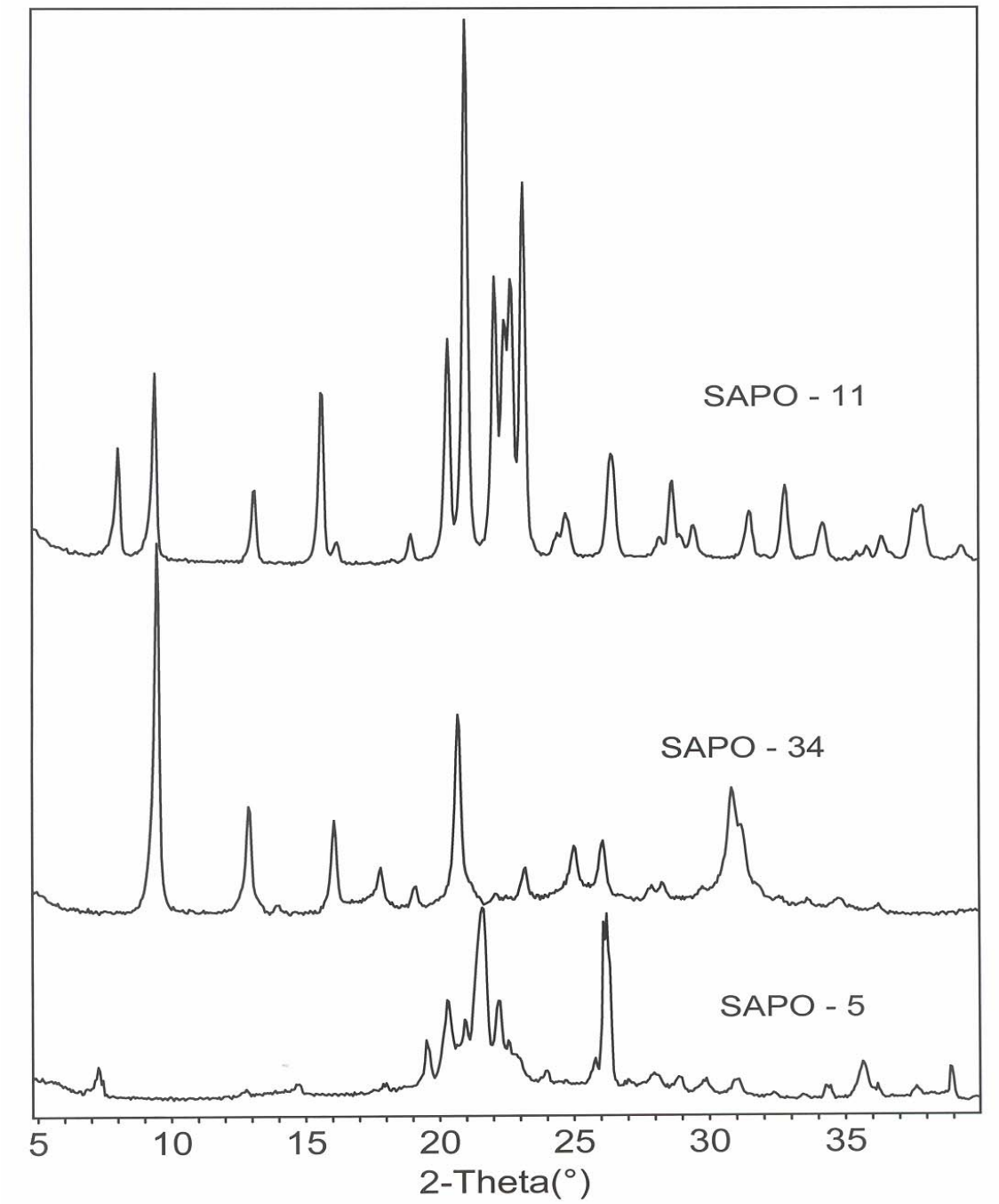

Fig. 9. XRD patterns of different SAPO samples.

Results from the WVU collaboration

During the past year, we have worked with the research group of Prof. Kugler and Prof. Dadyburjor in connection with their project on the dry reforming of methane to syngas using cobalt-tungsten-carbide catalysts. Our contribution was to characterize the catalysts by XRD, at different stages of the catalyst preparation and the post-reaction catalysts. Several dozen samples were analyzed and for details of these, see the report by Kugler and Dadyburjor.

Synthesis and properties of CuO nanoparticles

About two years ago, we undertook the synthesis of CuO nanoparticles by the sol-gel technique. These nanoparticles were supplied to the Utah group for testing them as catalyst in the synthesis of diethyl carbonate. CuO was found to have some activity although $PdCl_2/CuCl_2/AC$ catalysts were found to be more active. Nevertheless, we developed the protocols to synthesize CuO nanocrystals of size D = 4, 5, 7, 10, 15, 23, 30 and 34 nm, and we have investigated in detail their structural and magnetic properties [6,10,11]. One of the most interesting results is that the fractional change of the lattice constant b (viz. Δb/b) and the tensile strain Δd/d measured by XRD vary similarly as 1/D [Fig. 10]. Thus, as the particle size D is decreased, there are significant changes in the structural properties, along with changes in the magnetic properties, both sets varying as 1/D. These studies have established the important role of surface atoms in nanoparticles and established CuO as a prototype nanoparticle system with a ferromagnetic/antiferro-magnetic interface where the ferromagnetic component is provided by the uncompensated surface Cu^{2+} spins, with the core Cu^{2+} spins ordered antiferromagnetically. A sample of CuO has been submitted to the Los Alamos National Lab. for neutron diffraction studies of the magnetic state of this interesting nanoparticle system. Details of the magnetic properties are available in the cited references [6,10,11]. Dr. Punnoose presented an invited talk on "Finite Size Effects in CuO nanoparticles" at the Ninth International Conference on Composites Engineering, July 1-6, 2002 (San Diego, CA). An extended two page abstract was published in the Proceedings [12].

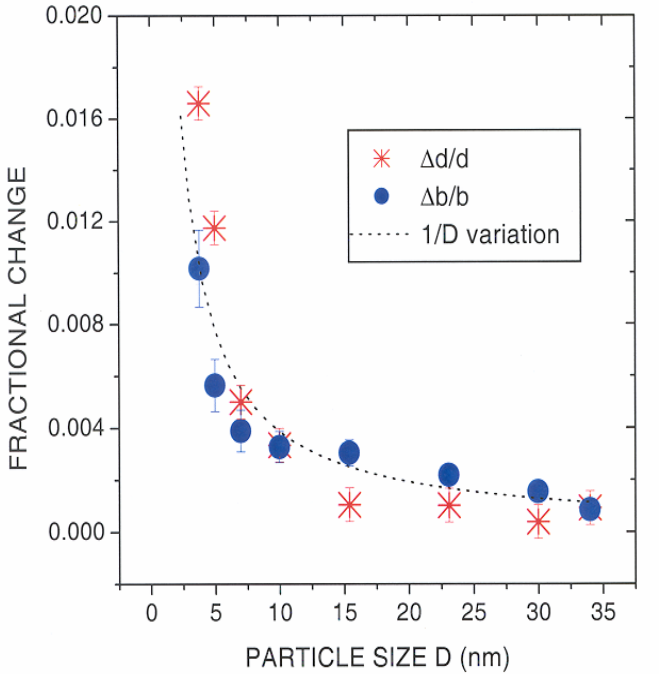

Fig. 10. Plot showing the 1/D type variation of lattice constant d and tensile strain.

Electron magnetic resonance spectroscopy of doped ferrihydrites (FHYD)

The temperature variation of the resonance field H_r and the linewidth ΔH of the magnetic resonance in pure FHYD and FHYD doped with Si, Ni, Mo and Ir has also been reported [13,14]. These systematic variations have been successfully interpretted in terms of changes in the magnetization and the resulting demagnetizing fields. Although most of the studies were carried out with the in-house spectrometer operating at 9.57 GHz [14,15], we have also carried

out studies at the much higher frequencies of 190 and 286 GHz available at the National Magnet Lab. in Tallahassee, Florida. These results will be written up for publication in the near future.

Concluding Remarks

A brief summary of the results obtained in our laboratory during the past year under the C-1 Chemistry program has been presented in this report. Our collaborations with the other researchers in the Consortium have been mutually very fruitful, in the true spirit of the Consortium. We thank our collaborators and it is our goal to continue these collaborations as suitable projects become available. Finally, a personal note. Dr. Alex Punnoose will be leaving my research group in mid August, 2002, to join Boise State University, Boise (Idaho) as an Assistant Professor of Physics. A search for his replacement is underway.

References

1. N. Shah, D. Panjala and G. P. Huffman, "Hydrogen production by catalytic decomposition of methane," Energy & Fuels 2001, 15, 1528-1534.
2. N. Shah, F. E. Huggins, D. Panjala, G. P. Huffman, A. Punnoose and M. S. Seehra, "Supported binary catalysts for dehydrogenation of methane," ACS Fuel Chem. Div. Preprints 2002, 47, 132-133.
3. A. Punnoose, N. Shah, G. P. Huffman, and M. S. Seehra, "X-ray diffraction and electron magnetic resonance studies of $M/Fe/Al_2O_3$ (M = Ni, Mo and Pd) catalysts for CH_4 to H_2 conversion," Fuel Process. Technol. (submitted).
4. A. Punnoose, M. S. Seehra, N. Shah and G. P. Huffman, "Magnetic properties of ferrihydrite nanoparticles doped with Ni, Mo and Ir," Phys. Rev. B (submitted).
5. M. S. Seehra and A. Punnoose, "Deviations from the Curie-law variation of magnetic susceptibility in antiferromagnetic nanoparticles," Phys. Rev. B 2001, 64, 132410 (4 pages).
6. A. Punnoose, M. S. Seehra, B. C. Dunn and E. M. Eyring, "Characterization of $PdCl_2/CuCl_2$/activated carbon catalysts for the synthesis of diethyl carbonate," Energy & Fuels 2002, 16, 182-188.
7. A. Punnoose and M. S. Seehra, "Hysteresis anomalies and exchange bias in 6.6 nm CuO nanoparticles," J. Appl. Phys. 2002, 91, 7766-7768; and references therein.
8. A. Punnoose, M. S. Seehra and I. Wender, "Structure, properties and roles of the different constituents of $Pt/WO_x/ZrO_2$ catalysts," Fuel Process. Technol. 2001, 74, 33-47.
9. A. Punnoose and M. S. Seehra, "ESR observation of W^{5+} and Zr^{3+} states in $Pt/WO_x/ZrO_2$ catalysts," Catalysis Letters 2002, 78, 157-160.
10. A. Punnoose, H. Magnone, M. S. Seehra and J. Bonevich, "Bulk to nanoscale magnetism and exchange-bias in CuO nanoparticles," Phys. Rev. B 2001, 64, 174420 (8 pages).
11. M. S. Seehra and A. Punnoose, "Size dependence of lattice parameters, Néel temperature, exchange-bias and coercivity in CuO nanoparticles," Phys. Rev. B (submitted).
12. A. Punnoose and M. S. Seehra, "Finite Size Effects in CuO nanoparticles," Proc. Ninth Intern. Conf. Composites Engg. San Diego, CA (July 2002), D. Hui, Editor, pp 639 – 640.
13. M. S. Seehra, A. Punnoose, P. Roy and A. Manivannan, "Effect of Si doping on the electron spin resonance properties of ferrihydrite nanoparticles," IEEE Transactions on Magnetics 2001, 37, 2207-2209.
14. A. Punnoose and M. S. Seehra, "Temperature dependence of paramagnetic resonance in pure and doped ferrihydrite nanoparticles," Proc. Third Asia-Pacific EPR/ESR Symposium, Nov. 2001, Kobe University, Japan (accepted, to be published by Elsevier).

NMR and ESR Studies of Particulate Matter in Model Compounds and Diesel Fuels

R. J. Pugmire Mark S. Solum and Yi Jin Jiang
University of Utah

Introduction

Particulate emission (PM) from combustion systems is undergoing increased scrutiny regarding the short/long term health effects. A number of population based epidemiological studies have reported associations between airborne particulates and a range of respiratory outcomes from symptoms to mortality.[1-3] Diesel engine powered vehicles account for a major fraction of particulate matter (up to 70%) in many cities. PM derived from diesel exhausts is predominantly carbon-rich material that contains a significant volatile organic component.

Data obtained on the particulate matter collected from a test diesel engine at Utah have provided some information on the volatile organic materials adsorbed on the PM (see data in reports of Meuzelaar and co-workers). In addition, intriguing aspects of the nature of the solid (insoluble) PM have been observed with and without the addition of oxygenates to the base fuel and, with addition of oxygenates, a significant reduction is noted in the quantity of PM released.[4] These data have also provided some clues as to the nature of the evolution of the PM. We have noted that the conductivity and concentration of free radicals in aerosols produced from model compounds increases with temperature as noted by Feitas, et. al.[5-7] A relationship between sample conductivity and the "graphite-like factor" of the PM has been observed[8] which we believe is related to the amount of electrons occupying conduction bands in the solid soot material.

One of the keys to understanding this behavior of PM (hereafter referred to as solvent extracted soot) is an understanding of the nature of the free radicals present. Pyrolyzed carbonaceous materials have on the order of 10^{17}-10^{20} spins/gram with extractable materials (tars) on the low end and residues (soots) on the high end. Two types of free radicals exist, those with 1) time independent (or static fixed free electrons) and 2) time dependent electrons that are associated with mobile or conduction electrons. Only the latter electrons give rise to sample conductivity.

Results

The amount of graphite-like structure in carbonaceous materials such as soots is an important parameter for understanding the composition of these materials. The structure of graphite has been studied extensively[9-14], and is described by the delocalization of the π electrons over the carbon structure. These delocalized π electrons contribute to the conductivity of graphitic material. A recently proposed structure of coals[15] and soots consists of regions or clusters that are graphite-like in nature, linked by non-conductive chain/bridging regions. The electrical conductivity of these materials will therefore depend on the extent of these graphitic regions. Therefore, by measuring the electrical conductivity of these samples it is possible to estimate the amount of graphitic materials present. Interestingly, anthracite coals are ideal materials for studying the conductivity of carbonaceous materials with low (≤ 0.3) H/C as described below.

The direct measurement of electrical conductivity is a classical method[16] in which a pair of electrodes is placed across the sample. However, due to the low resistivity (1.5×10^{-3} ohm-cm even in graphite),[17] the resistance of the electrical contact between the electrodes and the sample could seriously affect the measurement results, especially when the sample is a powder. In addition, the heterogeneity of the samples and the presence of nonconductive regions make it difficult to measure the electrical conductivity of the sample in this manner. In order to solve such problems, the method of measuring the quality factor (Q value) of a radio frequency (RF) coil at high frequency has been employed.[18,19] The experimental procedures have been reported[19] and the results obtained from anthracite coals and diesel soots[8] as well as model compounds have been obtained.[20,21]

The graphite factors reported represent a variety of samples studied in this laboratory over the last two years. The four anthracitic coals come from the LCNN, Jeddo, Harmony and Summit mines, all of which mine the Eastern Middle Field of Pennsylvania and were loaded to us by Professor Harold Schobert of The Pennsylvania State University. An elemental analysis of the four anthracite samples is given in Table 1.[16] Samples labeled as a residue are the insoluble portion after 24 hrs extraction with dichloromethane in a Soxlet extraction system. The diesel soots were produced from a Kubota 2-stroke diesel engine loaded to 10 fts. Three different fuel mixtures were used. Diesel #1 was made from pure diesel fuel. Diesel #2 was made from: 4.2 % ethanol, 1.3% diethyl carbonate, .1% diethoxymethane, .1% ethyl formate and 94.3 % diesel fuel. Diesel #3 was made from: 5 % diethylcarbonate and 95 % diesel fuel. The diesel particulate matter (DPM) 1650 sample was obtained from NIST. The exact conditions of the preparation of this DPM sample were not available although it is thought to come from large Caterpillar tractor engines. DPPH is 2,2-Di(4-*tert*-octylphenyl)-1-picrylhydrazyl free radical (Aldrich # 25,762-1).

Figure 1 shows a plot of the Q_i values associated with the standard diluted graphite samples vs the varying graphite content. The least squares fit of the data is:

$$G = -0.685Q_i + 179.0 \qquad (1)$$

This is used to calculate the graphite content of test samples. The marginal standard deviation of the slope is 0.041 and that of the intercept is 8.7. The graphite factors in this report are the values derived from equation 1 normalized by the weight of the sample (GF = G/wt).

The measured Q_i values, the graphite content, the atomic ratios C/H and the concentration of the unpaired electrons are given in Table 2 for the four anthracite coals. Data on these four coals have been reported previously.[22] Similar information for several soot samples is given in Table 3. This method has been applied for the first time to measure the graphite-like structures in the anthracites and soot samples that are being studied at Utah. Both of these highly aromatic materials are of complex composition containing mixtures of both amorphous and semi-ordered structures and, as far as the investigators can determine, no data of this type have previously appeared in the literature. However, based on results from other experiments, a possible qualitative explanation will be discussed.

The data in Table 2 indicate that the differences in graphitic carbon content of the four anthracites is significant, i. e., by an order of magnitude when one compares the data of the LCNN and Summit samples. However, the concentration of unpaired electrons in these four

samples is essentially constant, varying by less than a factor of 2. The graphite factor in the anthracite sample with the highest concentration of unpaired electrons (Harmony) is only 0.023. These results indicate that not all measured unpaired electrons contribute to the electrical conductivity. No change in the Q value of a coil is observed when a stable free radical (localized electron) such as DPPH (a standard free radical sample) is placed in the coil. These data indicate that there are at least two different types of electrons in the systems under study; 1) electrons such as found in DPPH where the electron is localized and, 2) electrons that can occupy conduction bands in graphite type structures made up of extended hexagonal ring systems. Electrons that have time independent electron-nuclear interactions or electrons where the electron-nuclear interaction is time dependent have been discussed before as they relate to DNP experiments.[23] These extended ring systems may contain, especially in the soot samples, some five-member rings.[24]

It is still not clear what size hexagonal ring systems is large enough to exhibit conduction behavior. For example, coronene, which has seven rings, has no effect on the Q value of the RF coil. Celzard[15] proposed that at least 70 hexagonal rings and a C/H weight ratio higher than 50 (atomic C/H ≈ 4.2) is where conductive behavior starts. According to the data shown in Table 2 the atomic C/H ratio of the anthracite coals from LCNN to Summit is 5.35, 4.44, 3.59, and 3.13, respectively. Comparison of these data with the graphitic carbon content seems to be reasonably in line with the results of Celzard. Pappano presented a model of the Jeddo sample that had 81 rings comprising each pre-graphitic sheet.[22]

The C-13 MAS spectra of five of the samples examined in this study are shown in Figure 2. The spectra of two anthracites, the NIST 1650 diesel engine soot residue and the anthracene soot residue were obtained using the CP technique. The Kubota diesel soot spectrum and a comparison graphite spectrum were taken with the single pulse technique due to a depletion of protons in the sample which renders the CP technique ineffective. These five samples have quite different percentages of the graphitic carbon. The graphite-factors for the five samples are: 0.015, 0.15, 0.34, 0.47 and 0.60 for Summit, LCNN, NIST 1650 residue, the 1400 K anthracene soot residue and the Kobota diesel soot #2, respectively. One can see that there is a great variation of line widths among the four samples that, to some degree, follows the graphite factor. However, all are narrower than the graphite sample. The NIST sample is broad in the aromatic region, but also contains some aliphatic material (about 22 %, the aliphatic material shows up with more relative intensity at shorter contact times) so the graphite-like factor is reduced (as correlated to the aromatic line width) as the aliphatic material is not conductive. The increased line width is due to anisotropy of the magnetic susceptibility of regions of graphene layering that is not totally removed under MAS conditions.[25,26] The Summit sample has the appearance of a normal diamagnetic sample with a very small graphite factor and no unusual line broadening. While the line width (FWHM) of the LCNN is essentially the same as that of the Summit, some line broadening appearing as Lorentzian wings are evident in the LCNN sample. The anthracene soot residue has even broader wings and the broadening of the main resonance is approximately 40% more than that of the LCCN. The Kubota diesel engine soot has an extremely broad resonance that is also noted in samples so deficient in proton content that the CP experiment is not effective.[27]

References

1. Schwartz, J., Dockery, D. W.,*An. Rev. Respir. Dis*., **1992**, 145, 600.
2. Ostro, B. D., *Arch. Envirn. Health* **1993**, 48, 336.
3. Dockery, D. W., Pope III, C. A., *Annu. Rev. Public Health*, **1994**, 15, 1994.
4. Unpublished data obtained at the University of Utah, 2001-2002.
5. Freitas, J. C. C., Cunha, A. G., Emmerich, F. G., **1997**, Fuel, 76, 229.
6. Freitas, J. C. C., Bonagamba, T. J., Emmerich, F. G. **1999**, Energy & Fuel, 13, 53.
7. Freitas, J. C. C., Emmerich, F. G., Cernicchiaro, G. R. C., Sampaio, L. C., Bonagamba, T. J., 2001, Solid State NMR, 20, 61.
8. Jiang, J. Y., Solum, M. S., Pugmire, R. J., Grant, D. M., Schobert, H., Pappano, P. J., A New Method for Measuring the Graphite Content of Anthracite Coals and Soots, Energy and Fuel, **2002**, in press.
9. Mantell, C. L., *Carbon and Graphite Handbook*; Interscience Publishers: New York, 1968, pp. 6-43.
10. Wallace, P. R., *Phys. Rev.*, **1947,** 71, 622.
11. Schobert, H. H., *The Chemistry of Hydrocarbon Fuels*; Butterworths: London, 1990, pp. 293-295.
12. McClure, J. W., *Phys. Rev*., **1956,** 104, 666.
13. Wagoner, G., *Phys. Rev*. **1960**, 118, 647.
14. Singer, L.S., Wagoner, G., In *Proc. Fifth Carbon Conf*; Pergamon Press: New York, 1963, pp. 65-71.
15. Celzard, A., Mareche, J. F., Payot, F.,Begin, D., Furdin, G., *Carbon*, **2000**, 38, 1207.
16. Terman, F. E., *Radio Engineer's Handbook, 1st. ed*; McGraw-Hill: New York, 1943, pp. 26-47.
17. Tyler, W. W., Wilson Jr., A. C., *Phys. Rev*. **1953**, 89, 870.
18. Terman, F. E., *Radio Engineer's Handbook, 1st. ed*; McGraw-Hill: New York, 1943, pp. 74-83.
19. Jiang, Y. J., *J. Magn. Reson*., **2000**, 142, 386.
20. Solum, M. S., Veranth, J., Jinag, Y. J., Orendt, A., Sarofim, A. F., Pugmire, R. J., "The Study of Anthracene Aerosols by Solid State NMR and ESR", manuscript in preparation.
21. Hunt, J. E., Winans, R. E., Tomczyk, N. A., Pugmire, R., Molecular Characterization of Hydrocarbons from Soots in Low Temperature Flames of Biphenyl and Illinois No. 6 Coal, *Am. Chem. Soc*., Fuel Chemistry Division Preprints, **2001**, 46(1), 294-295.
22. Pappano, P. J., Mathews, J. P., Schobert, H. H., *Prepr. Symp. - Am .Chem. Soc.,* Fuel Chemistry Division Preprints, **1999**, 44, 567.
23. Wind, R. A., Li, L., Maciel, G. E., Wooten, J. B., *Appl. Magn. Reson.*, **1993**, 5, 161.
24. Orendt, A. M., Facelli, J. C., Bai, S., Rai, A., Gossett, M., Scott, L., Boerio- Goates, J., Pugmire, R. J., Grant, D. M., *J. Phys. Chem. A*, **2000**, 104, 149.
25. Freitas, J. C. C., Emmerich, F. G., Cernicchiaro, G. R. C., Sampaio, L. C., Bonagamba, T. J., *Solid State NMR*, **2001**, 20, 61.
26. Kume, K., Hiroyama, Y., *Solid State Commun*., **1988**, 65, 617.
27. Solum, M. S., Sarofim, A. F., Pugmire, R. J., Fletcher, T. H., Zhang, H., *Energy Fuels*, **2001**, 15, 961.

Table 1. The Elemental Analyses of the Anthracite Coal Samples.[15]

Sample	C (%)	H (%)	N (%)	S (%)	O (%) (by diff)
LCNN	95.7	1.5	1.2	0.5	1.0
Jeddo	95.2	1.8	1.1	0.6	1.3
Harmony	94.0	2.2	1.0	0.5	2.3
Summit	93.2	2.5	1.6	0.6	2.2

Table 2. The Measured Graphite-Factor, C/H Atomic and Mass Ratios, Q_i Measurement, and Spin Concentration of Unpaired Electrons of the Anthracite Coal Samples.

Sample	Graphite Factor	Atomic C/H	C/H Weight Ratio	Q_i Value[a]	Spin Concentration (10^{19} spins/g)
LCNN	0.15[b]	5.35	63.8	184	3.3
Jeddo	0.11	4.44	52.9	200	3.5
Harmony	0.02_3	3.59	42.7	250	4.9
Summit	0.01_5	3.13	37.3	254	2.6

a) The frequency of the measurement was 100 MHz; at this frequency the Q value of the empty coil is 258.

b) Average of five repeat measurements with repacked rotors with a standard deviation of 0.01.

Table 3. The Measured Graphite-Factor and Unpaired Electron Spin Concentration of Some Soot Samples.

Sample	Sample Weight (mg)	Graphite Factor	Q_i Value[a]	Spin Concentration (10^{19}spins/g)
Anthracene 1400 K Soot Residue	164	0.47	149	11.00
Ethylene Soot Residue	150	0.48	157	3.78
NIST DPM 1650 Residue	181	0.34	172	1.11
Diesel Soot #1	174	0.46	144	3.99
Diesel Soot #2	186	0.60	98	3.82
Diesel Soot #3	186	0.60	98	3.00

a) The frequency of the measurement was 100 MHz; at this frequency the Q value of the empty coil is 258.

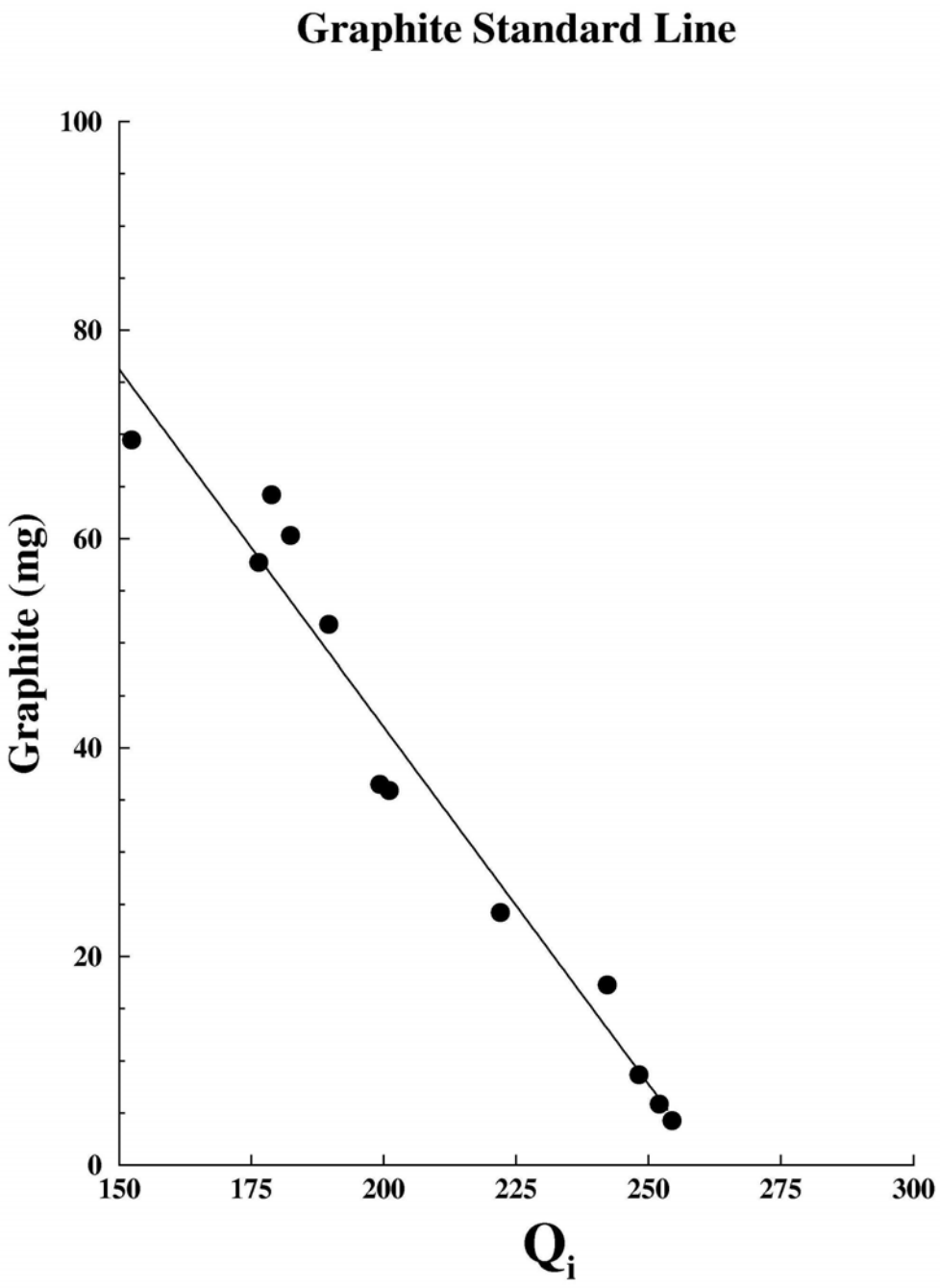

Figure 1. Plot of G vs. Q_i and the associated regression line.

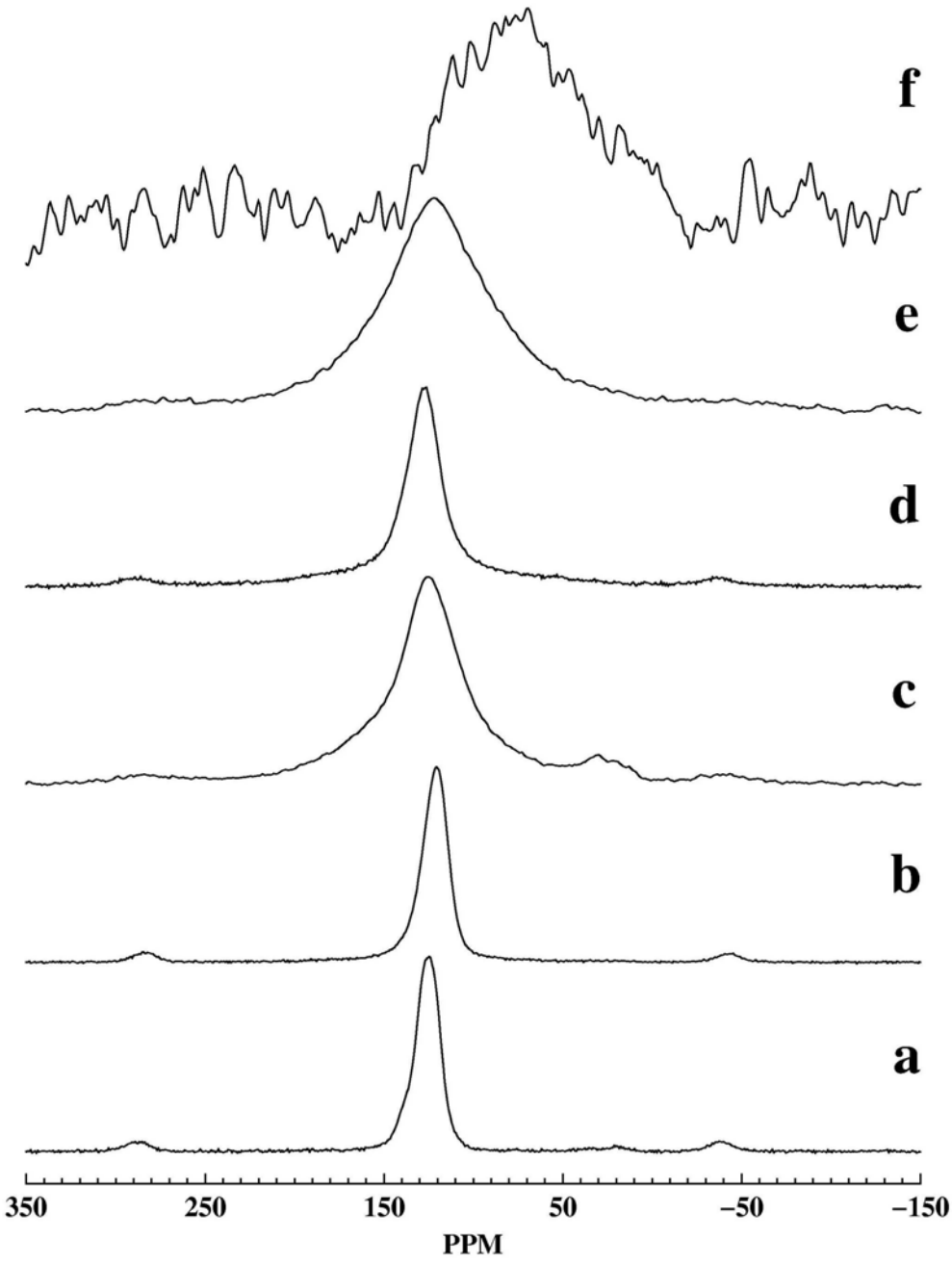

Figure 2. Carbon-13 MAS spectra of six of the highly aromatic samples. The spectra in a, b, c, d were taken with the CP technique all with a 1 s pulse delay. a) Summit anthracite coal taken with a 3 ms contact time. b) LCNN anthracite coal taken with a with a 10 ms contact time. c) NIST 1650 diesel particulate mater residue taken with a with a 10 ms contact time. d) Anthracene 1400 K aerosol residue taken with a 10 ms contact time. e) Kubota diesel engine soot, spectrum taken with the single pulse method and using a 10 s pulse delay. f) Graphite sample 20 % by weight in silica gel, single pulse method 864 scans and 600 s pulse delay.